

How Extreme Apparitions of the Volcanic and Anthropogenic South East Asian Aerosol Plume caused the Millennium Drought in South Eastern Australian. First Attribution and Mechanism using data from the Last Millennium Ensemble, Large Ensemble, MERRA-2 Reanalysis, four Satellites and the Global Volcanism Program.

Keith Alan Potts¹

¹Kyna Keju Pty Ltd

November 22, 2022

Abstract

The Last Millennium Ensemble, Large Ensemble, MERRA-2, four satellite data sets and the Global Volcanism Program database all show independently that drought in south eastern Australia (SEAus) is created by apparitions of the natural and anthropogenic aerosol plume over south east Asia which simultaneously create ENSO and IOD events. From 1997 to 2008 SEAus endured an exceptionally severe drought - the Millennium Drought. The River Murray, the major waterway in the region, experienced inflows at record low levels in 2006-07 which were more than 40% below the previous low. As the literature, Inter Governmental Panel on Climate Change (IPCC) and the USA Climate Change Science Program suggest that aerosols can affect the large-scale atmospheric circulation and hydrologic cycle I examine the relationship between aerosols and Australian droughts. The global aerosol coverage is highly inhomogeneous and variable at daily, monthly, annual and decadal scales. I show that the aerosol optical depth (AOD) and aerosol index (AI) of the South East Asian Plume (SEAP) and the volume of aerosols ejected by volcanoes (tephra) in south east Asia correlate with drought in Australia and conclude that the SEAP causes drought in Australia by Aerosol Regional Dimming (ARD), which, by altering the surface radiation budget under the plume and warming the upper atmosphere, forces the regional Inter Tropical Convergence Zone and Hadley Cells into abnormal seasonal positions. These effects alter the regional atmospheric circulation systems and hydrologic cycle thereby causing drought and, as the SEAP has intensified over time, created climate change.

1 **How Extreme Apparitions of the Volcanic and Anthropogenic South East Asian Aerosol**
2 **Plume caused the Millennium Drought in South Eastern Australian. First Attribution**
3 **and Mechanism using data from the Last Millennium Ensemble, Large Ensemble,**
4 **MERRA-2 Reanalysis, four Satellites and the Global Volcanism Program.**
5
6

7 **K. A. Potts¹**

8 ¹ Kyna Keju Pty Ltd.
9

10 Corresponding author: Keith Potts (Keith.Potts@bigpond.com)

11 **Key Points:**

- 12 • Drought in SE Australia, ENSO and IOD events are caused by apparitions of the South East
13 Asian aerosol Plume (SEAP)
- 14 • Volcanoes are and always have been the major source of the aerosols
- 15 • Post 1980 the anthropogenic SEAP has intensified the volcanic plume, drought, ENSO and
16 the IOD especially in Sep-Nov
17

18 **Abstract**

19 The Last Millennium Ensemble, Large Ensemble, MERRA-2, four satellite data sets and the Global
20 Volcanism Program database all show independently that drought in south eastern Australia (SEAus)
21 is created by apparitions of the natural and anthropogenic aerosol plume over south east Asia which
22 simultaneously create ENSO and IOD events. From 1997 to 2008 SEAus endured an exceptionally
23 severe drought - the Millennium Drought. The River Murray, the major waterway in the region,
24 experienced inflows at record low levels in 2006-07 which were more than 40% below the previous
25 low. As the literature, Inter Governmental Panel on Climate Change (IPCC) and the USA Climate
26 Change Science Program suggest that aerosols can affect the large-scale atmospheric circulation and
27 hydrologic cycle I examine the relationship between aerosols and Australian droughts. The global
28 aerosol coverage is highly inhomogeneous and variable at daily, monthly, annual and decadal scales.
29 I show that the aerosol optical depth (AOD) and aerosol index (AI) of the South East Asian Plume
30 (SEAP) and the volume of aerosols ejected by volcanoes (tephra) in south east Asia correlate with
31 drought in Australia and conclude that the SEAP causes drought in Australia by Aerosol Regional
32 Dimming (ARD), which, by altering the surface radiation budget under the plume and warming the
33 upper atmosphere, forces the regional Inter Tropical Convergence Zone and Hadley Cells into
34 abnormal seasonal positions. These effects alter the regional atmospheric circulation systems and
35 hydrologic cycle thereby causing drought and, as the SEAP has intensified over time, created climate
36 change.

37

1 INTRODUCTION

1.1 HYPOTHESIS AND PHYSICAL MODEL

38 This paper explores an explicit physical model and hypothesis to explain how the South East
39 Asia aerosol Plume (SEAP) causes drought in south eastern Australia (SEAus) and simultaneously
40 causes ENSO, described in the companion paper [K.A. Potts, 2020b], and IOD events.

41 Droughts in SEAus have always has been triggered and sustained by the natural volcanic
42 aerosol plume over south east Asia (SEAsia) which has, in recent decades, been intensified by the
43 anthropogenic aerosol plume especially from August to November (SON).

44 The sequence of events is:

- 45 1. The volcanic tephra aerosol plume forms over SEAsia and, in recent decades, is
46 intensified by the anthropogenic plume which is most intense from August to November
47 (ASON);
- 48 2. The aerosols absorb (and reflect) solar radiation which heats the atmosphere;
- 49 3. The aerosols reduce the solar radiation at the surface under the plume which cools the
50 surface;
- 51 4. 2 and 3 create a temperature inversion compared to times without a plume and this
52 reduces convection in the region;
- 53 5. The region to the south of the SEAP is now the driving force of the convective leg of the
54 southern regional Hadley cell;
- 55 6. This southerly move in convection shifts the entire southern Hadley Cell south;
- 56 7. This results in a southerly shift in the sub-tropical high over SEAus;
- 57 8. This results in higher pressure over SEAus;
- 58 9. This forces the cold fronts south and reduces rainfall over SEAus;
- 59 10. The cooler sea surface temperature (SST) in SEAsia reduces evaporation in the area
60 which supplies moisture to SEAus;
- 61 11. This results in less water vapour in the atmosphere over SEAus;
- 62 12. The combination of 9 and 11 above causes drought in SEAus.

1.2 Drought in south eastern Australia

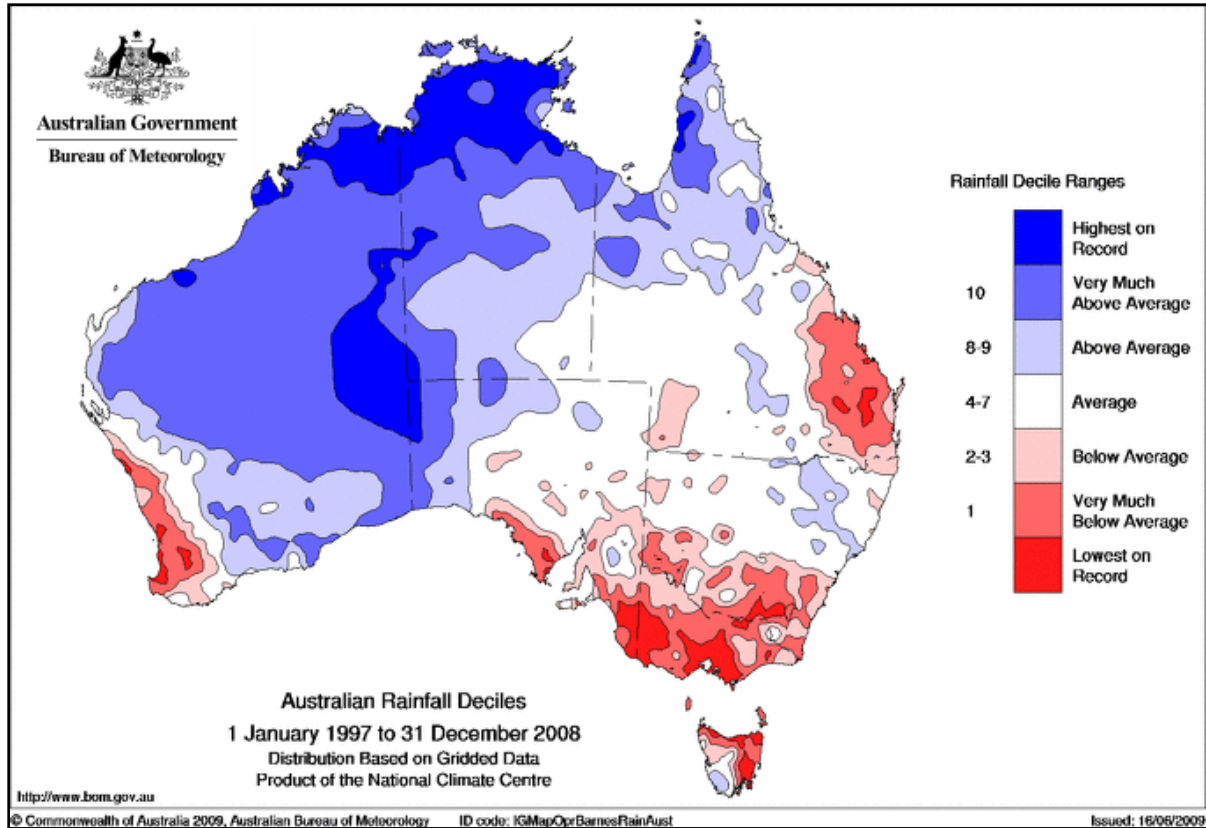
63 An exceptional and extended drought occurred in South Eastern Australia (SEAus) at the turn
64 of the century, the Millennium Drought [Timbal *et al.*, 2010] and [Ummenhofer *et al.*, 2009], and
65 Figure 1 shows the rainfall deficit from 1997 to 2008 when parts of SEAus received the lowest
66 rainfall on record. In this period all major cities in Australia were forced to build seawater
67 desalination plants to guarantee the urban water supply and the River Murray, the major waterway in
68 SEAus, received the lowest inflows on record [Murray Darling Basin Authority, 2011].

69 Whilst the Millennium Drought was exceptionally strong, drought has always occurred in
70 SEAus and must therefore be a natural phenomenon as historically anthropogenic forcing was
71 insufficient to impact the climate.

72 The drivers of such SEAus droughts have been identified as: El Niño – Southern Oscillation
73 Index (SOI) (ENSO) events by *Neville Nicholls et al.* [1996], *Power et al.* [1998] and *G Wang and*
74 *Hendon* [2007]; as Indian Ocean Dipole (IOD) events by *Ummenhofer et al.* [2009] and as variations
75 in the location and intensity of the sub-tropical ridge over SEAus by *Timbal and Drosowsky* [2013].
76 *Meyers et al.* [2007] investigated the effects of various combinations of ENSO and IOD events on
77 Australian rainfall concluding there is a need to develop the “capability to predict interannual SST
78 anomalies in the seas north of Australia in both the Pacific and the Indian Oceans.”

79 The Centre for Australian Weather and Climate Research (CAWCR) in *Timbal et al.* [2010]
80 reported the relationship between rainfall in south eastern Australia and the indices and parameters in
81 Figure 2 which shows that in Sept. Oct. and Nov (SON) the Niño 4 Sea Surface Temperature (SST)
82 and the local Mean Sea Level Pressure (SLP) exhibit the most significant and negative correlation
83 with rainfall. However, the climate model used for the analysis did not include carbonaceous aerosols
84 or small volcanic eruptions (personal communication).

85 I show that the element which must be included in the analysis of drought in SEAus is the
86 South East Asian aerosol Plume (SEAP) which simultaneously creates drought, ENSO and IOD
87 events



88
89
90
91

Figure 1: Figure 57 in *Timbal et al.* [2010] Australian rainfall deciles 1997 to 2008.

Correlation of Rainfall in Southern Hemisphere seasons with:	Autumn (MAM)	Winter (JJA)	Spring (SON)	Summer (DJF)
Local MSLP	-0.29	-0.74	-0.39	0.14
Niño 4 SST	-0.16	-0.20	-0.37	-0.18
NWS (North West Shelf) SST	0.07	0.30	0.26	-0.09
SAM (Southern Annular Mode)	-0.02	-0.27	0.31	0.31
NTS (Near Tasman Sea) SST	0.25	0.07	0.16	0.19

92
93
94

Figure 2: Correlations of parameters shown and rainfall south eastern Australia from Table 1 in *Timbal et al.* [2010].

1.3 Aerosols and Climate

95 The IPCC Assessment Report 4 (AR4) [Solomon *et al.*, 2007] identifies the two main
96 anthropogenic contributors to climate change as Long Lived Green House Gases (LLGHG) and
97 aerosols and defines Radiative Forcing (RF) as the global annual average of “the change in the net,
98 downward minus upward, irradiance (expressed in W m^{-2}) at the tropopause”. The IPCC AR4 also
99 discusses Surface Forcing (SF), the effects of the forcing agents at the surface of the Earth and Figure
100 3 from that report shows the evolution of RF and SF from 1850 to the present day. It can be clearly
101 seen that the net anthropogenic RF effect, black line – panel (A), follows the red line of LLGHG
102 reasonably closely. However, the net anthropogenic SF effect, black line – panel (B), clearly follows
103 the evolution of the aerosol direct effect which is much larger than the aerosol direct RF effect. The
104 SF graph also shows that the anthropogenic aerosol direct effect in 2000 at -1.6W/m^2 is comparable
105 to the explosive volcanic eruptions of Krakatau (1883) -2.2W/m^2 and Pinatubo (1991) -1.8W/m^2
106 which are considered to affect the mid to high latitude atmospheric circulation patterns [Solomon *et*
107 *al.*, 2007].

108 Absorbing aerosols, particularly black carbon, a product of incomplete combustion [Novakov
109 *et al.*, 2003], and organic carbon [Kirchstetter, 2004], have been linked to variations in the vertical
110 temperature profile of the atmosphere and the large scale atmospheric circulation [Solomon *et al.*,
111 2007], [Menon *et al.*, 2002] and [Chien Wang, 2004]. Aerosols may also have a greater influence on
112 the hydrologic cycle than other forcing agents through their SF effects [Solomon *et al.*, 2007].

113 Aerosols were believed to have mainly affected the northern hemisphere due to the greater
114 annually averaged aerosol optical depth north of the equator however Rotstayn *et al.* [2009b]
115 reviewed the impact of natural and anthropogenic aerosols on the Australian climate and suggested
116 that regional aerosol plumes with their associated large reductions in short wave flux at the surface
117 such as that derived from biomass burning in Indonesia may be important in understanding climate
118 variation in Australia and recommended that further research should be undertaken on a limited
119 number of topics including biomass burning in Indonesia as current aerosol inventories from this
120 region are poorly treated. Solomon *et al.* [2007] expressed the same concern that the distribution and
121 evolution of aerosol emissions during the 20th century were not well understood and Hegerl *et al.*
122 [2007] noted that most studies used in the IPCC AR4 omitted carbonaceous aerosols which could
123 have significant effects at regional scales.

124 The effects of short lived gases and aerosols were found to be substantial compared to
125 LLGHG and to account for as much as 40% of the warming over the summertime United States and
126 the climate response to these forcing agents was not confined to the area of their emission [Levy II *et*
127 *al.*, 2008].

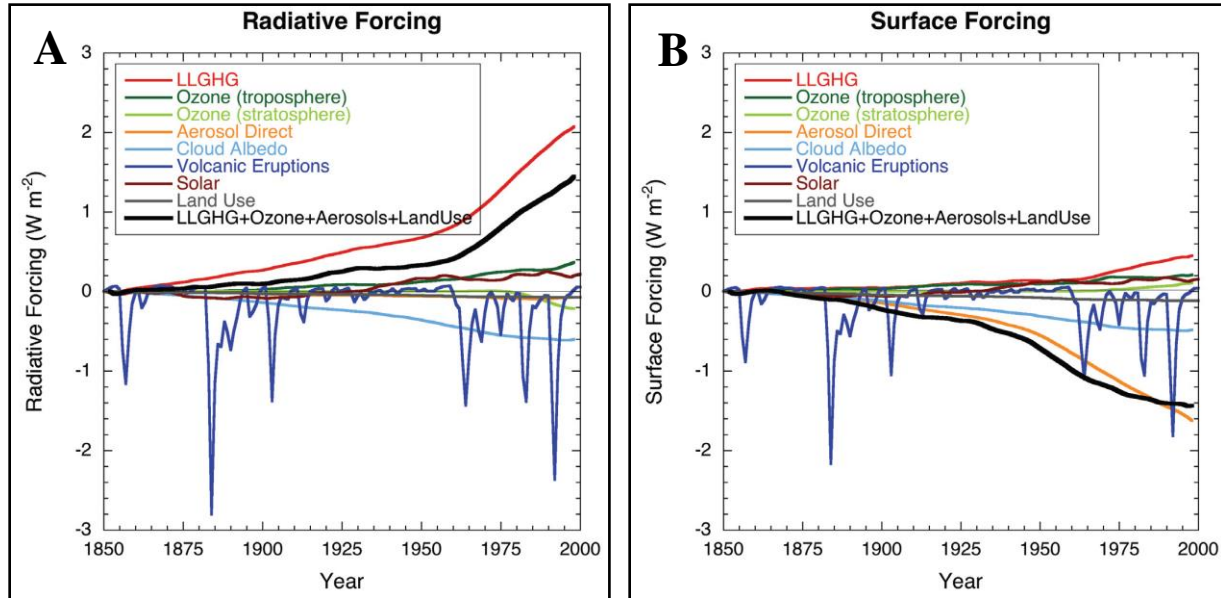
128 The global aerosol coverage and forcing is highly variable geographically and temporally and
129 it is “insufficient or even misleading” to emphasise the global average and the aerosol SF is greater
130 than the RF at the top of the atmosphere. Such SF affects the atmospheric circulation and the
131 hydrologic cycle [Remer *et al.*, 2009].

132 Rotstayn *et al.* [2007] concluded that anthropogenic aerosol forcing should be included in
133 modelling the Australian climate and that Asian anthropogenic aerosols may have affected the
134 hydrologic cycle in the Australian region.

135 Menon *et al.* [2002] investigating the climate of China and India found precipitation and
136 temperature changes in their model that were comparable to those observed only if the aerosol

137 ensemble included a large proportion of absorbing black carbon ("soot") which was similar to
 138 observed amounts and noted that absorbing aerosols heat the atmosphere and alter the regional
 139 atmospheric stability and vertical motions which affects the large-scale circulation and hydrologic
 140 cycle with significant regional climate effects.

141



142

143 Figure 3: IPCC AR4 Figure 2.23 Chapter 2 page 208 [Forster et al., 2007]. Globally and
 144 annually averaged temporal evolution of the instantaneous all-sky RF (A) and SF (B) due to various
 145 agents, as simulated in the MIROC+SPRINTARS model (Nozawa et al., 2005; Takemura et al.,
 146 2005). This is an illustrative example of the forcings as implemented and computed in one of the
 147 climate models participating in the AR4. Note that there could be differences in the RFs among
 148 models. Most models simulate roughly similar evolution of the LLGHGs' RF.

149 In a review of the simulation of the Australian climate with the new CSIRO global climate
 150 model (GCM) Mark 3.6 which includes an interactive aerosol scheme *Rotstayn et al.* [2009a] found
 151 that "Compared to its predecessors and several international GCMs, Mk 3.6 is best able to capture
 152 the spatial pattern of the leading rainfall mode, which represents variability due to the El Niño
 153 Southern Oscillation (ENSO)".

154 Anthropogenic aerosols have been linked to: the decadal variance in the North Atlantic SST
 155 and thus to drought in the Sahel and the Amazon with the dominant mechanism being the reduction
 156 in short wave surface radiation [Booth et al., 2012]; and the expansion of the tropics in the northern
 157 hemisphere evidenced by a poleward shift of the Hadley Cells, subtropical dry zones and extra-
 158 tropical storm tracks [Allen et al., 2012]. SE Asia is identified as one of the regions of the globe
 159 which has demonstrated the largest rates of increase in black carbon emissions from 1970 to 2009
 160 [Allen et al., 2012] and it is noted that future emissions of anthropogenic aerosols are "directly
 161 addressable by policy actions" [Booth et al., 2012]. However *R Zhang et al.* [2013b] investigated the
 162 claims in [Booth et al., 2012] and concluded that "key aspects of the HadGEM2-ES simulation
 163 exhibit substantial discrepancies with observations." Whilst noting that "Anthropogenic and natural
 164 aerosols have likely played some role in forcing the observed Atlantic multidecadal variability."

165 [Ott *et al.*, 2010] investigated the extreme biomass burning episode in the SEAP Area in 2006
166 and found that “temperatures over Indonesia were strongly modified by increased diabatic heating
167 during the period of burning. The largest increases were found in October and November between
168 150 and 400 hPa. In some regions, increases exceeded 0.7 K during SON.” and that It is necessary
169 for GCMs to include realistic representations of aerosols which fully represent the interannual
170 variability of biomass burning emissions in order to capture the effects discussed in the paper.

171 The carbonaceous aerosol emission inventories for the Coupled Model Intercomparison
172 Project phase 5 (CMIP5) are based on *Lamarque et al.* [2010] and are decadal averages designed to
173 investigate long term (decadal to century) climate change and *Lamarque et al.* [2010] specifically
174 state the emission inventories for CMIP5 are not designed to investigate “rapid” (i.e. less than a few
175 years) pollution changes which this paper addresses. The base year for the CMIP5 Representative
176 Concentration Pathways (RCP)’s is 2005 which was a low emission year in the SEAP Area and
177 contrasts starkly with 2006, a very high emission year, the effects of which would not be captured in
178 the CMIP5 analysis.

179 Finally [*K.A. Potts*, 2018] and [*K.A. Potts*, 2017] reported results that showed that drought
180 and local MSLP in SEAus are forced by the SEAP.

181 In summary then the literature states aerosols affect:

- 182 1. The hydrologic cycle;
- 183 2. The large-scale atmospheric circulation systems; and
- 184 3. are not well understood;

185 and that carbonaceous aerosols:

- 186 1. Are an essential parameter in climate models to correctly model observed changes in
187 precipitation;
- 188 2. Were omitted from most studies used in the IPCC AR4;
- 189 3. Have recently been linked to significant climate events; and
- 190 4. Are only included in the CMIP 5 RCP’s as decadal averages which cannot model the effects
191 this paper addresses.

1.4 The Anthropogenic South East Asian Aerosol Plume

192 The major anthropogenic aerosol plume in the Australian region occurs over SE Asia and is
193 referred to as the South East Asian aerosol Plume (SEAP).

194 The SEAP is one of eight great aerosol plumes which occur annually. It can be identified on
195 the monthly mean 0.55 micron AOD data from MODIS [*Kaufman et al.*, 2000] on the NASA Terra
196 and Aqua satellites distributed via the NASA MODIS Giovanni System (NMGs). *Remer et al.*
197 [2005] confirm that the uncertainty in the AOD measured by these two satellites is “ $\Delta\tau = \pm 0.05$
198 $\pm 0.15\tau$ over land” and that the AOD retrievals can be used in monitoring the aerosol radiative forcing
199 of the global climate. Two areas shown in Figure 4 are used to describe the SEAP: the “SEAP Area”
200 (latitude 10°S to 10°N and longitude 90°E to 160°E); and the Central SEAP (CSEAP) Area (latitude
201 5°S to 5°N and longitude 100°E to 120°E) where the SEAP is most intense. The monthly average
202 AOD of the CSEAP Area is shown in Figure 5 to demonstrate the peak anthropogenic aerosol

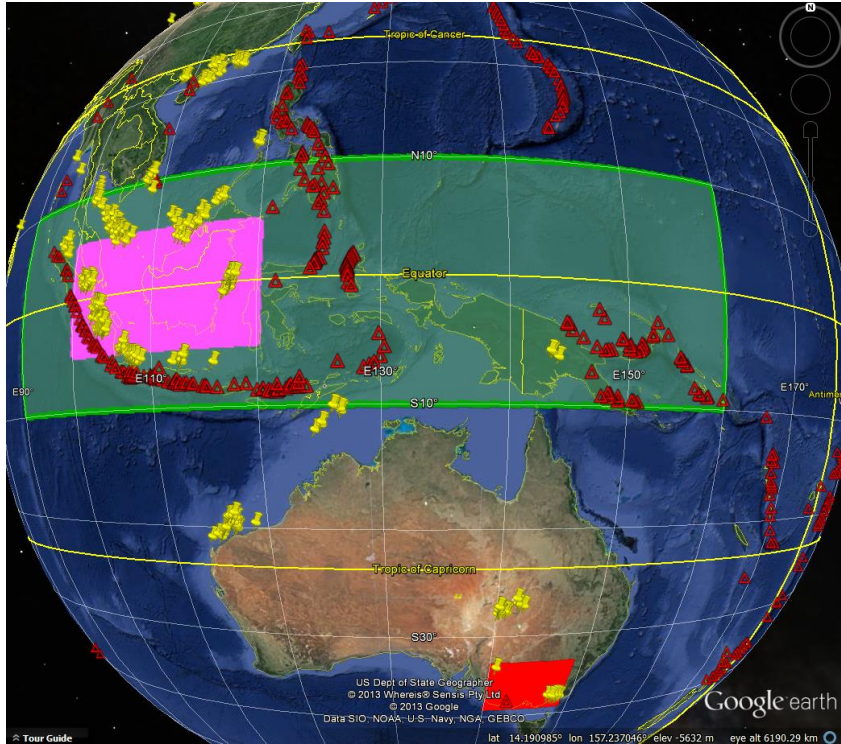
203 emission season is ASON, the end of the dry season in SE Asia, and was extremely high in 2002,
204 2004, 2006, 2009, 2014 and 2015 compared with the intervening years. In this analysis the AOD in
205 the SON season has been used as it matches the seasonal analysis by CAWCR in *Timbal et al.* [2010]
206 although in some years the AOD of the CSEAP Area is greater in August than in November.
207 However, the CSEAP Area AOD in SON correlates with the ASON and ASO AOD at over 0.99 and
208 0.98 respectively. Figure 6 shows the geographic extent of the October 2006 apparition of the SEAP
209 when the drought in SEAus was at its height (This image was included in the inaugural NASA
210 Giovanni Image Hall of Fame in 2013.) This paper therefore focuses on the anthropogenic SEAP in
211 SON because it is at its most intense in this season when it contains a preponderance of carbonaceous
212 aerosols from biomass burning and will therefore have its greatest effect at this time.

213 The average AI from the Total Ozone Mapping Spectrometer (TOMS) on the Nimbus 7 (N7)
214 and Earth Probe (EP) satellite platforms and from the Ozone Monitoring Instrument (OMI) on NASA
215 Aura and the AOD of the CSEAP Area from the Terra Platform from 1979 to 2018 in SON are
216 shown in Figure 7 which exhibits extreme interannual and interdecadal variation. The maximum
217 AOD and AI for the CSEAP Area was 1.60 (Oct 2015) and 1.811 (Sept 1997) and the AI of the
218 CSEAP Area increased from 0.038 in SON in 1979 to 0.193 in 1992 and to 0.296 in 2000 a 408%
219 and 679% increase respectively in years without extensive biomass burning. From 1979 to 1997, a
220 major biomass burning event year, the increase in AI in September was 3,499%.

1.5 The Natural South East Asian Aerosol Plume

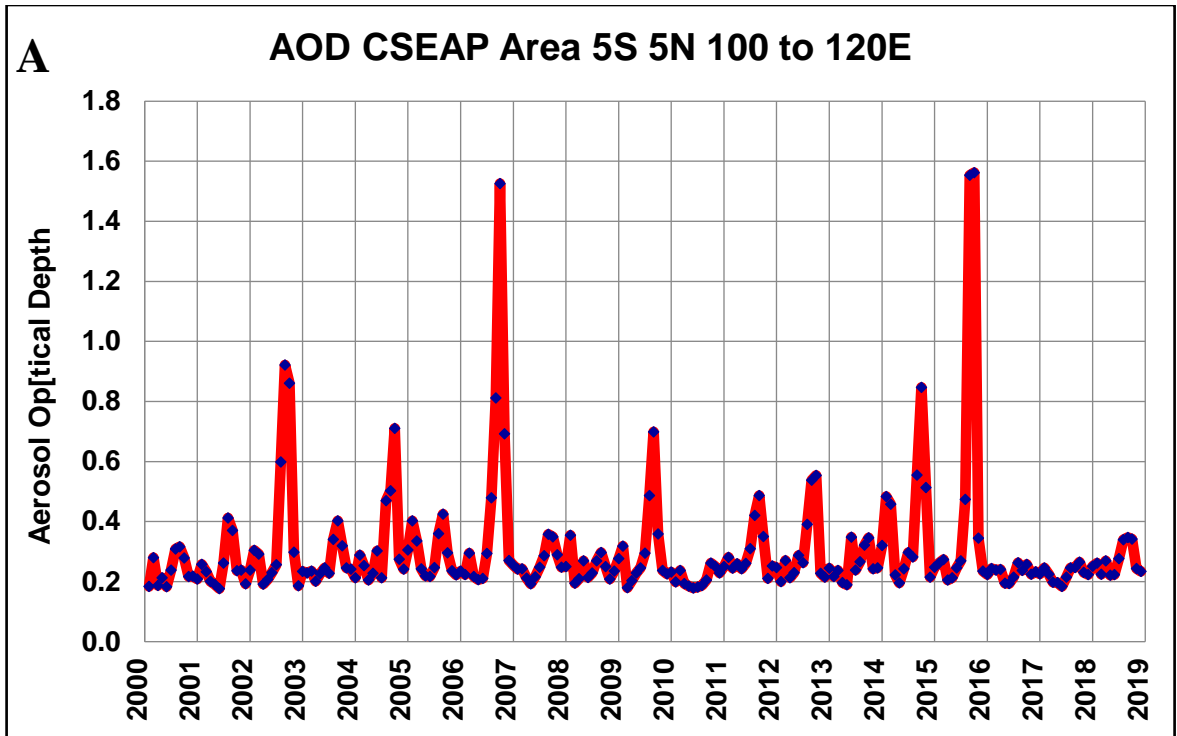
221 Indonesia, in the SEAP Area, is the most “is the most volcanically active nation on Earth”
222 (USGS at <https://www.usgs.gov/center-news/revolutionizing-volcano-monitoring-indonesia>) and the
223 Global Volcanism Program (GVP) database shows the SEAP Area hosts 18% of the total number of
224 volcanic eruptions in the World in about 3% of the global surface. *Simkin and Siebert* [2000] identify
225 16 volcanoes which have been erupting nearly continuously for 30 years and 5 (31%) are in the
226 SEAP Area.

227 Appendix A describes in detail how the three major aerosol sources in the SEAP Area:
228 biomass burning; gas flares; and volcanoes contributed to the extreme increases in the AOD or AI of
229 the SEAP Area in 1997, 2002, 2006, 2014 and 2015 and in the decade 2000 to 2009.

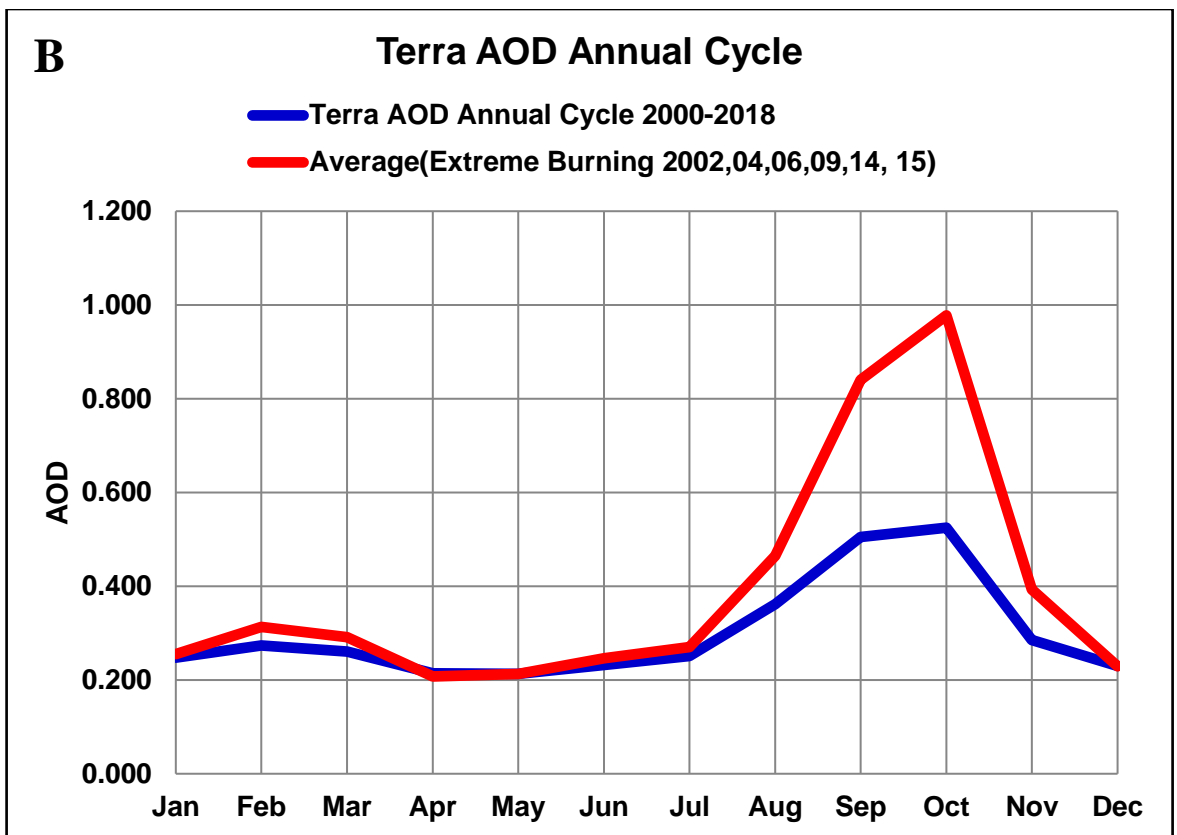


230
231 Figure 4: Google Earth image showing SEAP Area in Green, CSEAP Area in pink and the
232 area used to analyse rainfall in SEAus in red with the locations of gas flares (National Oceanic and
233 Atmospheric Administration (NOAA) and the Global Gas Flaring Reduction Partnership (GGFRP))
234 in yellow and volcanoes (GVP) in red.
235
236

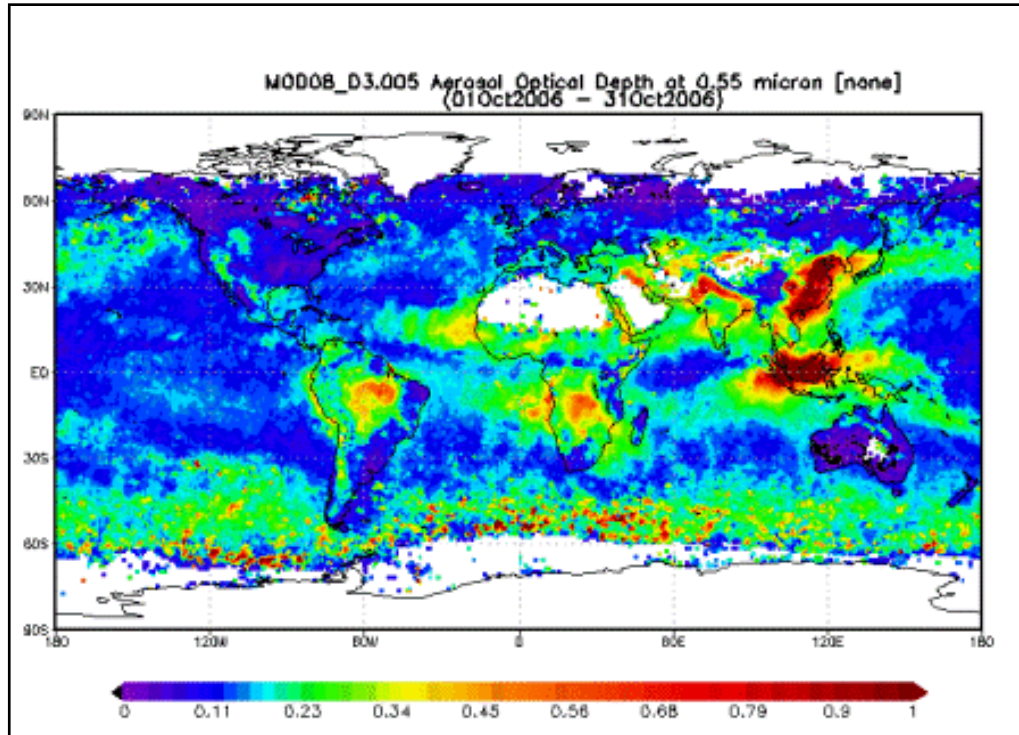
237



238

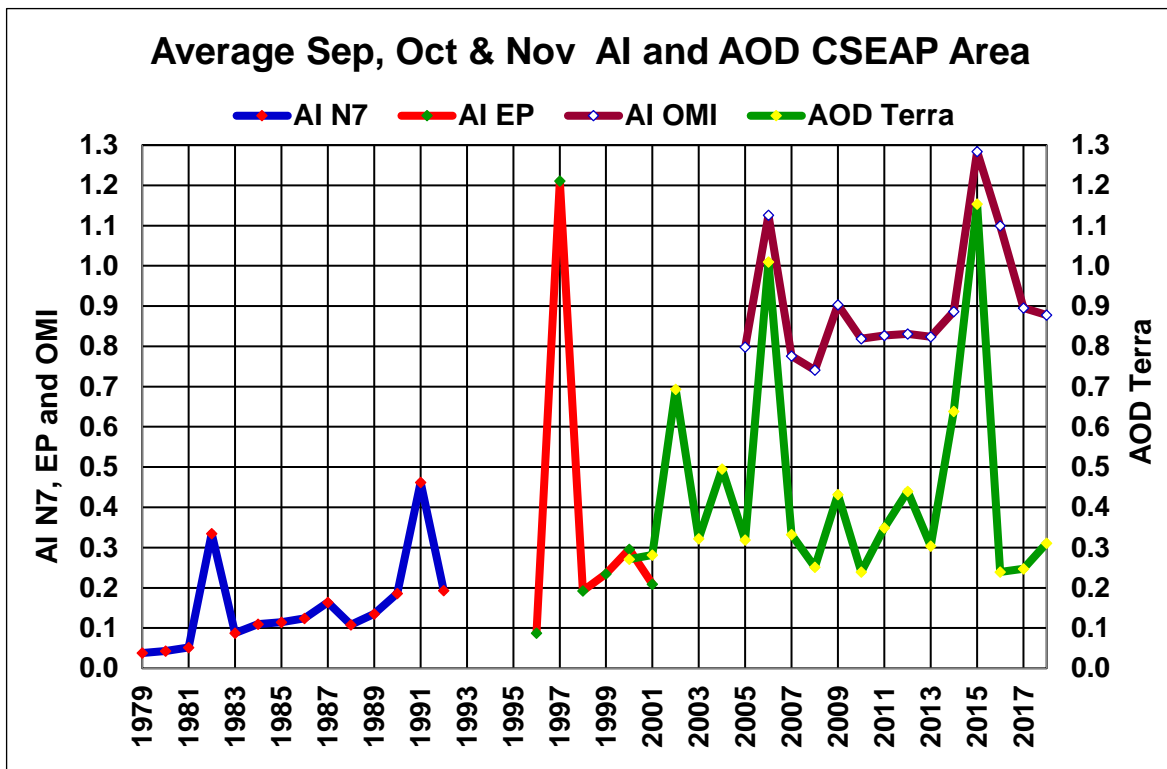


239 Figure 5: Terra AOD CSEAP Area. A: Monthly Average. B: Average annual cycle and cycle during
 240 years of extreme burning in SE Asia.



241
242
243

Figure 6: NASA Terra monthly mean AOD data October 2006.



244
245

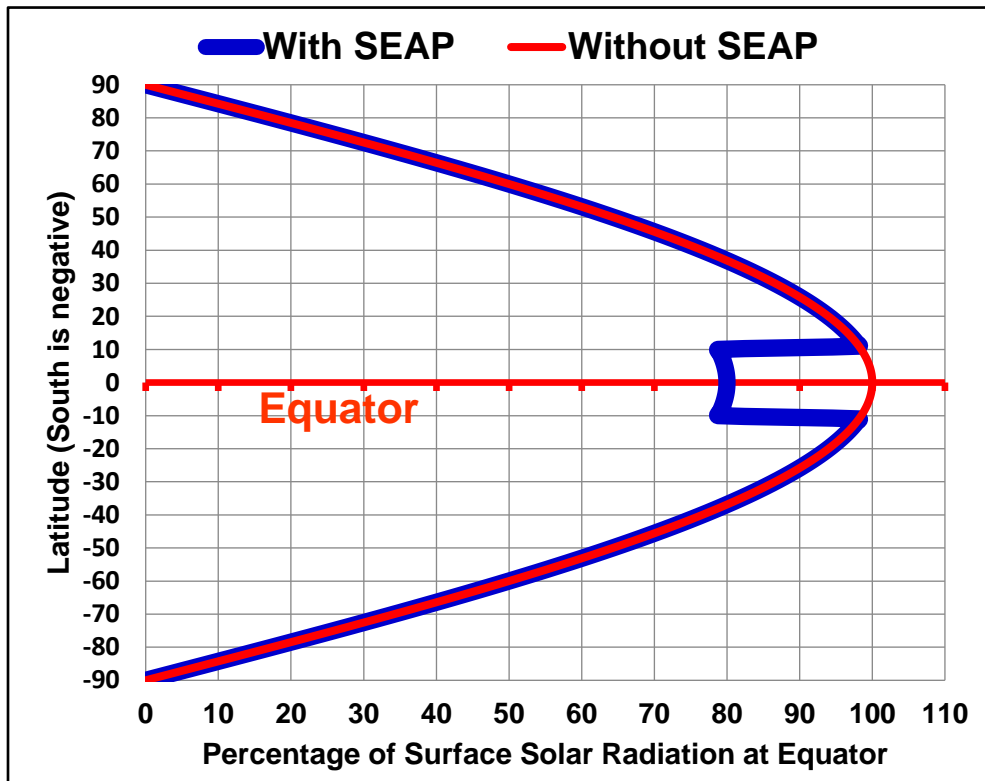
Figure 7: Average SON AI and AOD CSEAP Area.

1.6 Surface Radiative Forcing by the South East Asian Plume

246 The SF of aerosols is significant and the literature includes:

- 247 1. a 10% to 30% reduction of Photosynthetically Active Radiation recorded during
248 INDOEX in the Indian Ocean in 1999 [Ramanathan, 2006];
- 249 2. -150 W m^{-2} in an analysis of the Indonesian wildfires which occurred in 1997 in
250 [Duncan et al., 2003]; and
- 251 3. $\sim -286.0(\text{W/ m}^2)/\tau\alpha$ recorded during the Aerosol Characterization Experiment -Asia in
252 2001 [Hansell et al., 2003] ($\tau\alpha$ is the aerosol optical depth and its derivation is described
253 in the paper).

254 The idealised change in direct surface radiation when the SEAP is present is shown in Figure
255 8 with a plume AOD estimated at 0.52 compared with background 0.3 (Terra data Figure 7) giving a
256 20% reduction in surface radiation noting that 0.52 is much less than the maxima shown in the Terra
257 data in Figure 7. In this figure the sun is assumed to be over the equator and the phase lag between
258 the sun and the position of the ITCZ is ignored. It is clear that the highest level of surface solar
259 radiation is at the edges of the plume and that these regions will drive convection which, in turn,
260 drive the Hadley Cells. With the convective drive of the regional southern Hadley Cell moving south
261 the entire southern regional Hadley Cell moves south which in turn moves the regional sub-tropical
262 ridge south and creates anomalous, persistent high pressure over south eastern Australia as a direct
263 consequence of the SEAP.



264
265 Figure 8: Idealised surface solar radiation with and without the SEAP assuming an increase in
266 AOD from 0.3 to 0.52 which gives a 20% reduction under the SEAP.

267 The term Aerosol Regional Dimming (ARD) describes the surface radiative forcing effect of
268 continental scale aerosol plumes which immediately alters the large-scale atmospheric circulation
269 systems and regional hydrologic cycle and, crucially, only occurs when the plume exists.

1.7 The Connection Between the IOD and ENSO

270 The Australian Bureau of Meteorology (BOM) shows images of the atmospheric circulation
271 during IOD and ENSO events in its website at <http://www.bom.gov.au/climate/iod/> and
272 <http://www.bom.gov.au/climate/about/australian-climate-influences.shtml?bookmark=enso> .

273 From the diagrams of the IOD and ENSO it is clear that the connection between the two
274 effects is the SEAP Area. When the SST in the SEAP Area is warmer and convection occurs there
275 ENSO is in the neutral/La Nina phase and the IOD in the neutral/negative phase whilst when the SST
276 is cooler and convection reverses ENSO is in the El Niño phase and the IOD is in the positive phase.
277 Hence aerosol changes in the SEAP Area which affect convection and the SST can impact both
278 indices simultaneously.

2 METHOD and DATA

2.1 Modelling Data

279 The Last Millennium Ensemble (LME) [Otto-Bliesner *et al.*, 2016] data is available at
280 <https://www.earthsystemgrid.org/> . One member of each of the eight LME forcing simulations with
281 run number in () (850 (3), All (13), Ozone and Aerosol (Aero) (2), Green House Gas (GHG) (3),
282 Land use (Land) (3), Orbital (3), Solar (5) and Volcanic (5)) was used to create time series of 1,156
283 years and 13,872 months of: AOD; surface temperature; precipitation and omega; as well as indices
284 for: the Indian Ocean Dipole (IOD); Nino 3.4 SST and SOI (which the IPCC AR5 shows at Table 1
285 in Box 2.5 are used to monitor the status of ENSO). This LME data was processed as shown in
286 Appendix B and correlated as a time series to demonstrate that these indices and parameters are
287 directly connected to aerosols in the SEAP area.

288 The data was also segmented and averaged on the basis of AOD and then correlated and is
289 also presented graphically to show the effects of changes in AOD without using correlation.

290 Areas used for the LME and LE data were:

- 291 1. Rainfall: 137° 160°E 30° 40°S
- 292 2. Pressure: 130° 145°E 25° 40°S

293 A similar approach was used for:

- 294 1. The Large Ensemble (LE) [Kay *et al.*, 2015] using data from 1850 to 2005 with historic
295 forcings and from 2006 to 2100 using RCP 8.5 projections (run 001) Data as for LME.
- 296 2. The NASA Modern Era Retrospective analysis for Research and Applications release two
297 (MERRA-2) reanalysis dataset [Gelaro *et al.*, 2017] . Data
298 <http://giovanni.gsfc.nasa.gov/giovanni/>

2.2 Satellite Data

299 Figure 5 shows the anthropogenic SEAP is at its height in SON, the end of the dry season in
300 SE Asia, and will therefore have its greatest impact in this season. Aerosol data from four NASA
301 satellites, N7 (AI), EP (AI), Terra (AOD) and OMI (AI) was downloaded from the NASA Giovanni
302 system and correlated on an average SON basis with the following datasets:

- 303 1. **Rainfall:** Data NASA MERRA-2 reanalysis, area 36° to 39°S 140° to 149°E;
- 304 2. **MSLP:** Data NCEP reanalysis [*Kalnay et al.*, 1996]; area 30° to 35°S 140° to 147.4°E
- 305 3. **SEAP Area SST:** to the north and northwest of Australia reported by the BOM to influence
306 the hydrologic cycle over SEAus (ENSO Wrap-Up Sept 2007) at
307 <http://www.bom.gov.au/climate/search/ensowrap-up.shtml?bookmark=no-rm>. Data NCEP
308 reanalysis;
- 309 4. **Omega:** Data from NCEP reanalysis at <http://www.esrl.noaa.gov/psd/data/timeseries/>
- 310 5. **IOD:** Data from NOAA ESRL at
311 https://www.esrl.noaa.gov/psd/gcos_wgsp/Timeseries/Data/dmi.long.data
- 312 6. **ENSO:** ENSO Nino 3.4 index from NOAA at
313 <http://www.cpc.ncep.noaa.gov/data/indices/ersst4.nino.mth.81-10.ascii>
- 314 **SOI:** The Southern Oscillation Index from the BOM at
315 <ftp://ftp.bom.gov.au/anon/home/ncc/www/sco/soi/soiplaintext.html>

316 to demonstrate the connection between the SEAP, SON drought in SE Australia, ENSO and the IOD.
317 As some aerosol datasets exhibit significant trends the data was also detrended using the PAST
318 software version 3.22 [*Hammer et al.*, 2001].

319 Note: AI, unlike AOD, is “only sensitive to desert dust and elevated smoke layers. Therefore,
320 it does not account for aerosols of industrial origin or any kind of aerosol in the lowest 2 km of the
321 atmosphere” (Personal Communication - NASA). However in the SEAP Area it is useful as we are
322 investigating biomass burning “smoke” in SON and the CALIPSO data at
323 https://eosweb.larc.nasa.gov/project/calipso/calipso_table shows smoke at an altitude of 3Km in
324 October 2015, above the lower limit of AI data.

2.3 Global Volcanism Program Data

325 Volcanoes are the major source of natural aerosols in the SEAP Area which existed prior to
326 the anthropogenic SEAP of recent decades as described in Appendix A.

327 The Global Volcanism Program (GVP) database [*Venzke*, 2013] includes the Volcanic
328 Explosivity Index (VEI) for most eruptions. The VEI was converted to tephra using the table in
329 [*Newhall and Self*, 1982] which relates the VEI of an eruption to an estimated volume of Tephra
330 (VEIT), the material explosively ejected into the atmosphere during the eruption. The IPCC AR5
331 [*Stocker et al.*, 2013] shows that tropospheric, tropical/sub-tropical, volcanic aerosols have a
332 residence time of one to three weeks in the atmosphere and *Simkin and Siebert* [2000] state that the
333 median duration of a volcanic eruption is seven weeks which results in a median plume duration of
334 eight to ten weeks. Under the plume the eruption produces “Cooling because reduction of sunlight
335 overwhelms any increased downward energy emitted by volcanic cloud” [*Kirtman et al.*, 2013].

336 *Simkin and Siebert* [2000] state that 16 volcanoes have been erupting nearly continuously for
337 24 years and that 5 of them are in the SEAP Area.

338 Appendix A describes the processing route for the GVP eruption data which is available at
339 http://volcano.si.edu/list_volcano_holocene.cfm. This data was then correlated with:

- 340 **1. Rainfall in the Riverina West Rainfall District:** Data: BOM CD and 2009 -2016 data by
341 personal communication;
- 342 **2. Rainfall in Melbourne, Adelaide and Echuca:** data from BOM;
- 343 **3. The inflows into the River Murray:** Data: Murray Darling Basin Authority (MDBA)
344 (personal communication) 1892 to 2015;
- 345 **4. Convection in the SEAP Area:** Data NCEP reanalysis 1948 to 2016
- 346 **5. Mean SLP in Echuca and Melbourne:** Data BOM Australian Climate data CD

3 RESULTS

347 The climate is highly variable with more than one agent usually contributing to any variation
348 and therefore whilst useful information can be extracted from such data using only time series
349 analysis it is preferable to also analyse the data by segmenting the data on the basis of the forcing
350 agent being investigated, averaging and then correlating as the averaging process improves the signal
351 to noise ratio in the data significantly and the range of the forced parameter from the lowest to the
352 highest forcing segment is a good indicator of the effects of the forcing agent without relying on
353 correlation.

354 Some of the correlations from the LME and LE show significance levels that are much less
355 than 0.01 due to the correlation magnitude and the length of the time series.

356 Note: Colour coding for the correlation significance in all results is Blue < 0.1, Green <0.05,
357 Orange <0.02, Yellow < 0.01.

3.1 Modelling Data

3.1.1 Last Millennium Ensemble

359 Segment analysis results in the extraordinary correlations shown in the last two rows of
360 Figure 9, the majority are 0.97 or greater magnitude. The segments boundaries for all runs except the
361 “All” and “Aero” were set at AODVIS levels of: 0, 0.025, 0.028, 0.032, 0.038, 0.046, 0.055, 0.065
362 and 25 for all the CSEAP Area correlations and 0, 0.043, 0.046, 0.049, 0.053, 0.059, 0.068, 0.078
363 and 25 for the SEAP Area correlations. The AODVIS levels in the SEAP and CSEAP Areas are
364 different with annual averages of 0.100 and 0.077 respectively and hence require different segments
365 for analysis. The “All” and “Aero” runs show very different aerosol levels and therefore very
366 different segments have to be used and, although they show similar levels of correlation with the
367 IOD, and PSL and PRECL in SEAus they were not included in this analysis for simplicity. A graph
368 of annual average SE Australian rainfall (PRECL), SLP (PSL) and AODVIS is at Figure 10 and
369 shows that precipitation falls from an average of 398 to 162 mm/annum from the segment with the
370 lowest AODVIS to the segment with the highest, a fall of 59%.

371 The AODVIS and the IOD graph is at Figure 11 showing an IOD rise from -1.2 to 1.0 from
372 the lowest AODVIS segment to the highest. This compares well with the NOAA IOD data which has
373 a range of -1.2 to 1.5 noting that the highest monthly maximum of the LME AODVIS (Aero (2)) at
374 0.28 is much lower than the Terra AOD at 1.56 with only three years showing maximum monthly
375 AOD in the Terra data less than 0.28. Correcting this bias in the LME data would be expected to
376 increase the maximum of the IOD in the LME data to at least the level in the instrument record.

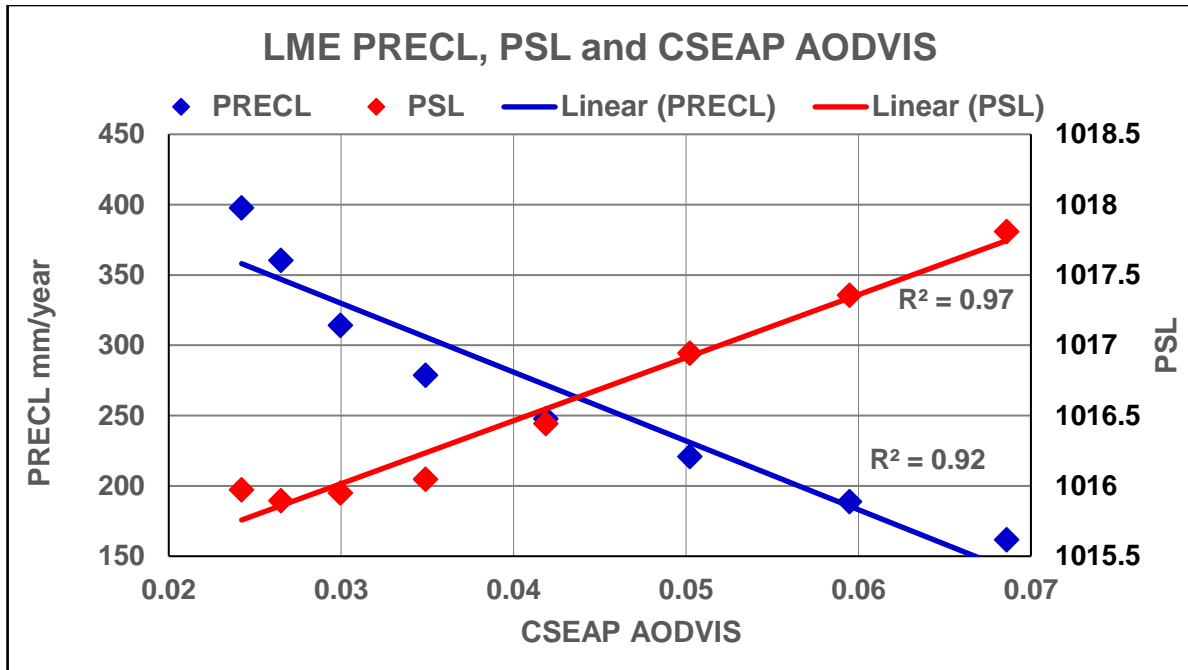
377 Graphs of the Nino 3.4 SST, the SOI and omega in the SEAP Area are in the companion
378 paper [K.A. Potts, 2020b].

379 Note: The volcanic forcing data in the LME cannot of itself demonstrate the connection
380 between the natural volcanic SEAP and rainfall and SLP in SEAus, the IOD and ENSO as it does not
381 have the resolution required to do so. It is derived from ice cores in the Arctic and Antarctic [*Otto-*
382 *Bliesner et al., 2016*] and [*Gao et al., 2008*] who provide the data as only stratospheric sulfate
383 forcing in latitude bands (ten degrees wide), by altitude and month. For volcanic tephra to travel to
384 the polar regions the tephra must be injected into the stratosphere requiring a minimum VEI of 3 to 4.
385 Hence all the VEI 0,1,2 and some (50% assumed) of the VEI 3 eruptions in the SEAP Area must be
386 missing from the dataset. Since this excludes over 94% of the eruptions in the SEAP Area since 1850
387 which are used in this paper the resolution of this LME volcanic forcing dataset is inadequate in itself
388 in terms of eruption size, geospace and aerosol type to prove the causation of the effects of volcanic
389 tephra described in this paper. Although these volcanic forcing runs do provide another independent
390 LME aerosol forcing dataset which is used.

391

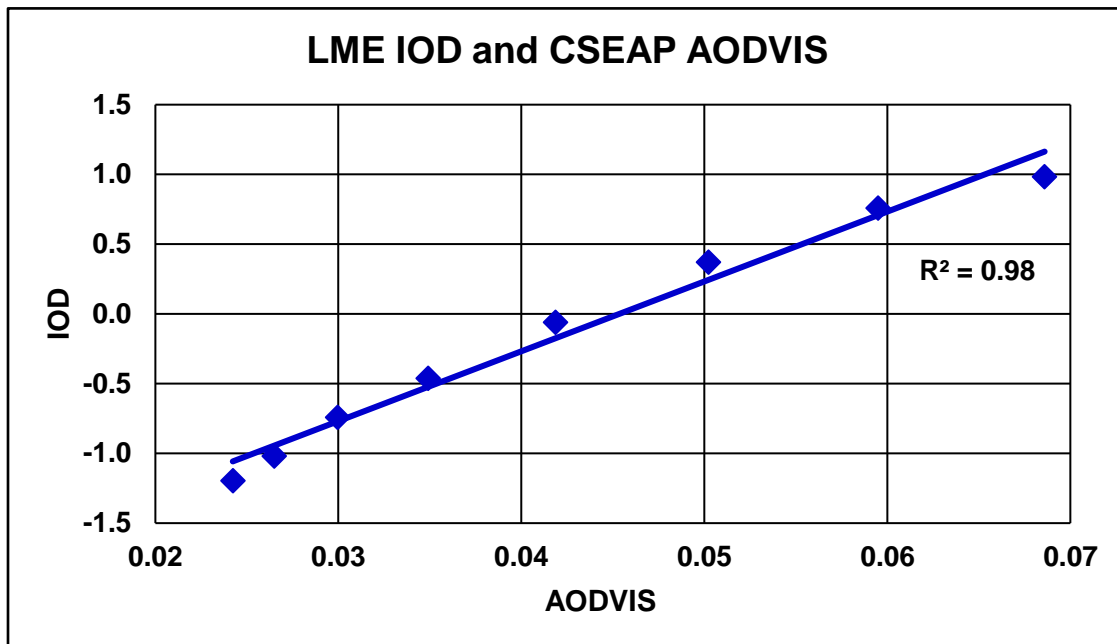
AODVIS	Omega (609mb)	SST Nino 3.4 TS	SOI	IOD	Pressure SEAus	Rainfall SEAus
Monthly (Segmented)						
CSEAP Area	0.95	0.96	-0.97	0.94	0.82	-0.83
SEAP Area	0.76	0.93	-0.98	0.94	0.84	-0.98
September to November Averages						
CSEAP Area	0.82	0.79	-0.79	0.85	0.42	-0.76
SEAP Area	0.87	0.77	-0.78	0.82	0.50	-0.72
April to October Averages						
CSEAP Area	0.80	0.85	-0.89	0.88	0.68	-0.79
SEAP Area	0.81	0.83	-0.80	0.83	0.75	-0.65
Annual Averages						
CSEAP Area	0.79	0.90	-0.86	0.89	0.70	-0.78
SEAP Area	0.83	0.84	-0.79	0.76	0.78	-0.59
Annual Average - Segmented						
CSEAP Area	0.92	1.00	-1.00	0.97	0.97	-0.95
SEAP Area	0.98	0.99	-0.97	0.90	0.99	-0.87

392 Figure 9 LME correlations of AODVIS in the CSEAP and SEAP Areas with the parameters
393 shown.
394



395
396
397
398

Figure 10: Segmented Annual LME AODVIS with SEAus Precipitation and SLP. Averaged using the 850 GHG, Land, Orbital, Solar and Volcanic runs.



399
400
401

Figure 11: Segmented Annual LME AODVIS and the Indian Ocean Dipole. Averaged using the 850, GHG, Land, Orbital Solar and Volcanic runs.

402 3.1.2 Large Ensemble

403 The LE data was analysed in the same way as the LME data for the historic data from 1850 to
 404 2005 and the RCP 8.5 data from 2006 to 2100 separately and the results were then averaged and are
 405 shown in Figure 12.

406

AODVIS	Omega (609mb)	SST Nino 3.4 TS	SOI	IOD	Pressure SEAus	Rainfall SEAus
Monthly (Segmented)						
CSEAP Area	0.96	0.90	-0.86	0.85	0.96	-0.76
SEAP Area	0.83	0.93	-0.95	0.91	0.82	-0.89
September to November Averages						
CSEAP Area	0.90	0.78	-0.73	0.78	0.41	-0.75
SEAP Area	0.85	0.63	-0.72	0.80	0.42	-0.66
April to October Averages						
CSEAP Area	0.91	0.88	-0.84	0.81	0.71	-0.78
SEAP Area	0.83	0.76	-0.76	0.87	0.73	-0.70
Annual Averages						
CSEAP Area	0.92	0.92	-0.82	0.84	0.70	-0.74
SEAP Area	0.91	0.86	-0.77	0.87	0.78	-0.73
Annual Average – Segmented						
CSEAP Area	0.98	0.99	-0.97	0.96	0.97	-0.96
SEAP Area	0.98	0.99	-0.97	0.99	0.98	-0.96

407 Figure 12 LE average correlations of AODVIS in the CSEAP and SEAP Areas with the
 408 parameters shown.

409 3.1.3 MERRA-2

410 The NASA MERRA-2 reanalysis is an atmospheric reanalysis of the modern satellite era
 411 produced by NASA's Global Modelling and Assimilation Office. MERRA-2 is especially useful for
 412 the analysis in this paper as it includes the assimilation of aerosol observations and extended for 39
 413 years in 2019. The aerosol loading in the CSEAP area is highly variable with significant spikes at
 414 near random intervals making it especially useful in correlation analysis. Results from the analysis of
 415 the MERRA-2 data are shown in Figure 13 (right hand column) where all the data is derived from the
 416 MERRA-2 dataset. These results support the LME and LE analysis. The areas used for the MERRA-
 417 2 analysis SLP and rainfall analysis are longitude 140° 149°E and latitude 36° 39°S.

418 Graphs of the MERRA-2 SON AOD, precipitation in SEAus, the IOD and SLP in SEAus are
 419 at Figures 14 and 15 which show a fall in precipitation of 39% from the segment with lowest AOD to
 420 the highest whilst the IOD rises from -0.38 to 0.74 across the same segments.

421

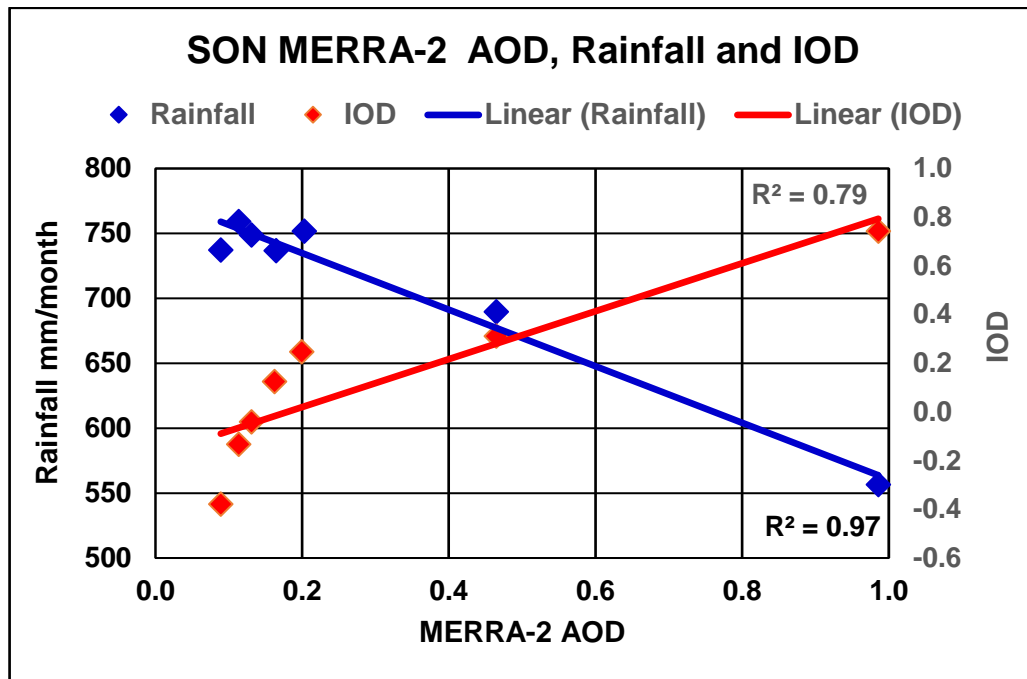
422

A		Sept Oct Nov – Correlations						
		AOD Terra 2000-18	AI Nimbus 7 1979-1992	AI E Probe 1996-2001	AI OMI 2004 - 18	AI N7 + EP 1979...2001	AI N7+EP+OMI 1979...2018	MERRA-2 MERRA-2 1980-2018
1	MERRA Rainfall	-0.66	-0.41	-0.45	-0.23	-0.24	-0.17	-0.52
2	MSL Pressure	0.69	0.26	0.69	0.46	0.49	0.47	0.42
3	SST SEAP Area	-0.66	-0.68	-0.85	-0.20	-0.41	0.11	-0.54
4	CSEAP Omega	0.91	0.57	0.96	0.62	0.56	0.31	0.79
5	IOD	0.57	0.62	0.95	0.30	0.79	0.63	0.62
6	Nino 3.4 SST	0.77	0.56	0.91	0.65	0.61	0.34	0.73
7	SOI	-0.75	-0.64	-0.85	-0.69	-0.45	-0.13	-0.73

B		Sept Oct Nov - Detrended (PAST 3) Correlations						
		AOD Terra 2000-18	AI Nimbus 7 1979-1992	AI E Probe 1996-2001	AI OMI 2004 - 18	AI N7 + EP 1979...2001	AI N7+EP+OMI 1979...2018	MERRA-2 MERRA-2 1980-2018
1	MERRA Rainfall	-0.66	-0.69	-0.46	-0.29	-0.37	-0.39	-0.52
2	MSL Pressure	0.70	0.42	0.67	0.48	0.54	0.51	0.45
3	SST SEAP Area	-0.67	-0.83	-0.83	-0.33	-0.75	-0.65	-0.58
4	CSEAP Omega	0.92	0.79	0.98	0.68	0.74	0.71	0.78
5	IOD	0.58	0.69	0.92	0.25	0.83	0.66	0.67
6	Nino 3.4 SST	0.77	0.67	0.92	0.61	0.73	0.63	0.75
7	SOI	-0.74	-0.76	-0.87	-0.65	-0.65	-0.60	-0.73

423
424 Figure 13: Correlations of time series (A) and detrended (using PAST 3) time series (B) AI and AOD
425 over the CSEAP Area with characteristics of Australian drought, CSEAP Area Omega and the IOD
426 in SON. In the MERRA-2 MERRA-2 column only data from the MERRA-2 reanalysis is used using
427 the same areas as is used in all the other columns.
428

429



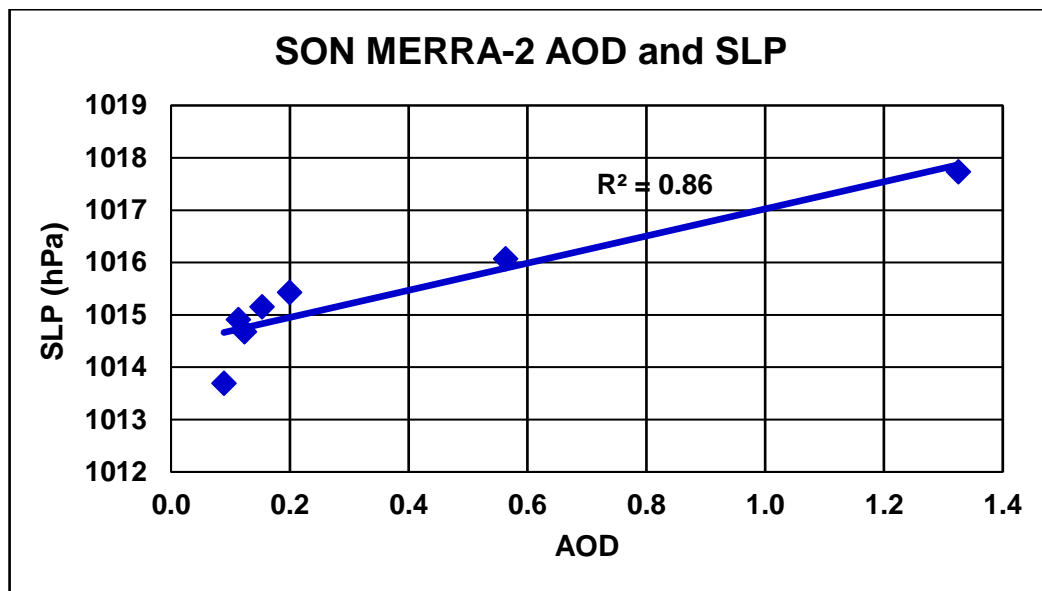
430

431

Figure 14: SON MERRA-2 AOD CSEAP Area, Rainfall SEAus and the IOD segmented and averaged

432

433



434

435

Figure 15: SON MERRA-2 AOD CSEAP Area and SLP segmented and averaged

3.2 Satellite Data

436

437

438

439

As shown in Figure 7 the CSEAP AI data contains a significant trend and therefore the SON AI, AOD and other data was detrended using PAST 3 [Hammer *et al.*, 2001] and then correlated both as a times series and a detrended time series. The results are shown in Figures 13(A) and (B) which show statistically significant correlations with all seven (AOD) and six of seven (N7 AI) detrended

440 parameters respectively. The EP and OMI AI data are shown correlated alone and the EP data with
441 the N7 data and the OMI data with both the N7 and EP data. Due to the short duration of the EP data,
442 the extreme 1997 biomass burning event in Indonesia and the very unusual 1997 biomass burning
443 event in north western Australia the EP data should be interpreted with caution. However, it is
444 considered to support the N7, OMI and AOD correlations. The EP data was detrended with PAST 3
445 by detrending the data without the extreme 1997 data and then reinserting the 1997 data as
446 detrending with the 1997 data introduces a different, significant trend.

447 The lower correlation coefficients for the N7 AI time series data cf. the Terra AOD data are
448 suggested to relate to the much lower AI level in the SEAP Area in the early years of the data when
449 the effects of the plume would have been much smaller and to the effects of the significant trend in
450 the AI data which is demonstrated by the higher correlation coefficients of the detrended data.

451 The OMI AI data shows lower correlation magnitudes than the AOD data with reduced
452 significance caused at least partially by the shorter duration of this data. The detrended OMI AI and
453 Terra AOD data correlate at 0.85 and the significance of the OMI data is therefore expected to
454 increase as its duration increases.

455 The detrended time series of the AI and AOD of the CSEAP Area with SEAus rainfall and
456 pressure are shown in Figures 16 and 17. The AI and AOD are shown on the same scale in these
457 graphs to minimise the number of graphs although the AI and AOD measure different aspects of the
458 aerosol plume.

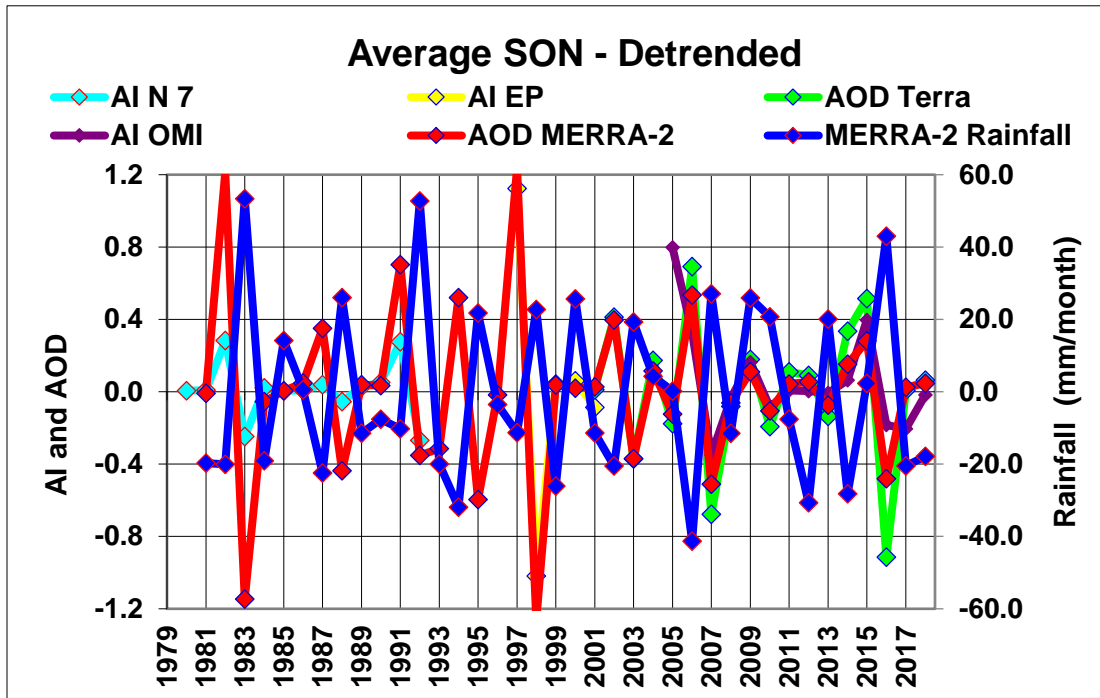
459 Segmenting the Terra AOD and rainfall data in the same way as the MERRA-2 data shows a
460 decline in rainfall in SON of 47% from the segment with the lowest AOD to the highest.

461 Note: The AI derived from OMI is significantly higher than that derived from the N7 and EP
462 satellites at about 0.8 base level compared with 0.2 (EP) and 0.1 (N7). This disparity is not seen in
463 data from the aerosol plumes over the Amazon and West Africa. It may be due to several causes
464 including instrumentation differences, aerosol height, the actual increase in aerosol loading over
465 time, volcanic aerosols in the SEAP which are not present in the other areas and the non-volcanic
466 aerosol types present. The OMI data is therefore useful as an independent dataset and detrended in
467 combination with the detrended N7 and EP data. In Figure 13A the combined N7, EP and OMI data
468 has been retained for completeness but should be viewed with caution due to the discontinuity
469 discussed above.

470

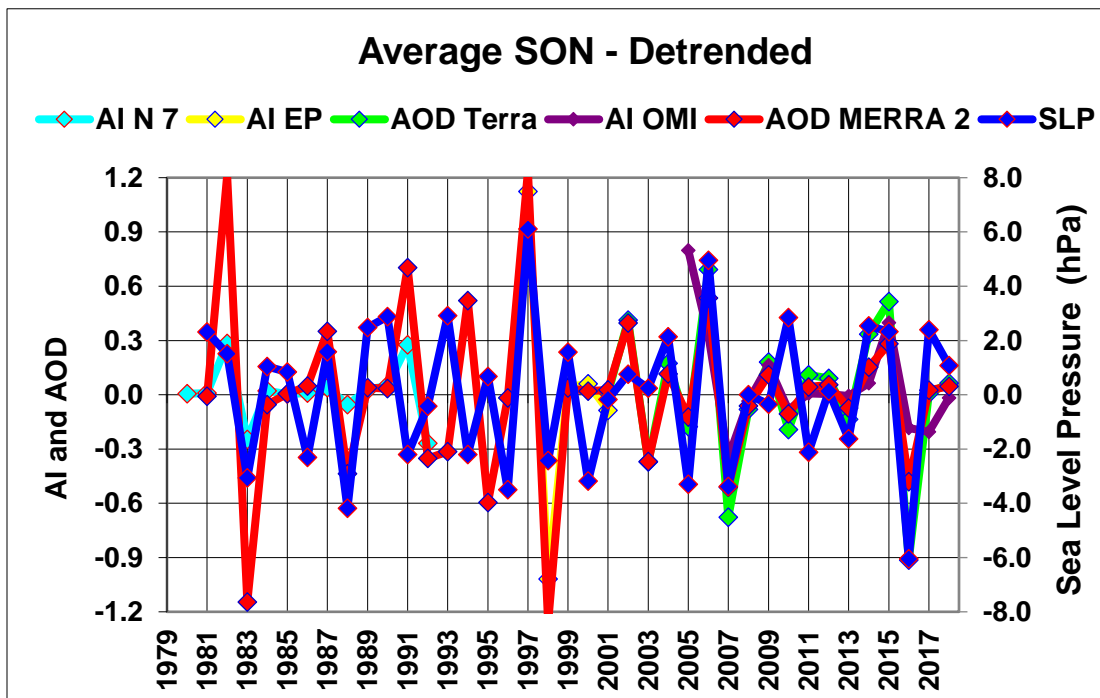
471

472



473
474
475
476
477
478

Figure 16: Average SON AI and AOD CSEAP Area and Rainfall south eastern Australia (from NASA MERRA converted to mm/month.) PAST 3 detrended



479
480
481
482

Figure 17: Average SON AOD and AI CSEAP Area and MERRA-2 SLP south eastern Australia PAST 3 detrended.

3.3 Global Volcanism Program Data

483 The SEAP Area VEIT data was processed into monthly totals as shown in Appendix A, then
484 smoothed with a 12-month running average before segmenting and averaging which is expected to
485 improve the signal to noise level in the data as both the VEI(T) and Murray River data have caveats
486 on accuracy.

487 Figure 18 shows the correlations of the segmented and averaged SEAP Area VEIT with
488 rainfall, pressure, inflows into the River Murray and CSEAP Area omega and demonstrates
489 statistically significant correlations exists. The three locations, Adelaide, Melbourne and Echuca, are
490 spread across the area used in the analysis of the satellite data from north to south and east to west to
491 demonstrate the spread of reduced rainfall across SEAus using measured rainfall data.

492 It is worth noting here that the SEAP Area covers 70° of longitude, 19% of the Earth's
493 circumference, and the effect of volcanic tephra ejected in the eastern part of the SEAP Area on
494 SEAus may be different to volcanic tephra ejected in the central or western part.

495 The plots of the segmented and averaged data are shown in Figure 19 (RWRD rainfall) and
496 Figure 20 (Murray River inflows). It is worth noting that from the lowest VEIT at 0.000167Km³ to
497 the fourth segment with VEIT at 0.0011 Km³ the inflows into the River Murray declined by 15% to
498 820 Gl/month and with VEIT at 0.017, the highest, by 63% to 360 Gl/month.
499

500

Index	Correlation (Monthly)	Period
RWRD Rainfall (BOM)	-0.99	1890 – 2016
Adelaide Rainfall (BOM)	-0.89	1870 - 2018
Melbourne Rainfall (BOM)	-0.91	1890 - 2018
Echuca Rainfall (BOM)	-0.97	1890 - 2018
Murray River Inflow (MDBA)	-0.98	1892 – 2015
SLP Melbourne	0.96	1903 - 2008
SLP Echuca	0.84	1908 - 2008
CSEAP Area Omega (NCEP/NCAR)	0.98	1948 – 2018

501

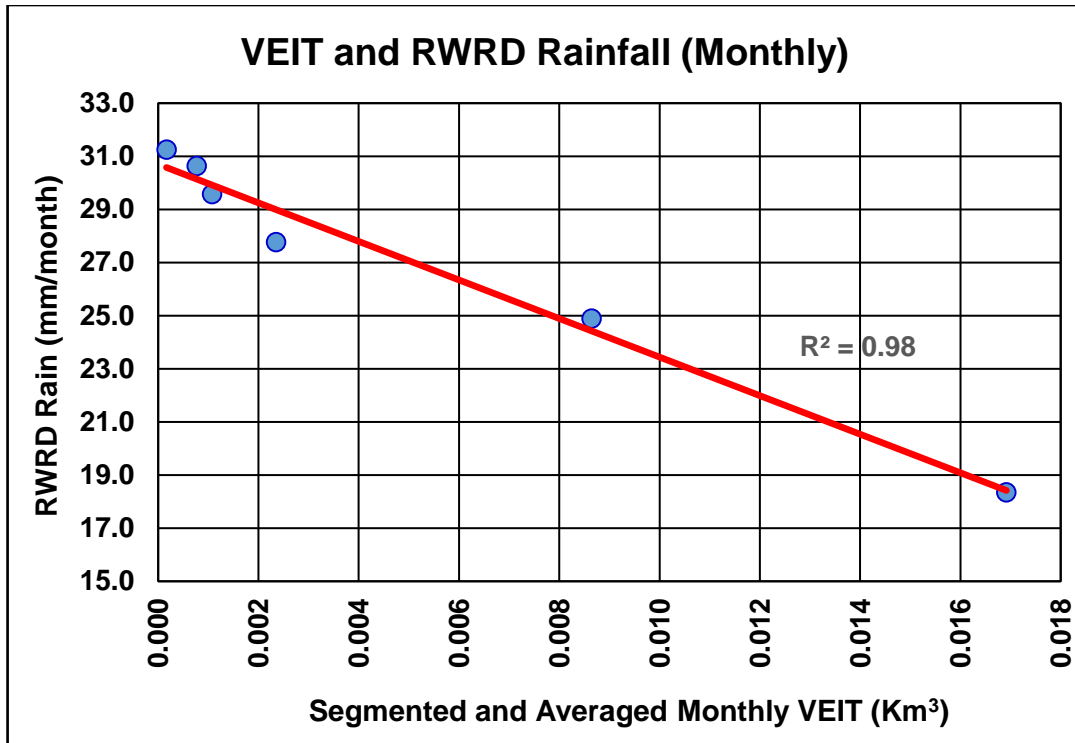
502

503

504

505

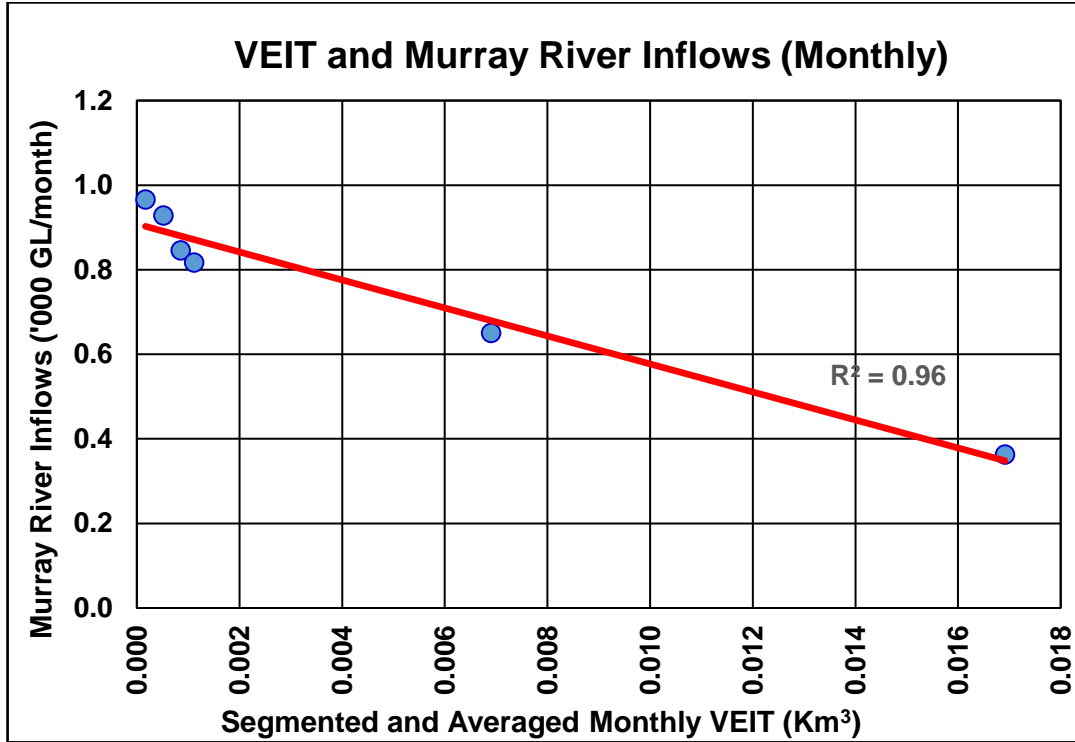
Figure 18: Correlations of segmented and averaged SEAP Area VEIT with parameters shown for the periods shown. All annual data except for SLP which is April to October average.



506

507 Figure 19: Monthly RWRD Rainfall and SEAP Area VEIT 1890 to 2016 data segmented and
508 averaged.

509



510

511 Figure 20: Annual Murray River Inflows and VEIT from the SEAP Area. 1892 to 2015 data
512 segmented and averaged.

3.4 Convection in the CSEAP Area

513 Radical changes in convection occur in the CSEAP Area when the SEAP exists and the
514 detrended AOD and AI of this area was correlated with the detrended NCEP/NCAR reanalysis
515 omega at the 400hPa level in the same area. Omega is a measure of vertical velocity in the
516 atmosphere at specific pressure levels. Positive values indicate falling motion and negative values
517 rising and a reduction in convection produces a positive change in omega. The correlations of the
518 detrended data are shown in Figure 13 (B) (4) at 0.68 or greater magnitude showing that when an
519 aerosol plume is present over the CSEAP area convection decreases. The segmented and averaged
520 VEIT data was also correlated with the CSEAP Area omega. Figure 18 shows the statistically
521 significant correlation. Graphs of the data are in the companion paper [K.A. Potts, 2020b].

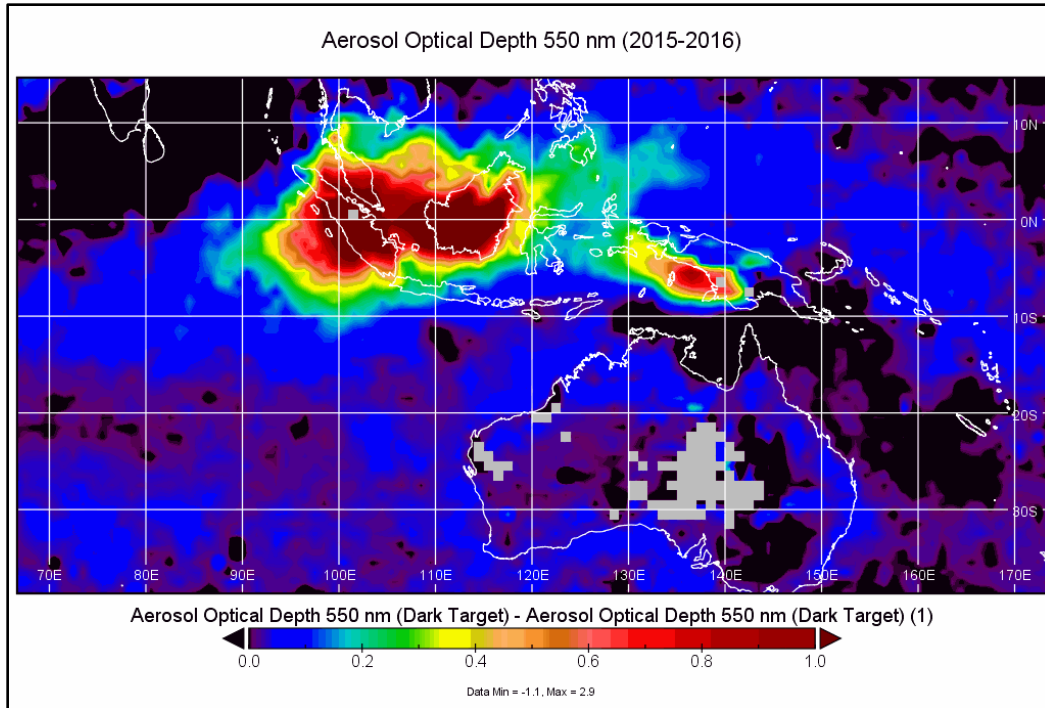
4 MECHANISMS – FOLLOWING THE HYPOTHESIS

522 Timbal et al. [2010] state that “Many of the influences of the climate indices on SEA (South
523 Eastern Australia) come about through modulations of the atmospheric circulation”. This section
524 explains how ARD caused by apparitions of the SEAP drives these modulations of rainfall and SLP
525 in SEAus and the IOD via the effects outlined in the hypothesis and physical model. ENSO is
526 addressed in the companion paper [K.A. Potts, 2020b].

527 The extreme interannual variation in the AOD of the SEAP is used to show the changes
528 wrought by the SEAP using the NCEP/NCAR reanalysis and MERRA-2 data by subtracting the
529 SON data in 2016, low AOD, from 2015, high AOD (as shown in Figures 5 and 7), which shows the
530 effect of the 2015 apparition of the SEAP.

4.1 The SEAP Forms

531 In recent decades the AOD of the SEAP Area has increased as Figures 5 and 7 and Appendix
532 A show due to increases in both the natural and anthropogenic plumes. In SON the anthropogenic
533 SEAP has increased significantly in some years as Figure 7 also shows. Figure 21 shows the extreme
534 change in the SEAP in SON between 2015 to 2016. The actual extent of the 2015 apparition of the
535 SEAP is similar to the 2006 apparition shown in Figure 6.



536

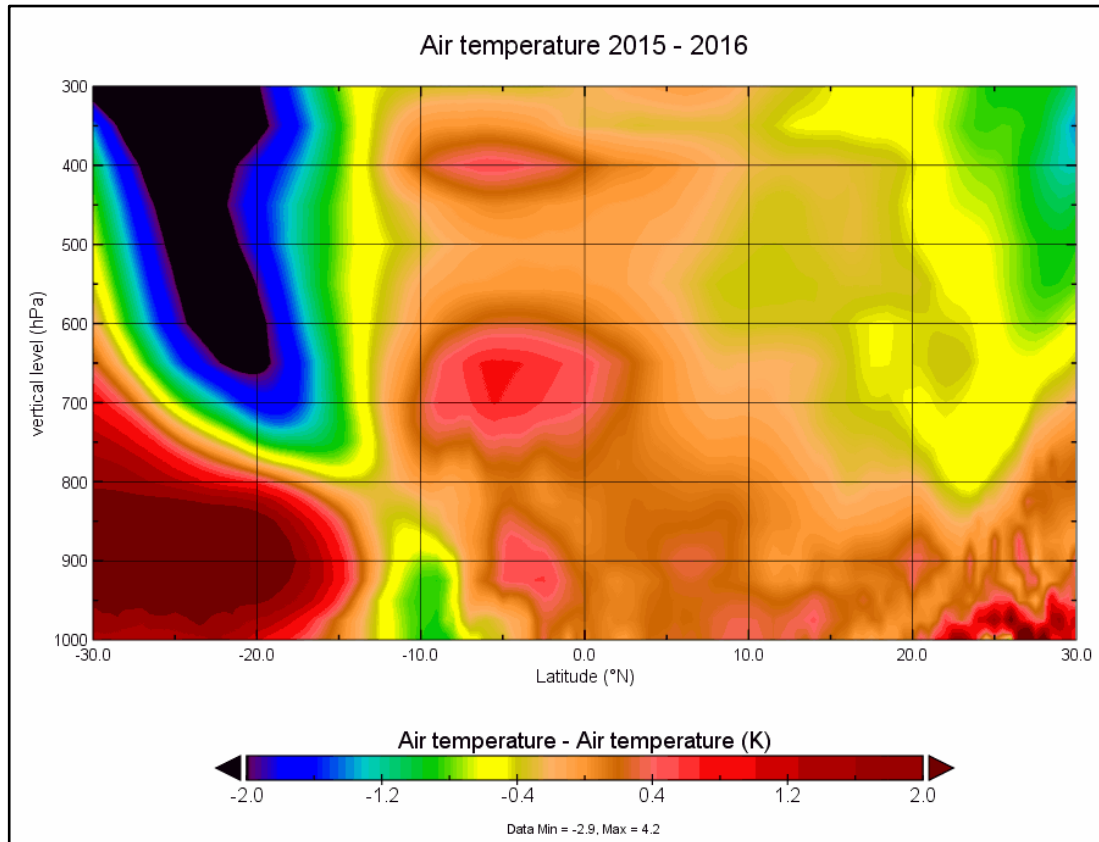
537

538

Figure 21: Terra AOD SON 2015-2016 (NASA Panoply)

4.2 The SEAP absorbs solar radiation and heats the atmosphere

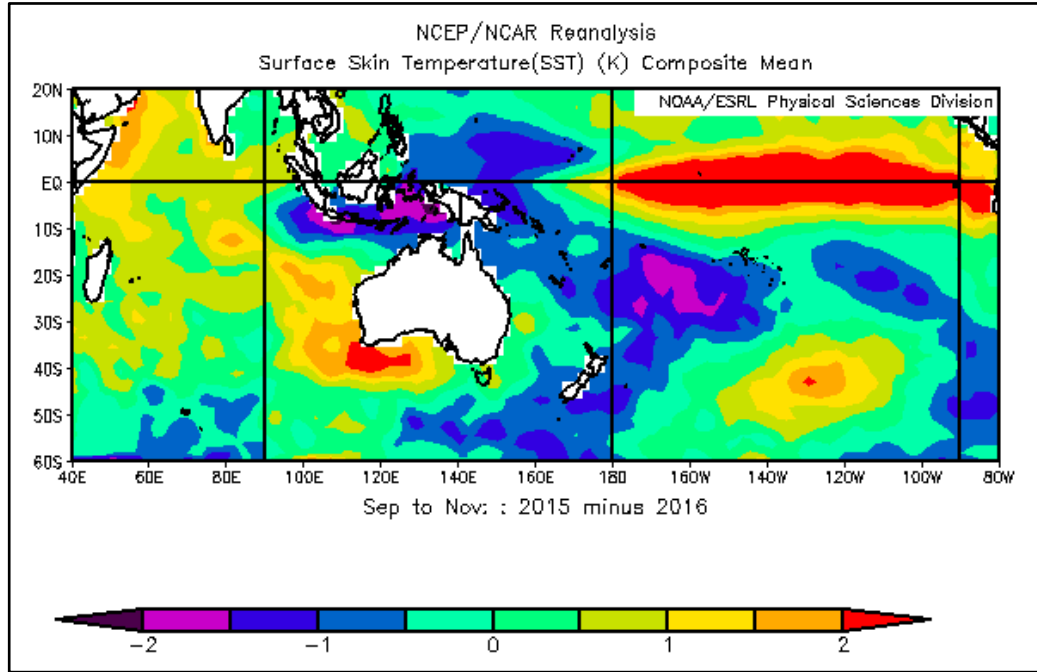
539 Figure 22 shows the MERRA-2 air temperature averaged across the CSEAP Area longitudes
540 from 30°S to 30°N and it can be clearly seen that in the high AOD year the air temperature within the
541 plume at 400hPa and 650hPa is higher which correlates with estimated aerosol height from the
542 Calipso data reasonably well.



543
544 Figure 22: MERRA-2 SON Air Temperature averaged across the CSEAP Longitudes 2015-
545 2016
546

4.3 The SEAP reduces surface solar radiation which cools the surface

547 The NCEP/NCAR reanalysis dataset SON SST in Figure 23 with 2016 subtracted from 2015
548 shows nearly all the SEAP Area sea surface is cooler except the extreme north and west.



549

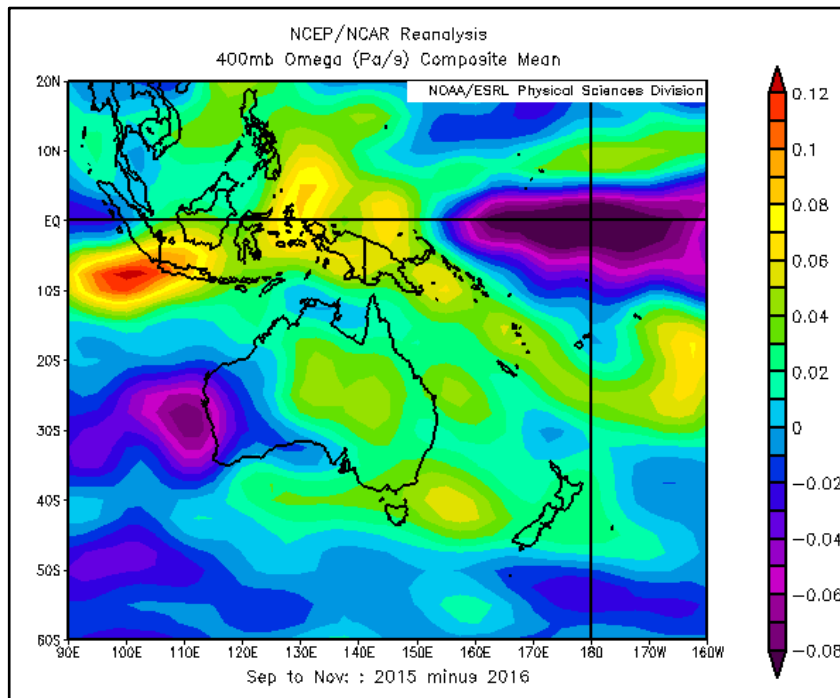
550

Figure 23: NCEP/NCAR SST 2015-2016

551

4.4 Convection in the SEAP Area:

552 The effects of aerosols on convection and atmospheric circulation have been extensively
553 described in the literature as discussed in the introduction. The SEAP absorbs solar radiation which
554 warms the upper atmosphere and reduces solar radiation at the surface which cools the lower
555 atmosphere. This alters the vertical temperature profile of the atmosphere with warmer air above
556 cooler air (relative to the temperatures without the plume) and this stabilises the atmosphere and
557 reduces convection. This well understood process is confirmed in the SEAP Area in this paper with
558 the demonstrated correlation of omega with the AOD, AI and ejected volcanic ash in the area and in
559 Figures 13, 18 and 24 where again nearly all the SEAP Area is affected except the extreme north and
560 west.



561

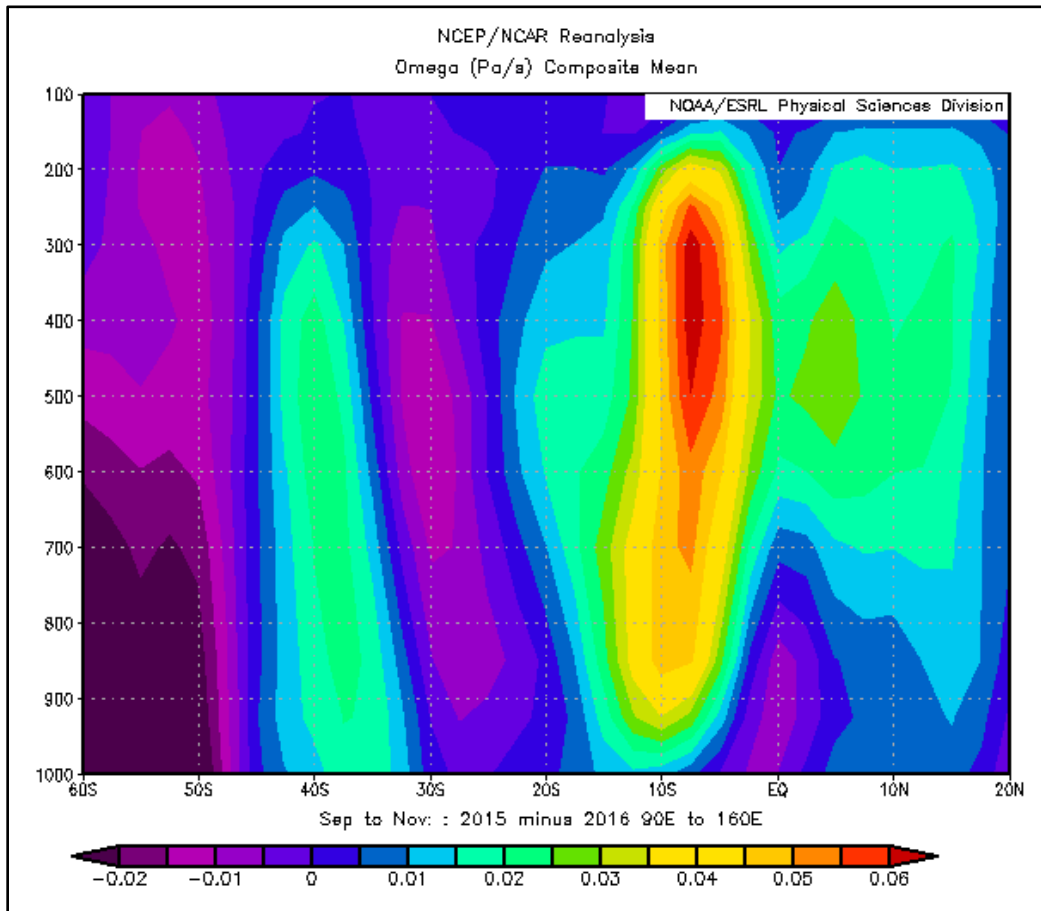
562

Figure 24: NCEP/NCAR convection at the 400 mb level 2015-2016

563

4.5 Hadley Cells:

564 The Hadley Cells are thermally driven [*G R McGregor and Nieuwolf, 1977*], [*Barry and*
 565 *Chorley, 2010*] and [*IPCC, 2007*]. Reduced convection in the SEAP Area alters the regional Hadley
 566 Cells and this can be clearly seen in Figure 25 where the rising limb of the southern Hadley Cell has
 567 been altered in the year of high AI or AOD in the SEAP Area relative to the low AI or AOD years
 568 and the region driving the greatest convection is between 20° and 30° south.



569

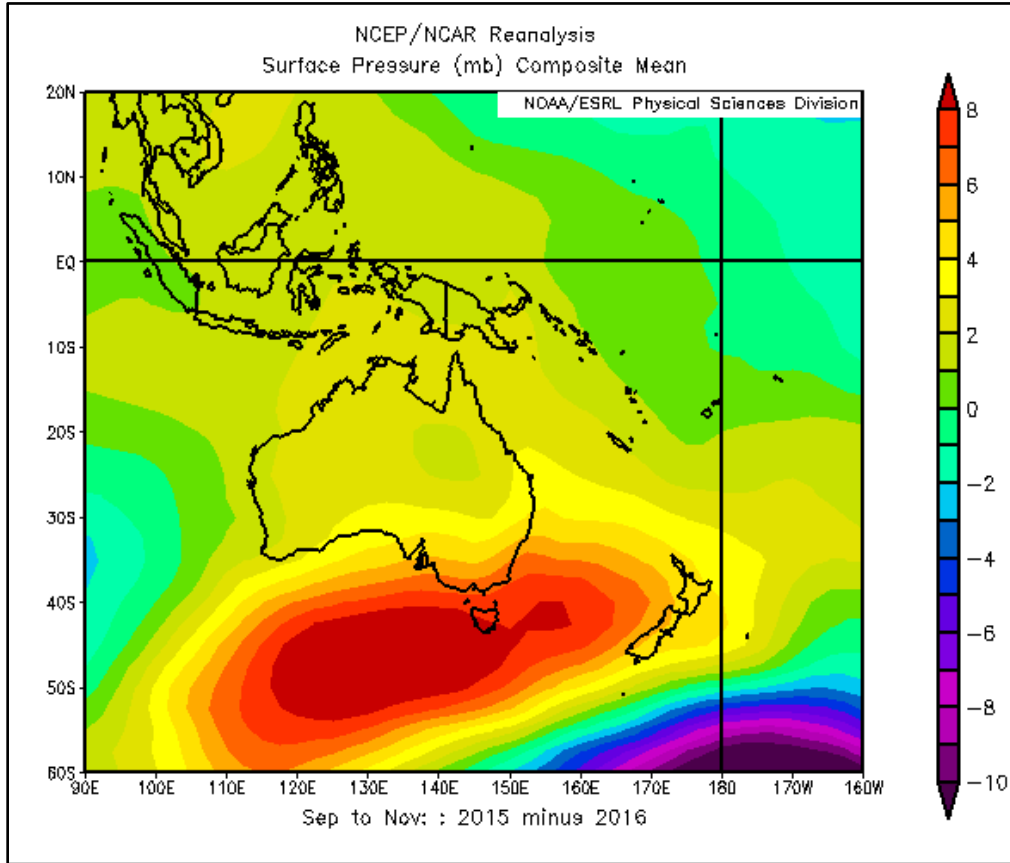
570 Figure 25: NCEP/NCAR omega averaged across the SEAP Area longitudes 2015-2016

571

572

4.6 High Pressure over SE Australia

573 The perturbation of the “Southern Hadley Cell” shown in Figure 25 creates falling motion
574 and therefore anomalous high pressure over SEAus as Figure 26 shows.



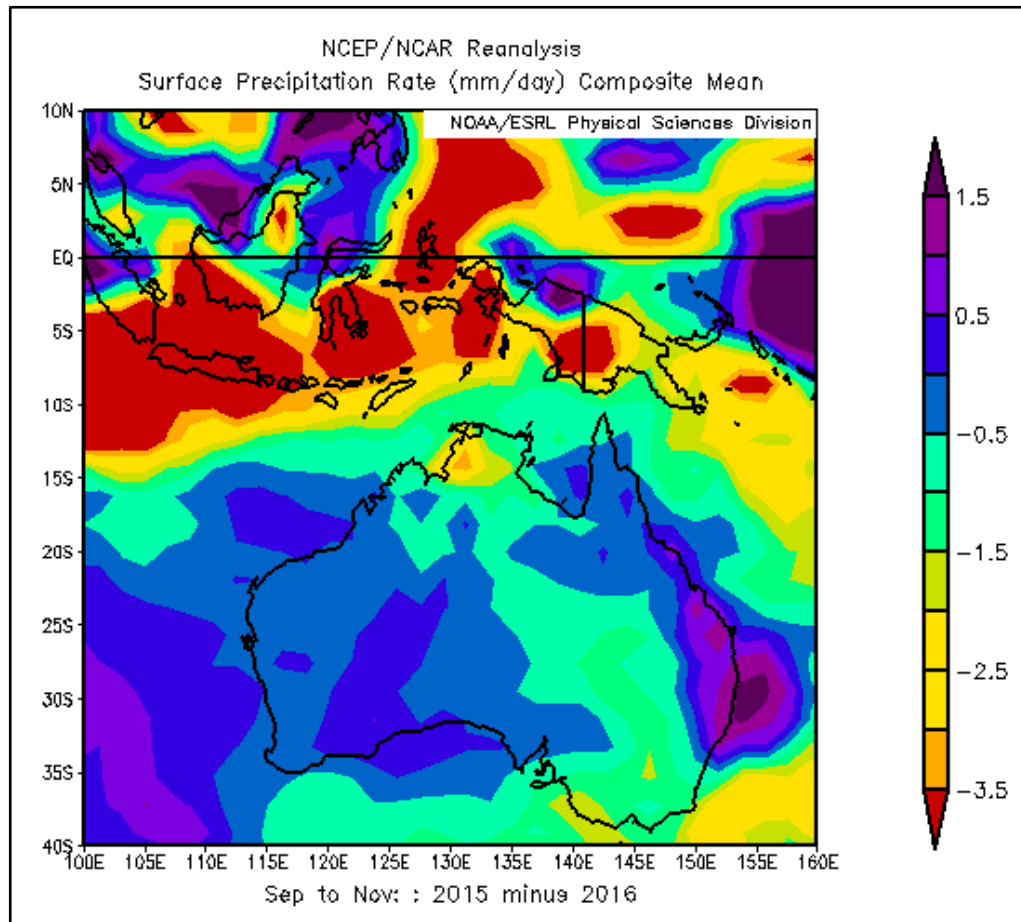
575

576 Figure 26: NCEP/NCAR Surface Pressure 2016 -2015.

577

4.7 Rainfall in SE Australia

578 Rainfall reduces in SEAus when ARD occurs in the SEAP Area because: The SEAP reduces
 579 the SST in the SEAP Area and this reduces evaporation in an area which is a major source of
 580 precipitation for SEAus; and the SEAP also forces the perturbation of the “Southern Hadley Cell”
 581 which creates a persistent high pressure system over SEAus which then forces the low pressure
 582 systems and cold fronts to the south resulting in fewer rain events and, as each rain event deposits
 583 less rain due to the lower humidity, drought ensues as Figure 27 shows. Note the band of reduced
 584 rainfall extends from SEAus to the NNW and points directly at the CSEAP Area, the southern part of
 585 which is also experiencing a significant reduction in rainfall.



586

587

Figure 27: NCEP/NCAR Reanalysis surface precipitation 2015-2016.

588

4.8 The IOD

589 In Figure 23 the SST (2015-2016) is cooler in the eastern IOD Area, as it is shaded by the
590 SEAP, and warmer in the western IOD Area as the surface wind speed reduces which drives the IOD
591 into a positive phase when the AOD in the SEAP Area is high.

5 CAUSATION ANALYSIS

592 It is clearly understood that correlation between events A and B does not prove causation
593 from A to B or vice versa. Thus, the causal relationship between the SEAP and the ENSO must be
594 demonstrated in other ways.

5.1 Volcanic Eruptions

595 Volcanic eruptions are caused by deep earth tectonic processes and cannot be caused by
596 rainfall or SLP thirty degrees of latitude away. Therefore, given the clear correlation between
597 volcanic tephra, rainfall and SLP demonstrated in this paper the causal relationship must be from the
598 volcanic tephra to the rainfall and SLP.

5.2 Analysis without Correlation

599 Figure 10 shows that the LME annual precipitation in SEAus falls from 398mm to 162 mm a
600 fall of 59% from the segment with the lowest AODVIS to the one with the highest and this is
601 comparable to the fall in the measured annual RWRD rainfall in 2006 from 2005 of -56% without
602 using correlation.

5.3 ENSO and the IOD

603 This paper and its companion [K.A. Potts, 2020b] show that the SEAP is simultaneously the
604 cause of drought in SEAus, and the IOD and ENSO events which have historically been cited as the
605 cause of drought in SEAus. The IOD and ENSO are therefore not the drivers of drought in SEAus.

5.4 Modelling

606 **LME:** there is no physical mechanism by which drought or SLP in SEAus can create aerosols
607 in the LME over south east Asia hence the causal direction must run from the aerosols to the rainfall
608 and SLP.

609 In addition, the aerosol forcings in all LME runs are fixed at 1850 values except for the
610 “ozone and aerosol” and “all” runs and there can therefore be no forcing of the aerosols by any agent
611 within these six runs and the causal direction must flow from the aerosols to the rainfall and SLP.

612 **LE:** Aerosols are included as forcing agents in the LE and rainfall and SLP in SEAus cannot
613 therefore affect the aerosols over SEAsia and the causal direction must run from the aerosols to
614 rainfall and SLP.

615 **MERRA-2** reanalysis assimilates measured aerosol data and therefore the causal direction
616 must be from the aerosols to the rainfall and SLP.

5.5 Multiple Independent Datasets

617 Seven of eight LME modelling runs (excluding the aerosol forced run as it correlates with
618 the All forcing run) and the MERRA-2 reanalysis exhibit very low or negative correlations between
619 the CSEAP AODVIS in the individual runs as shown in the correlation matrix in Appendix C with an
620 overall average 0.0016. Hence the datasets are independent. The LE is excluded as it correlates with
621 the LME ALL forcing run.

622 All the datasets show correlations with the rainfall and SLP at significance of <0.01 or less
623 and the chance that all these eight independent datasets show the same result and are wrong is the
624 product of the significance i.e. 0.01^{-8} or 10.0^{-16} , a vanishingly small number.

5.6 Companion Paper

625 The companion paper [K.A. Potts, 2020b] demonstrates that ENSO events which have
626 commonly been linked to drought in south eastern Australia are also caused by the SEAP and this
627 further confirms that the causal relationship flows from the SEAP to all these events.

5.7 Segmented Data

628 The climate is a chaotic system and my preferred way to analyse climate data is to segment,
629 average the data as the averaging process will improve the signal to noise ratio of the analysis. When
630 the LME CSEAP annual AODVIS and rainfall and SLP data in SEAus is segmented on the basis of
631 the AODVIS data and then averaged and correlated R^2 values of 0.92 and 0.97 (Figure 10) are found.
632 This demonstrates clearly that the SEAP is the major and possibly the only driver of reduced rainfall
633 and increased SLP in SEAus.

634 The difference between the lowest LME CSEAP Area AODVIS segment and the highest
635 shows a reduction in annual precipitation in SEAus of 236mm or 59% in Figure 10 with an obvious,
636 well-established trend. Similarly, the same Figure shows an increase in SLP of 1.8 hPa also with a
637 well-established trend. This analysis does not depend on correlation.

5.8 Causal Direction

638 Therefore with:

- 639 1. The volcanic aerosols demonstrating conclusively that SEAP Area aerosols must be the cause
640 of reduced rainfall and increased SLP in SEAus;
- 641 2. The segmented LME data showing a reduction in rainfall in SEAus as the AODVIS level of
642 the SEAP rises without using correlation;
- 643 3. The LME and MERRA-2 time series analysis showing the same results across multiple
644 independent datasets with a vanishingly small chance of error;
- 645 4. The LME data showing, by a preferred analysis method, extremely high correlations of
646 AODVIS, PRECL and PSL ($R^2 = 0.92$ and 0.97) which leave no possibility of other
647 significant drivers;
- 648 5. The demonstration that IOD and ENSO (in the companion paper) events which are commonly
649 cited as the cause of drought in SEAus are also caused by the SEAP;

650 6. The support of four satellite datasets showing the same results;

651 The inevitable conclusion is that the hypothesis is proven and the SEAP is the primary driver
 652 of reduced rainfall and increased SLP in SEAus and may even be the sole driver.

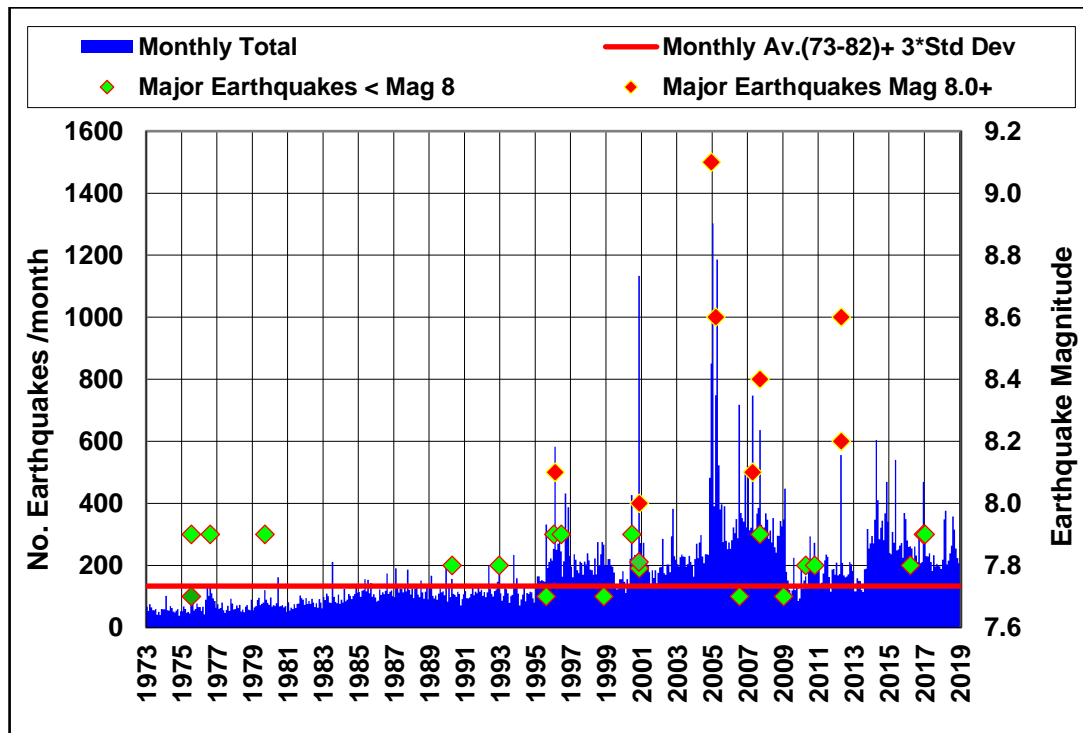
6 THE CAUSE OF THE MILLENNIUM DROUGHT IN SOUTH EASTERN AUSTRALIA

653 This paper shows that volcanic and anthropogenic aerosol plumes in the SEAP Area are the
 654 primary cause of drought in SEAus and this allows the causes of the Millennium Drought to be
 655 determined.

6.1 Changes in the Natural SEAP

656 The level of tectonic activity in the SEAP Area during the Millennium Drought was at an
 657 extremely high level (Figure 28) with five of the twenty largest earthquakes (magnitude 8.4+) in the
 658 world between 1900 and 2015 occurring in the SEAP Area and four of them occurring between 2000
 659 and 2015 (United States Geological Survey (USGS) database). In concert with this increased tectonic
 660 activity the volcanic activity in the SEAP Area also intensified significantly and Figure 29 shows that
 661 in the decade from 2000 to 2009 there were 79 eruptions and 0.50 km³ of tephra ejected against
 662 averages of 40.9 and 0.17 km³ per decade over the twentieth century an approximate doubling and
 663 trebling respectively.

664

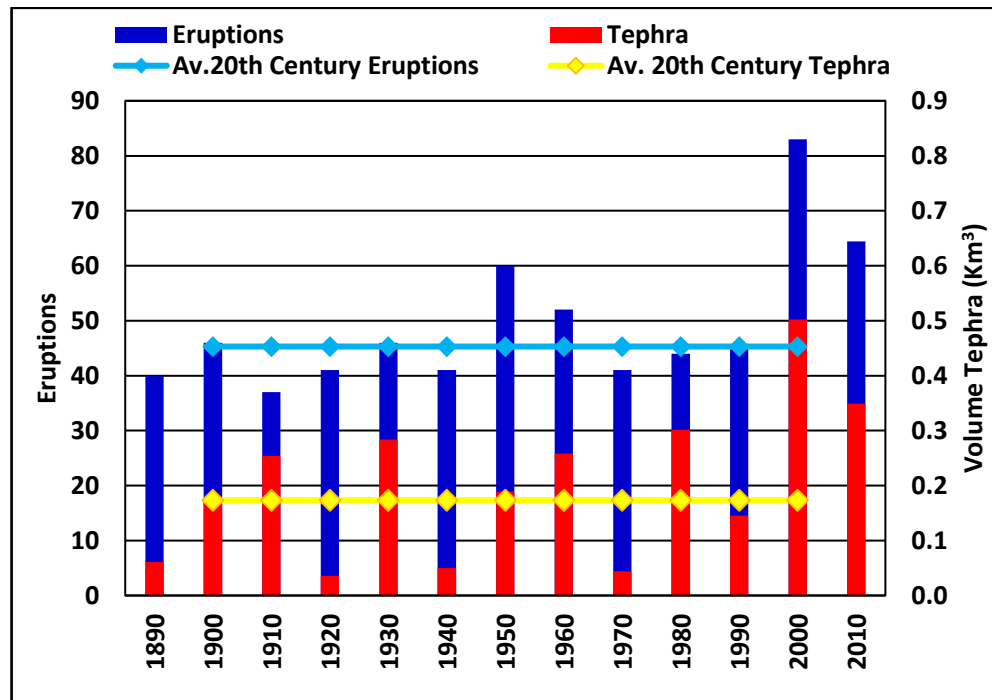


665

666 Figure 28: Total Monthly Earthquakes SEAP Area with major events Magnitude 7.7+ shown.
 667 USGS Earthquake database.

668

669



670

671 Figure 29: Decadal total and average volcanic eruptions and tephra volume in the SEAP Area
 672 from April to October. Averages from 1900 to 1999. The 2010 data has been increased pro rata to
 673 enable comparison with other decades.

6.2 Changes in the Anthropogenic SEAP

674 The background level of AOD in the SEAP Area was significantly higher during the
 675 Millennium Drought having increased by 679% in SON from 1979 to 2000 and it is worth noting
 676 here that this background level has not reduced in the last decade (Figures 5 and 7). There was also a
 677 large increase in the frequency and intensity of rainforest clearing events in the SEAP Area (seen as
 678 the AI and AOD peaks in 1997, 2002, 2004, 2006 and 2009 in Figures 5 and 7) with the associated
 679 increased extent and AOD of the carbonaceous aerosol plume in the SEAP Area in SON.

6.3 The Cause

680 In the segmented model data the correlations of the LME CSEAP AODVIS and precipitation
 681 and SLP data for SEAus in Figure 9 are -0.95 and 0.97 respectively (LE correlations -0.96 and 0.97)
 682 which give $r^2 = 0.90$ and 0.94 and conclusively shows that the SEAP is the prime cause of drought in
 683 SEAus.

684 During the Millennium Drought I have shown there was a significant increase in volcanic
 685 activity, background AOD levels and rainforest clearing in the SEAP Area which drove the AOD of
 686 the SEAP Area higher and which:

- 687 1. Cooled the sea surface under the plume resulting in lower evaporation in the region
 688 where the water which falls as rain in SEAus evaporates;

- 689 2. Perturbed the southern, regional Hadley Cell resulting in anomalous high pressure
690 over SEAus; which
- 691 3. Forced cold fronts, which normally cross SEAus, to the south and away from the
692 continent.

693 Therefore, large increase in the natural and anthropogenic SEAP during the years of the
694 Millennium Drought was the cause of the Millennium Drought in SEAus.

7 FUTURE RESEARCH

695 To finally confirm the findings above I suggest that a further LME analysis is undertaken in
696 which an aerosol plume is created in the model which ramps up from the naturally low level in
697 January to reach the same AOD as the extreme SEAP of October 2006 or 2015 in February,
698 continues at the same level to October and ramps down in November to the naturally low level in
699 December. This plume to be applied in the model with random returns from 2 to 10 years to mimic
700 the actual known return frequency of ENSO events with all other forcing agents held constant.

701 This modelling should be repeated with AOD levels reduced by perhaps 0.1 between runs to
702 determine the level of AOD in the SEAP Area which is required to create the effects outlined in this
703 paper.

704 This will confirm the analysis in this paper and conclusively demonstrate that reduced rainfall
705 and increased SLP in SEAus and IOD and ENSO events are caused by the SEAP.

706 8 CONCLUSIONS

707 The LME with 1.156 annual and 13,872 monthly time series data points, the LE including the
708 RCP 8.5 forcing to 2100, MERRA-2, measured aerosol datasets from four satellites and the GVP
709 volcanic eruption data all confirm the direct connection between the SEAP and drought in SEAus in
710 multiple independent ways and my analysis clearly shows that the relationship must be causal.

711 I therefore conclude that Aerosol Regional Dimming by apparitions of the SEAP is the prime
712 trigger for and sustaining influence on drought in SEAus, ENSO and IOD events.

713 Applying this conclusion to the Millennium Drought, it is obvious that this unprecedented
714 drought was caused by:

- 715 1. The increased level of tectonic activity, earthquakes and volcanic eruptions which led to a
716 tripling of the volcanic tephra ejected in the SEAP Area;
- 717 2. The increase in background AOD in the SEAP Area; and
- 718 3. The increase in the intensity and frequency of the anthropogenic SEAP in SON

719 These conclusions demonstrate the importance of accurately modelling in climate analysis:

- 720 1. The natural volcanic tephra plumes from both small and large volcanic eruptions;
- 721 2. The other seven continental scale, anthropogenic, carbonaceous, aerosol plumes in
722 Africa the Americas, the Middle East and Asia;

723 at adequate spatial and temporal resolutions.

724 Finally I concur with *Booth et al.* [2012] that emissions of carbonaceous aerosols are directly
725 addressable by government policy actions and suggest that this is an urgent necessity to avoid future
726 anthropogenic droughts in the Austral spring in south eastern Australia.

727 **9 APPENDICES**

9.1 Appendix A: The Three Major Sources of the SEAP and the Volcanic Data Processing Route

9.2 Appendix B: The LME and LE Processing Route

9.3 Appendix C: LME and MERRA-2 Aerosol Correlation Matrix

728 The appendices are included in the companion paper [K.A. Potts, 2020b].

729 **ACKNOWLEDGEMENTS**

730 I acknowledge:

731 NASA: Analyses and visualizations used in this paper were produced with the Giovanni
732 online data system, developed and maintained by the NASA GES DISC; the mission scientists and
733 Principal Investigators who provided the data used in this paper including the CALIPSO data; and Dr
734 Robert Schmunk for the Panoply data viewer;

735 The CESM1(CAM5) Last Millennium Ensemble Community Project and supercomputing
736 resources provided by NSF/CISL/Yellowstone;

737 The CESM Large Ensemble Community Project and supercomputing resources provided by
738 NSF/CISL/Yellowstone;

739 Google EarthTM and the copyright holders noted on the image for the image of the Earth;

740 The Murray Darling Basin Authority, Australia for the Murray River inflow data;

741 The Climate and Global Dynamics Division of ESSL at NCAR for the SEAP SST and
742 Omega data;

743 NOAA: Data and images provided by the NOAA/OAR/ESRL PSD, Boulder, Colorado, USA,
744 from their Web site at <http://www.esrl.noaa.gov/psd/> and the IOD at
745 https://www.esrl.noaa.gov/psd/gcos_wgsp/Timeseries/DMI/

746 The United Nations Department of Economic and Social Affairs Population Division for the
747 world population statistics;

748 The Australian Bureau of Meteorology for the Australian climate information and data at
749 <http://www.bom.gov.au>

750 The U.S. Geological Survey for the earthquake and volcano information at:
751 [https://www.usgs.gov/natural-hazards/earthquake-hazards/science/20-largest-earthquakes-world?qt-](https://www.usgs.gov/natural-hazards/earthquake-hazards/science/20-largest-earthquakes-world?qt-science_center_objects=0#qt-science_center_objects)
752 [science_center_objects=0#qt-science_center_objects](https://www.usgs.gov/natural-hazards/earthquake-hazards/science/20-largest-earthquakes-world?qt-science_center_objects=0#qt-science_center_objects)

753 BP for the oil production statistics at [https://www.bp.com/en/global/corporate/energy-](https://www.bp.com/en/global/corporate/energy-economics/statistical-review-of-world-energy.html)
754 [economics/statistical-review-of-world-energy.html](https://www.bp.com/en/global/corporate/energy-economics/statistical-review-of-world-energy.html)

755 The Global Volcanism Program at the Smithsonian Institution for the volcano eruption data.
756 <http://dx.doi.org/10.5479/si.GVP.VOTW4-2013> ;

757 Warwick Goldsworthy and Andrew Metcalfe for discussion and comments;

758 The anonymous reviewers whose comments greatly improved the paper.

759 All data supporting the conclusions is available from the sources shown in the text.

760 This research project was funded personally by the author and his wife Julie.

761 **References**

- 762 Allen, R. J., S. C. Sherwood, J. R. Norris, and C. S. Zender (2012), Recent Northern Hemisphere tropical expansion
763 primarily driven by black carbon and tropospheric ozone, *Nature*, 485(7398), 350-354, doi:10.1038/nature11097.
- 764 Barry, R. G., and R. J. Chorley (2010), *Atmosphere Weather and Climate* Routledge, Abingdon UK.
- 765 Booth, B. B., N. J. Dunstone, P. R. Halloran, T. Andrews, and N. Bellouin (2012), Aerosols implicated as a prime driver
766 of twentieth-century North Atlantic climate variability, *Nature*, 484(7393), 228-232, doi:10.1038/nature10946.
- 767 Duncan, B. N., I. Bey, M. Chin, L. J. Mickley, T. D. Fairlie, R. V. Martin, and H. Matsueda (2003), Indonesian wildfires
768 of 1997: Impact on tropospheric chemistry, *Journal of Geophysical Research: Atmospheres*, 108(D15), 4458,
769 doi:10.1029/2002JD003195.
- 770 Forster, P., et al. (2007), Changes in Atmospheric Constituents and in Radiative Forcing. In: *Climate Change 2007: The*
771 *Physical Science Basis. Contribution of Working Group I to the Fourth Assessment Report of the*
772 *Intergovernmental Panel on Climate Change* [Solomon, S., D. Qin, M. Manning, Z. Chen, M. Marquis, K.B.
773 Averyt, M. Tignor and H.L. Miller (eds.)] Cambridge University Press, Cambridge, United Kingdom and New
774 York, NY, USA.
- 775 Gao, C., A. Robock, and C. Ammann (2008), Volcanic forcing of climate over the past 1500 years: An improved ice
776 core-based index for climate models, *Journal of Geophysical Research: Atmospheres*, 113(D23),
777 doi:10.1029/2008jd010239.
- 778 Gelaro, R., et al. (2017), The Modern-Era Retrospective Analysis for Research and Applications, Version 2 (MERRA-2),
779 *Journal of Climate*, 30(14), 5419-5454, doi:10.1175/jcli-d-16-0758.1.
- 780 Hammer, Ø., D. A. T. Harper, and P. D. Ryan (2001), PAST: Paleontological statistics software package for education
781 and data analysis. , *Palaeontologia Electronica* 4(1): 9pp, 9pp.
- 782 Hansell, R. A., S. C. Tsay, Q. Ji, K. N. Liou, and S. C. Ou (2003), Surface aerosol radiative forcing derived from
783 collocated ground-based radiometric observations during PRIDE, SAFARI, and ACE-Asia, *Appl Opt*, 42(27),
784 5533-5544.
- 785 Hegerl, G. C., F. W. Zwiers, P. Braconnot, N. P. Gillett, Y. Luo, J. A. Marengo Orsini, N. Nicholls, J. E. Penner, and P.
786 A. Stott (2007), Understanding and Attributing Climate Change. In: *Climate Change 2007: The Physical Science*
787 *Basis. Contribution of Working Group I to the Fourth Assessment Report of the Intergovernmental Panel on*
788 *Climate Change* [Solomon, S., D. Qin, M. Manning, Z. Chen, M. Marquis, K.B. Averyt, M. Tignor and H.L.
789 Miller (eds.)]. Cambridge University Press, Cambridge, United Kingdom and New York, NY, USA.
- 790 IPCC (2007), IPCC Assessment Report 4 Glossary.
- 791 Kalnay, E., et al. (1996), The NCEP/NCAR 40-Year Reanalysis Project, *Bulletin of the American Meteorological*
792 *Society*, 77(3), 437-471, doi:10.1175/1520-0477(1996)077<0437:TNYRP>2.0.CO;2.
- 793 Kaufman, Y. J., B. N. Holben, D. Tanré, I. Slutsker, A. Smirnov, and T. F. Eck (2000), Will aerosol measurements from
794 Terra and Aqua Polar Orbiting satellites represent the daily aerosol abundance and properties?, *Geophysical*
795 *Research Letters*, 27(23), 3861-3864, doi:10.1029/2000GL011968.
- 796 Kay, J. E., et al. (2015), The Community Earth System Model (CESM) Large Ensemble Project: A Community Resource
797 for Studying Climate Change in the Presence of Internal Climate Variability, *Bulletin of the American*
798 *Meteorological Society*, 96(8), 1333-1349, doi:10.1175/bams-d-13-00255.1.
- 799 Kirchstetter, T. W. (2004), Evidence that the spectral dependence of light absorption by aerosols is affected by organic
800 carbon, *Journal of Geophysical Research*, 109(D21), doi:10.1029/2004jd004999.
- 801 Kirtman, B., et al. (2013), Near-term Climate Change: Projections and Predictability. In: *Climate Change 2013: The*
802 *Physical Science Basis. Contribution of Working Group I to the Fifth Assessment Report of the Intergovernmental*
803 *Panel on Climate Change* Stocker, T.F., D. Qin, G.-K. Plattner, M. Tignor, S.K. Allen, J. Boschung, A. Nauels, Y.
804 Xia, V. Bex and P.M. Midgley (eds.)]. *Rep.*, IPCC, Cambridge, United Kingdom and New York, NY, USA.
- 805 Lamarque, J. F., et al. (2010), Historical (1850–2000) gridded anthropogenic and biomass burning emissions of reactive
806 gases and aerosols: methodology and application, *Atmospheric Chemistry and Physics*, 10(15), 7017-7039,
807 doi:10.5194/acp-10-7017-2010.
- 808 Levy II, H., D. T. Shindell, A. Gilliland, M. D. Schwarzkopf, and L. W. Horowitz (2008), Executive Summary in
809 *Climate Projections Based on Emissions Scenarios for Long-Lived and Short-Lived Radiatively Active Gases and*
810 *Aerosols*. H. Levy II, D.T. Shindell, A. Gilliland, M.D. Schwarzkopf, L.W. Horowitz, (eds.). A Report by the U.S.
811 *Climate Change Science Program and the Subcommittee on Global Change Research*, Washington, D.C.
- 812 McGregor, G. R., and S. Nieuwof (1977), *Tropical Climatology*, 207 pp., John Wiley and Sons.
- 813 Menon, S., J. Hansen, L. Nazarenko, and Y. Luo (2002), Climate Effects of Black Carbon Aerosols in China and India,
814 *Science*, 297(5590), 2250-2253, doi:10.1126/science.1075159.

- 815 Meyers, G., P. McIntosh, L. Pigot, and M. Pook (2007), The Years of El Niño, La Niña, and Interactions with the
 816 Tropical Indian Ocean, *Journal of Climate*, 20(13), 2872-2880, doi:10.1175/jcli4152.1.
- 817 Murray Darling Basin Authority (2011), Annual Report 2010-11Rep.
- 818 Newhall, C. G., and S. Self (1982), The volcanic explosivity index (VEI) an estimate of explosive magnitude for
 819 historical volcanism, *Journal of Geophysical Research: Oceans*, 87(C2), 1231-1238,
 820 doi:10.1029/JC087iC02p01231.
- 821 Nicholls, N., B. Lavery, C. Frederiksen, W. Drosowsky, and S. Torok (1996), Recent apparent changes in relationships
 822 between the El Niño-Southern Oscillation and Australian rainfall and temperature, *Geophysical Research Letters*,
 823 23(23), 3357-3360, doi:10.1029/96GL03166.
- 824 Novakov, T., V. Ramanathan, J. E. Hansen, T. W. Kirchstetter, M. Sato, J. E. Sinton, and J. A. Sathaye (2003), Large
 825 historical changes of fossil-fuel black carbon aerosols, *Geophysical Research Letters*, 30(6), 1324,
 826 doi:10.1029/2002GL016345.
- 827 Ott, L., B. Duncan, S. Pawson, P. Colarco, M. Chin, C. Randles, T. Diehl, and E. Nielsen (2010), Influence of the 2006
 828 Indonesian biomass burning aerosols on tropical dynamics studied with the GEOS-5 AGCM, *Journal of*
 829 *Geophysical Research: Atmospheres*, 115(D14), D14121, doi:10.1029/2009JD013181.
- 830 Otto-Bliesner, B. L., E. C. Brady, J. Fasullo, A. Jahn, L. Landrum, S. Stevenson, N. Rosenbloom, A. Mai, and G. Strand
 831 (2016), Climate Variability and Change since 850 CE: An Ensemble Approach with the Community Earth System
 832 Model, *Bulletin of the American Meteorological Society*, 97(5), 735-754, doi:10.1175/bams-d-14-00233.1.
- 833 Potts, K. A. (2017), Poster: The South East Asian Aerosol Plume: The Cause of All El Niño Events, in *AGU 2017 Fall*
 834 *Meeting*, edited, Earth and Space Science Open Archive (ESSOAr, New Orleans, USA,
 835 doi:<https://doi.org/10.1002/essoar.10500075.1>.
- 836 Potts, K. A. (2018), Poster: How the Natural & Anthropogenic Aerosol Plume over S. E. Asia caused the Millennium
 837 Drought, in *AMOS-ICSHMO 2018*, edited, Sydney, Australia, doi:<https://doi.org/10.1002/essoar.10500083.1>.
- 838 Potts, K. A. (2020), How Extreme Apparitions of the Volcanic and Anthropogenic South East Asian Aerosol Plume
 839 Trigger and Sustain El Niño Events. First Attribution and Mechanism using data from the Last Millennium
 840 Ensemble, Large Ensemble, MERRA-2 Reanalysis, four Satellites and the Global Volcanism Program.
- 841 Power, S., F. Tseitkin, S. Torok, B. Lavery, R. Dahni, and B. McAvaney (1998), Australian temperature, Australian
 842 rainfall and the Southern Oscillation, 1910-1992: coherent variability and recent changes, *Aust. Met. Mag.*, 47.
- 843 Ramanathan, V. (2006), ATMOSPHERIC BROWN CLOUDS: HEALTH, CLIMATE AND AGRICULTURE
 844 IMPACTS, *Scripta Varia 106*.
- 845 Remer, L. A., et al. (2009), Executive Summary, in *Atmospheric Aerosol Properties and Climate Impacts, A Report by*
 846 *the U.S. Climate Change Science Program and the Subcommittee on Global Change Research [Mian Chin, Ralph*
 847 *A. Kahn, and Stephen E. Schwartz (eds.)]. National Aeronautics and Space Administration, Washington, D.C.,*
 848 *USA.*
- 849 Remer, L. A., et al. (2005), The MODIS Aerosol Algorithm, Products, and Validation, *Journal of the Atmospheric*
 850 *Sciences*, 62(4), 947-973, doi:10.1175/JAS3385.1.
- 851 Rotstajn, L. D., et al. (2007), Have Australian rainfall and cloudiness increased due to the remote effects of Asian
 852 anthropogenic aerosols?, *Journal of Geophysical Research: Atmospheres*, 112(D9), D09202,
 853 doi:10.1029/2006JD007712.
- 854 Rotstajn, L. D., M. A. Collier, M. R. Dix, Y. Feng, H. B. Gordon, S. P. O'Farrell, I. N. Smith, and J. Syktus (2009a),
 855 Improved simulation of Australian climate and ENSO-related rainfall variability in a global climate model with an
 856 interactive aerosol treatment, *International Journal of Climatology*, n/a-n/a, doi:10.1002/joc.1952.
- 857 Rotstajn, L. D., M. D. Keywood, B. W. Forgan, A. J. Gabric, I. E. Galbally, J. L. Gras, A. K. Luvar, G. H. McTainsh, R.
 858 M. Mitchell, and S. A. Young (2009b), Possible impacts of anthropogenic and natural aerosols on Australian
 859 climate: a review, *International Journal of Climatology*, 29(4), 461-479, doi:10.1002/joc.1729.
- 860 Simkin, T., and L. Siebert (2000), Earth's volcanoes and eruptions: an overview p. 249-261. , in *Encyclopedia of*
 861 *Volcanoes*, , edited by S. H. Academic Press, San Diego.
- 862 Solomon, S., et al. (2007), Technical Summary. In: *Climate Change 2007: The Physical Science Basis. Contribution of*
 863 *Working Group I to the Fourth Assessment Report of the Intergovernmental Panel on Climate Change [Solomon,*
 864 *S., D. Qin, M. Manning, Z. Chen, M. Marquis, K.B. Averyt, M. Tignor and H.L. Miller (eds.)]. Cambridge*
 865 *University Press, Cambridge, United Kingdom and New York, NY, USA.*
- 866 Stocker, T. F., et al. (2013), Technical Summary. In: *Climate Change 2013: The Physical Science Basis. Contribution of*
 867 *Working Group I to the Fifth Assessment Report of the Intergovernmental Panel on Climate ChangeRep.,*
 868 *Intergovernmental Panel on Climate Change, Cambridge, United Kingdom and New York, NY, USA.*
- 869 Timbal, B., et al. (2010), Understanding the anthropogenic nature of the observed rainfall decline across south-eastern
 870 Australia, *Centre for Australian Weather and Climate Research, Technical Report 026*.

- 871 Timbal, B., and W. Drosowsky (2013), The relationship between the decline of Southeastern Australian rainfall and the
872 strengthening of the subtropical ridge, *International Journal of Climatology*, 33(4), 1021-1034,
873 doi:10.1002/joc.3492.
- 874 Ummenhofer, C. C., M. H. England, P. C. McIntosh, G. A. Meyers, M. J. Pook, J. S. Risbey, A. S. Gupta, and A. S.
875 Taschetto (2009), What causes southeast Australia's worst droughts?, *Geophysical Research Letters*, 36(4),
876 doi:10.1029/2008gl036801.
- 877 Venzke, E. (2013), Volcanoes of the World v. 4.4.3, edited by S. I. G. V. Program, doi:
878 <http://dx.doi.org/10.5479/si.GVP.VOTW4-2013>.
- 879 Wang, C. (2004), A modeling study on the climate impacts of black carbon aerosols, *Journal of Geophysical Research:*
880 *Atmospheres*, 109(D3), D03106, doi:10.1029/2003JD004084.
- 881 Wang, G., and H. H. Hendon (2007), Sensitivity of Australian Rainfall to Inter–El Niño Variations, *Journal of Climate*,
882 20(16), 4211-4226, doi:10.1175/jcli4228.1.
- 883 Zhang, R., et al. (2013), Have Aerosols Caused the Observed Atlantic Multidecadal Variability?, *Journal of the*
884 *Atmospheric Sciences*, 70(4), 1135-1144, doi:doi:10.1175/JAS-D-12-0331.1.
- 885
- 886

887 **How Extreme Apparitions of the Volcanic and Anthropogenic South East Asian Aerosol**
888 **Plume Trigger and Sustain El Niño Events. First Attribution and Mechanism using data**
889 **from the Last Millennium Ensemble, Large Ensemble, MERRA-2 Reanalysis, four**
890 **Satellites and the Global Volcanism Program.**

891

892

893 **K. A. Potts¹**

894 ¹Kyna Keju Pty Ltd.

895 Corresponding author: Keith Potts (Keith.Potts@bigpond.com)

1. Key Points:

896 • Volcanic aerosol plumes over SE Asia are and always have been the trigger and sustaining
897 force for ENSO events

898 • The anthropogenic aerosol plume has intensified the volcanic plume and ENSO events in
899 recent decades

900 • Analysis of the Last Millennium Ensemble, Large Ensemble, MERRA-2, 4 satellite's and
901 Global Volcanism Program data confirms this

902

2. Abstract

903 Volcanic aerosols over south east Asia have always been the trigger and sustaining cause of ENSO
904 events. In recent decades this natural plume has been augmented by the anthropogenic plume which
905 has intensified ENSO events especially in SON. Data from the Last Millennium Ensemble (13,972
906 months), and Large Ensemble (3,012 months) demonstrate this connection with three ENSO indices
907 and aerosol data derived from the same datasets correlating at 1.00 (LME), 0.97 and 0.99 magnitude
908 (segmented and averaged). ENSO events are the dominant mode of variability in the global climate
909 responsible for Australian, Indian and Indonesian droughts, American floods and increased global
910 temperatures. Understanding the mechanism which enables aerosols over SE Asia and only over SE
911 Asia to create ENSO events is crucial to understanding the global climate. I show that the South East
912 Asian aerosol Plume causes ENSO events by: reflecting/absorbing solar radiation which warms the
913 upper troposphere; and reducing surface radiation which cools the surface under the plume. This
914 inversion reduces convection in the region thereby suppressing the Walker Circulation and the Trade
915 Winds which causes the SST to rise in the central Pacific Ocean and creates convection there. This
916 further weakens/reverses the Walker Circulation driving the climate into an ENSO state which is
917 maintained until the aerosols dissipate and the climate system relaxes into a non-ENSO state.
918 Measured aerosol data from four NASA satellites, estimates of volcanic tephra from the Global
919 Volcanism Program (GVP) for over 100 years and the NASA MERRA-2 reanalysis dataset all
920 confirm this analysis.

921 **1 INTRODUCTION**

922 **1.1 The Hypothesis and Physical Model**

923 This paper explores an explicit physical model and hypothesis to explain how the occurrence
924 of ENSO events is and always has been triggered and sustained by the natural volcanic aerosol plume
925 over south east Asia (SEAsia) which has, in recent decades, been intensified by the anthropogenic
926 aerosol plume especially from September to November (SON).

927 The sequence of events is:

- 928 13. The volcanic tephra aerosol plume forms and, in recent decades, is intensified by the
929 anthropogenic plume which is most intense from September to November (SON);
- 930 14. The aerosols absorb (and reflect) solar radiation which heats the atmosphere;
- 931 15. The aerosols reduce the solar radiation at the surface under the plume which cools the
932 surface;
- 933 16. 2 and 3 create a temperature inversion compared to times without a plume and this
934 reduces convection;
- 935 17. Reducing convection over SEAsia causes the Trade Winds blowing from east to west
936 over the Pacific Ocean to reduce in intensity as there is no exit into the convection and the
937 Hadley and Walker Circulation;
- 938 18. Reducing the Trade Wind speed over the Pacific Ocean cause the sea surface temperature
939 to rise;
- 940 19. The increased temperature in the central Pacific Ocean causes convection in this region
941 and the Walker circulation further relaxes or even reverses;
- 942 20. The SOI is forced into a negative phase by these changes
- 943 21. The western Pacific warm pool then migrates east as the wind stress on the ocean has
944 reduced;
- 945 22. The ENSO event continues until the aerosol plume over SEAsia dissipates which is
946 typically when the SEAsian monsoon starts;
- 947 23. With the revived Trade Wind speed over the Pacific Ocean the warm pool then migrates
948 west again and the ENSO event ends.

949 **1.2 ENSO**

950 El Niño Southern Oscillation Index (SOI) (ENSO) events are defined in the
951 Intergovernmental Panel on Climate Change (IPCC) Assessment Report Four (AR4) Glossary as a
952 coupled atmosphere-ocean phenomenon with a two to seven year time scale during which “the
953 prevailing trade winds weaken, reducing upwelling and altering ocean currents such that the sea
954 surface temperatures warm, further weakening the trade winds. This event has a great impact on the
955 wind, sea surface temperature and precipitation patterns in the tropical Pacific. It has climatic effects
956 throughout the Pacific region and in many other parts of the world, through global teleconnections.”

957 Three national meteorological organisations together with The National Aeronautics and
958 Space Administration (NASA) define ENSO in similar ways on their websites and there is also an
959 extensive body of literature which describes the characteristics of ENSO events including:

- 960 1. “All [El Niño or ENSO] events are preceded by westerly wind anomalies on the equator near
961 the date line.” [Enfield, 1989];
- 962 2. “El Niño (EN) is characterized by a large-scale weakening of the trade winds and warming of
963 the surface layers in the eastern and central equatorial Pacific Ocean.” McPhaden et al. [1998]
964 in a review of the history of El Niño events;
- 965 3. “The onset of an El Niño is characterized by a decrease in wind power that leads to a decrease
966 in available potential energy, and hence a flatter thermocline.” [Brown and Fedorov, 2010];
- 967 4. “the principal factor that affected model ENSO behavior is the change in the basic-state
968 equatorial winds and associated equatorial upwelling.” [B. Wang and An, 2002];
- 969 5. “Our model experiments reproduce the empirical observations of a short-term ENSO response
970 to explosive tropical eruptions” [Mann et al., 2005]
- 971 6. “The El Niño–Southern Oscillation (ENSO) cycle of alternating warm El Niño and cold La
972 Niña events is the dominant year-to-year climate signal on Earth. ENSO, originates in the
973 tropical Pacific through interactions between the ocean and the atmosphere” [McPhaden et al.,
974 2006]
- 975 7. Zebiak and Cane [1987] in exploring the reproduction of ENSO events in a climate model
976 noted that “ENSO is largely controlled by deterministic processes in the tropical Pacific
977 atmosphere-ocean system”.
- 978 8. Timmreck [2012] explored the impact of low latitude strong explosive eruptions on climate and
979 ENSO finding that the climate response depends on the initial ENSO phase and the eruption
980 season;
- 981 9. S Mcgregor et al. [2014] investigated the pause in global warming and suggested that the
982 Atlantic SST increase contributed to the strengthening of the Walker circulation.
- 983 10. Maher et al. [2015] investigated the effects of large tropical eruptions on the Indian-Pacific
984 variability and found they are associated with “co-occurring El Niño and positive IOD events”
985 which peak “6-12 months after the volcanic forcing peaks”;
- 986 11. Predybaylo et al. [2017] also investigated the large, low latitude Pinatubo eruption in 1991 but
987 only used SO₂ emissions and found that the ENSO response depends on season and initial
988 ENSO state.
- 989 12. Blake et al. [2018] investigated the effects of the six largest tropical volcanic eruptions using
990 the Last Millennium Ensemble (LME) data from 850 to 1850 on Australian rainfall, the IOD
991 and ENSO finding that the eruptions “increased the likelihood of El Niño and a positive IOD
992 condition for up to four years following an eruption”.

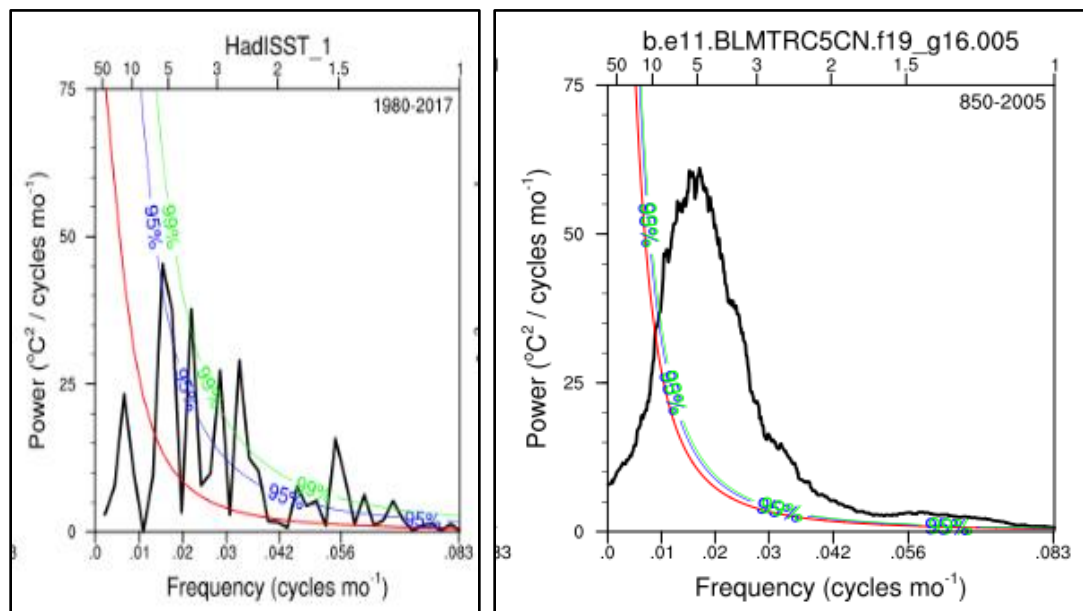
993 It is therefore clear that the Trade Winds and therefore the Walker Circulation are intimately
994 connected with ENSO events and determining the cause of the weakening of the Trade Winds and
995 Walker Circulation may well reveal the cause of ENSO events.

996 It is also worth noting that many of the references above only include large eruptions at any
 997 location and SO₂ emissions. Whereas this paper examines the role the natural and anthropogenic (all
 998 eruptions and aerosols) South East Asian aerosol Plume (SEAP) plays in reducing convection,
 999 weakening the Walker Circulation and thus in initiating and maintaining ENSO events. Aerosol
 1000 plumes can alter the major atmospheric circulation systems [Solomon *et al.*, 2007], [Remer *et al.*,
 1001 2009] and the SEAP is uniquely positioned to influence the Walker Circulation as it exists in the
 1002 region of normal (non-ENSO) Walker Circulation convection.

1003 1.3 ENSO Return Frequency

1004 The literature describes ENSO events as exhibiting a return frequency of two to seven to ten
 1005 years and the University Corporation for Atmospheric Research (UCAR) website at
 1006 http://webext.cgd.ucar.edu/Multi-Case/CVDP_repository/cesm1.lm in the ENSO section shows the
 1007 ENSO power spectra for all the LME runs and the same information for the HadISST_1 [Rayner *et al.*
 1008 *et al.*, 2003] and ERSST v5_1 [Huang *et al.*, 2017]. The HadISST_1 and ERSST v5_1 spectra are
 1009 similar and Figure 1 shows the multiple peaks in the HadISST_1 data whilst all the LME runs show a
 1010 single peak at about 5 years and are nearly identical even with different forcings whilst they are all
 1011 very different to the two spectra based on real data as Figure 1 shows. The reasons for this variation
 1012 are discussed in the results section.

1013



1014

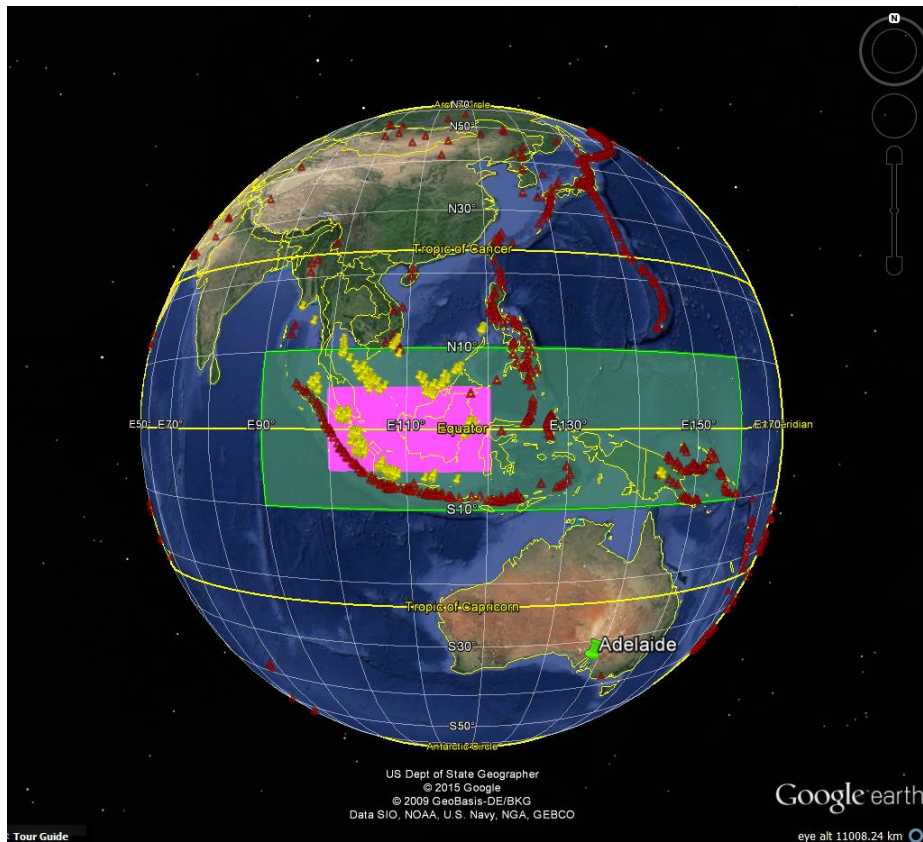
1015 Figure 1: ENSO Power Spectra: Left: HadISST_1 and Right: run 5 LME all forcings

1016 1.4 The SEAP and CSEAP Areas

1017 In this analysis two areas are used which are shown in Figure 2:

- 1018 1. The SEAP Area 10°S-10°N and 90°E-160°E which is the area covered by the SEAP;
- 1019 2. The Central SEAP (CSEAP) Area 5°S-5°N and 100°E-120°E where the anthropogenic SEAP is
 1020 most intense.

1021



1022

1023 Figure 2: The SEAP Area, Green and CSEAP Area, pink with the locations of gas flares
 1024 (from National Oceanic and Atmospheric Administration (NOAA) and the Global Gas Flaring
 1025 Reduction Partnership (GGFRP)) in yellow and volcanoes (Global Volcanism Program (GVP)) in
 1026 red. Image source: Google Earth.

1027 1.5 The South East Asian Plume (SEAP)

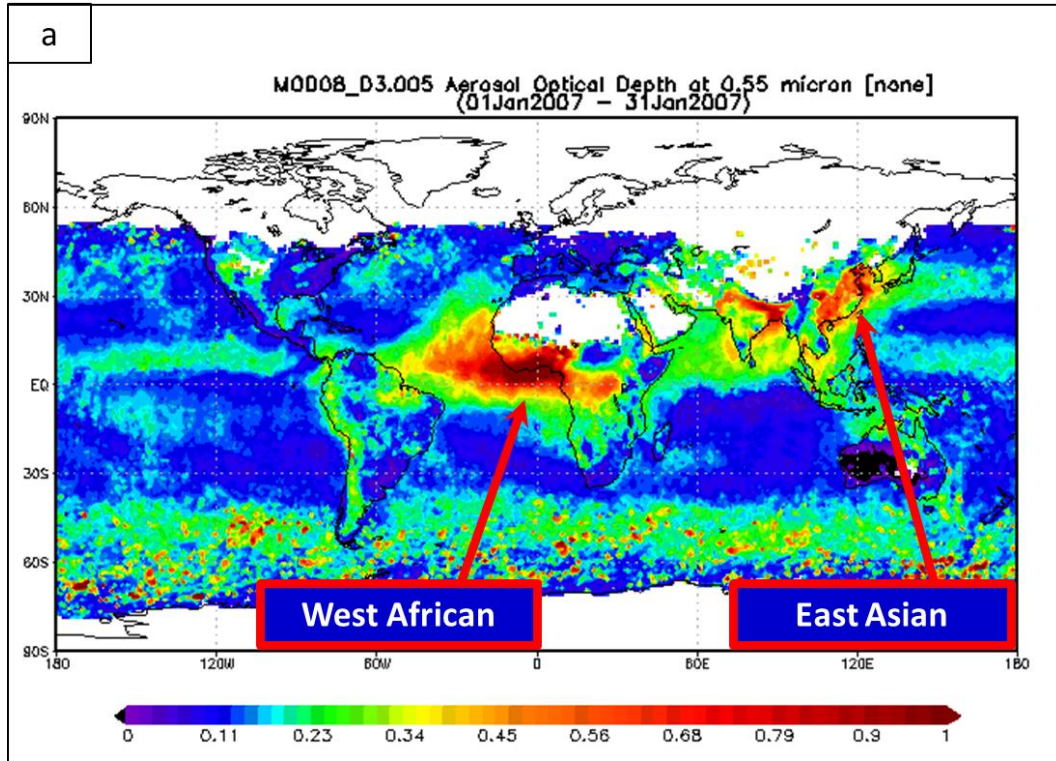
1028 This paper focuses on south east Asia as this region is where convection, which drives the
 1029 Walker Circulation, occurs and is therefore where aerosols can have a significant effect. Appendix A
 1030 describes the sources of aerosols in the SEAP Area, the Natural SEAP derived from volcanic
 1031 eruptions and the Anthropogenic SEAP derived mainly from biomass burning and gas flares in the
 1032 oil production industry.

1033 1.5.1 The Natural SEAP

1034 The SEAP Area, which covers about 3.4% of the globe, is the world's most tectonically
 1035 active area with the United States Geological Survey (USGS) earthquake database showing 29% (5
 1036 of 17) of the major earthquakes (magnitude > 8.4) in the world since 1900 occurred in the SEAP
 1037 Area and the GVP's database showing that from 1500 to 2018 over 18% of the global volcanic
 1038 eruptions occurred in the SEAP Area. *Simkin and Siebert* [2000] state that 5 of 16 (31%) of the
 1039 continuously erupting volcanoes in the world for the past 24 years are located in the SEAP Area and
 1040 that one more, in Vanuatu, is just to the south east of the SEAP Area.

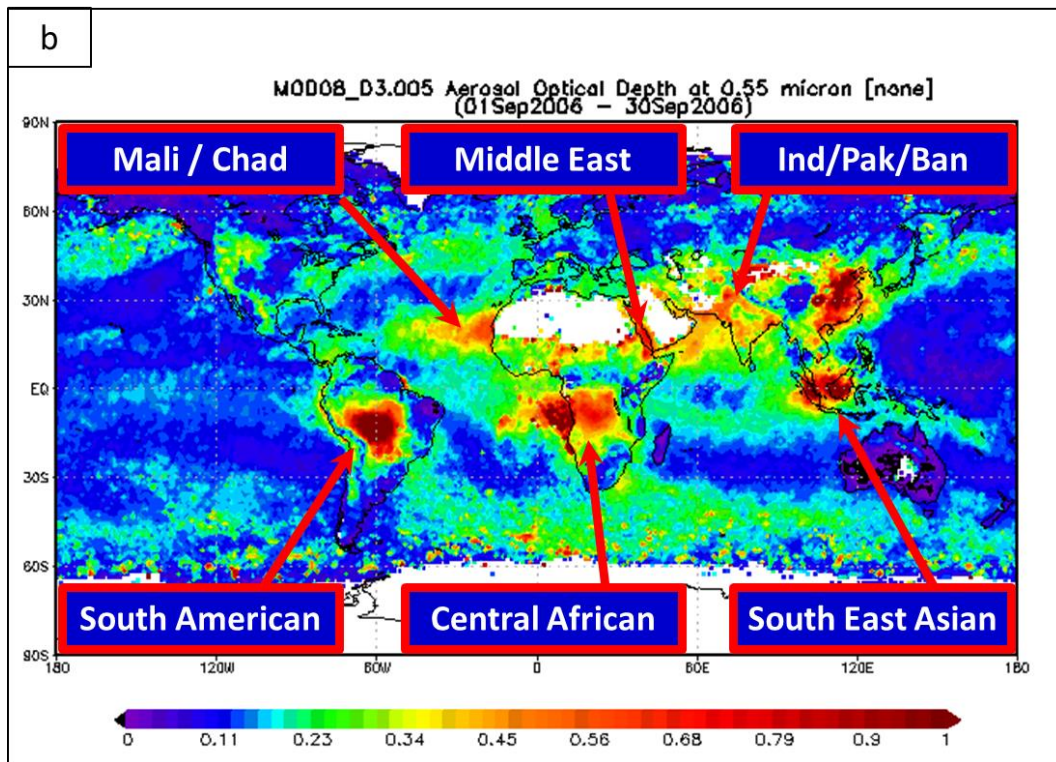
1041 1.5.2 The Anthropogenic SEAP

1042 The anthropogenic SEAP is one of eight continental scale, anthropogenic, aerosol plumes
1043 which occur annually and are shown in Figure 3. These extreme plumes typically exist for a few
1044 months each year at the end of the regional dry season when biomass burning can occur. The SEAP
1045 is easily identified on the monthly mean 0.55 micron Aerosol Optical Depth (AOD) data from
1046 MODIS [*Kaufman et al.*, 2000] on the NASA Terra and Aqua satellites. The monthly average AOD
1047 of the CSEAP Area observed by Terra is shown in Figure 4 to demonstrate the peak anthropogenic
1048 aerosol emission season is SON, the end of the dry season in SE Asia, and was extremely high (AOD
1049 > 0.6) in 2002, 2004, 2006, 2009, 2014 and 2015 compared with the intervening years. Peaks in the
1050 MODIS AOD in SON are attributed to seasonal biomass burning in south east Asia (Appendix A).
1051 CALIPSO (Cloud-Aerosol Lidar and Infrared Pathfinder Satellite Observations) [*Winker et al.*, 2009]
1052 profiles confirm a layer of smoke existed at about 3Km altitude in October 2015 in the SEAP Area
1053 and Figure 5 shows the geographic extent of the extreme October 2006 apparition of the SEAP. This
1054 paper analyses the effects of the SEAP on an annual, April to October (wet season in south eastern
1055 Australia) and SON (when the anthropogenic plume is at its most intense and will therefore have its
1056 greatest effect.) basis.



1057

1058



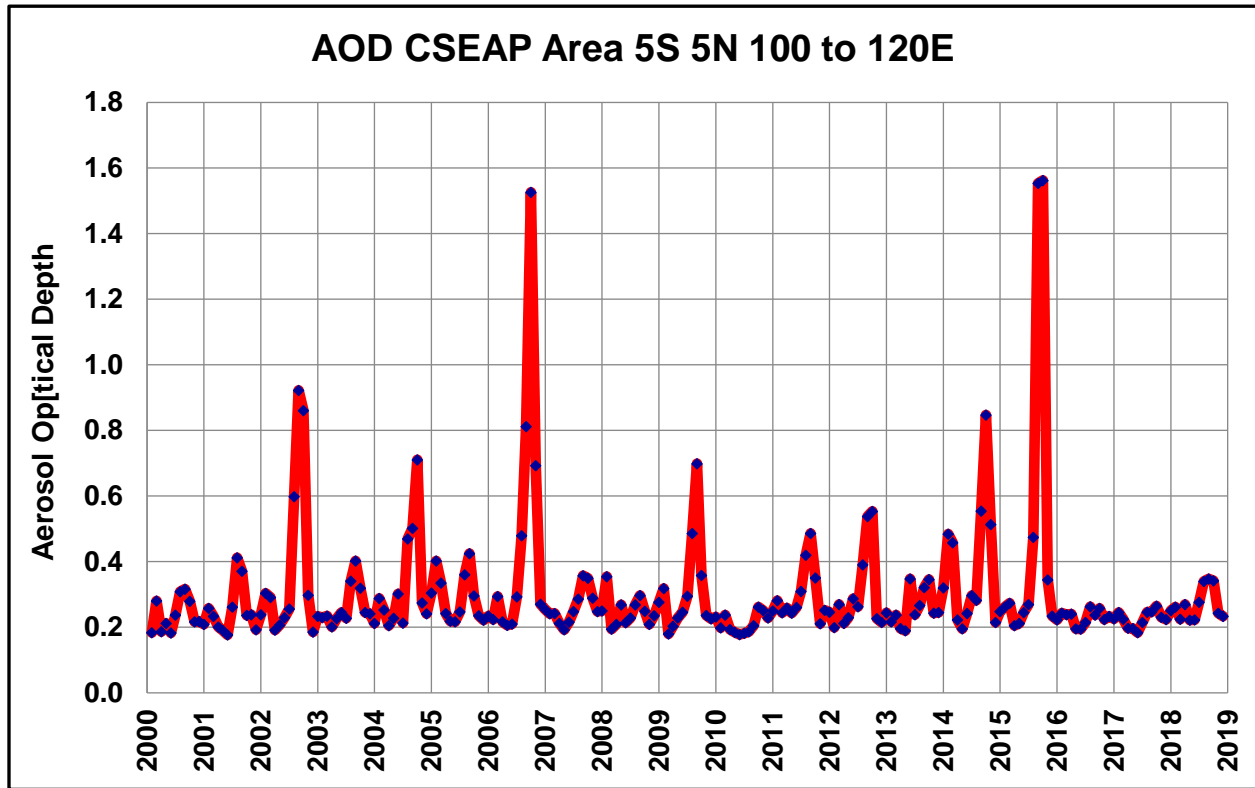
1059

1060

1061

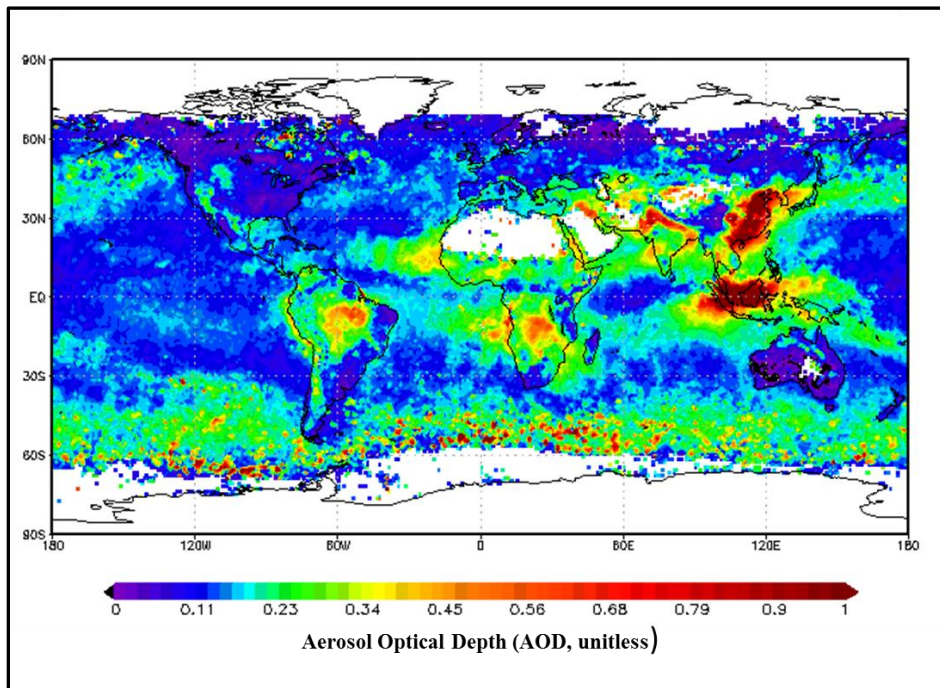
Figure 3: The Eight Continental Scale Aerosol Plumes. NASA Giovanni AOD (a) January 2007 (b) September 2006. Source: NASA Giovanni.

1062



1063

1064 Figure 4: Monthly average MODIS Terra AOD in the CSEAP Area 5°S-5°N and 100°E-120°E.

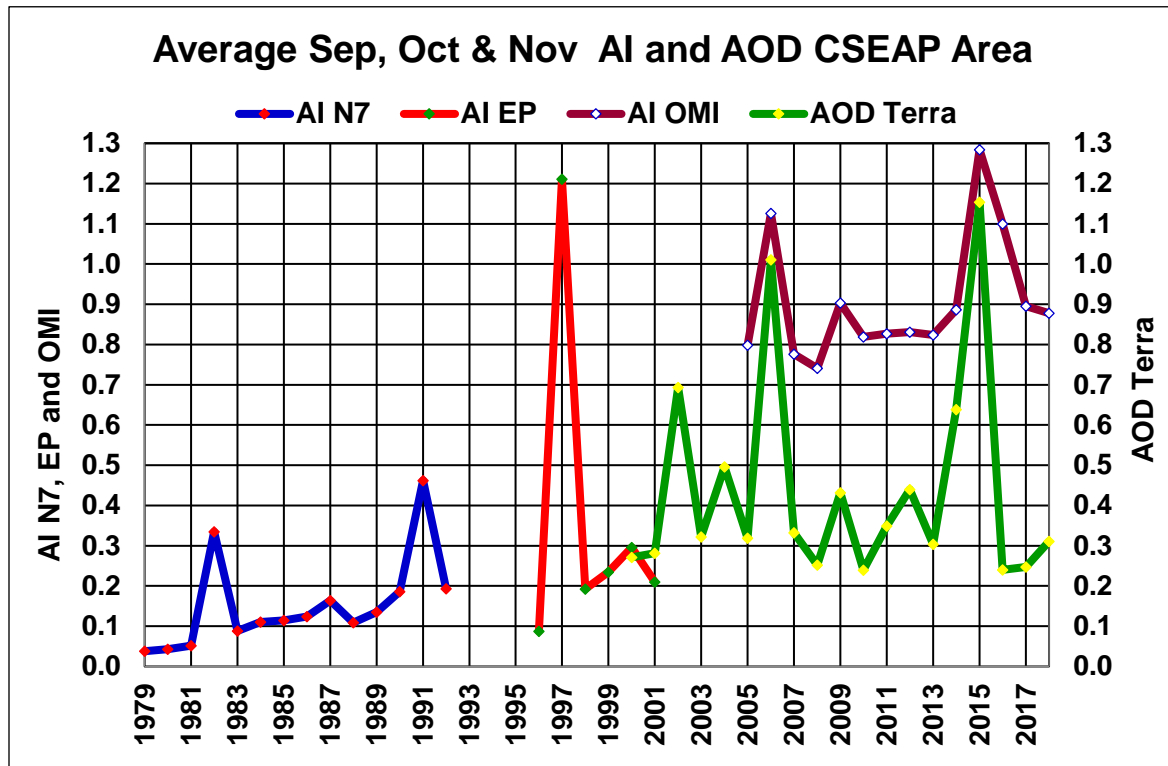


1065

1066 Figure 5: NASA MODIS monthly mean AOD data for October 2006. Source: NASA Giovanni.

1067 The SON average Aerosol Index (AI) and AOD of the CSEAP Area from 1979 to 2018 in
 1068 SON is shown in Figure 6. The maximum AOD was 1.60 (Oct 2015) and the maximum Nimbus 7
 1069 (N7) and Earth Probe (EP) AI was 1.81 (Sept 1997). The AI of the CSEAP Area increased from
 1070 0.050 in Sep 1979 to 0.297 in 1992 and to 0.396 in 2000 a 491% and 687% increase respectively in
 1071 years without extensive biomass burning. From 1979 to 1997, a major biomass burning event year
 1072 [Applegate *et al.*, 2001], the increase in September in AI is 3,499%.

1073
 1074



1075

1076 Figure 6: Average SON AI (N7, EP and OMI) and AOD (MODIS on Terra) CSEAP Area.
 1077 (N7 – TOMS instrument, EP – TOMS instrument, OMI Ozone Monitoring Instrument)

1078 The surface radiative forcing of the anthropogenic SEAP is significant and the literature
1079 includes:

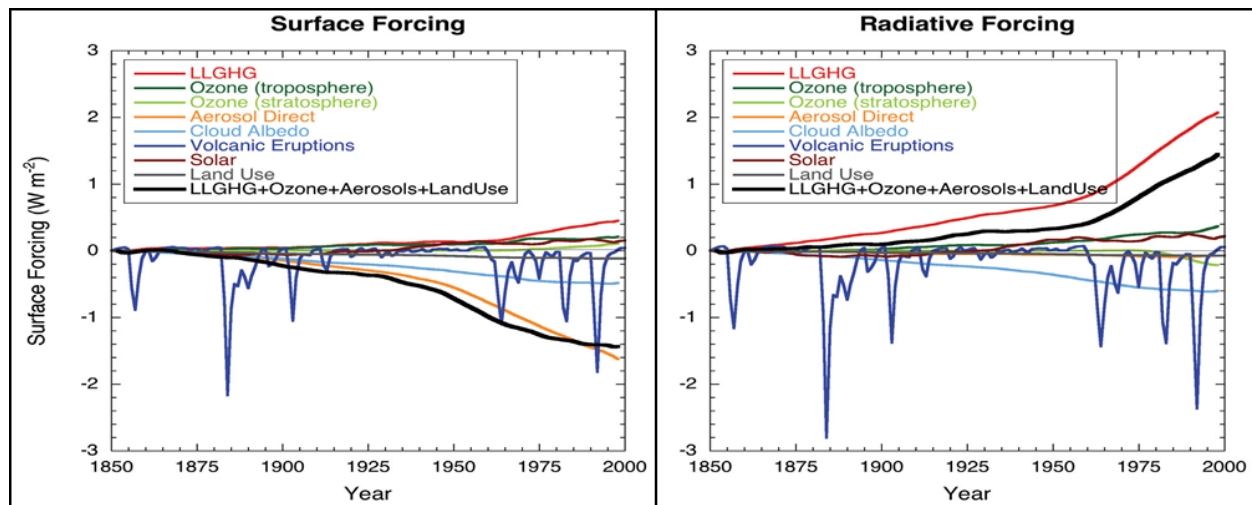
- 1080 1. A 10% to 30% reduction of Photosynthetically Active Radiation [Ramanathan, 2006];
- 1081 2. -150 W m^{-2} [Duncan et al., 2003]; and
- 1082 3. During ACE-Asia, $\sim -286.0 \text{ W/m}^2/\tau\alpha$ [Hansell et al., 2003] ($\tau\alpha$ is the aerosol optical depth and
1083 its derivation is described in the paper in detail).

1084 **1.6 The Walker Circulation**

1085 The Walker Circulation is defined in the IPCC AR4 Glossary as “Direct thermally driven
1086 zonal overturning circulation in the atmosphere over the tropical Pacific Ocean, with rising air in the
1087 western and sinking air in the eastern Pacific” (See also [Chunzai Wang, 2002], [Barry and Chorley,
1088 2010], [Trenberth et al., 2000] and [Sturman and Tapper, 1996]).

1089 The Australian Bureau of Meteorology (BOM) shows images of the atmospheric circulation
1090 during El Niño, La Nina and neutral seasons on its website at:
1091 <http://www.bom.gov.au/climate/about/australian-climate-influences.shtml?bookmark=enso>. It is
1092 clear from these figures that the “direct thermal drive” for the La Niña and neutral Walker
1093 Circulation must be located at ground level in the SEAP Area where solar radiation heats the Earth’s
1094 surface which in turn heats the atmosphere as the rising limb of the non-ENSO Walker Circulation is
1095 located there in exactly the same location as the SEAP which is therefore uniquely positioned to
1096 directly affect the Walker Circulation and ENSO.

1097 Since variations in the solar energy at the top of the atmosphere cannot explain the reduction
1098 in the surface heating in the SEAP Area which causes the Walker Circulation to relax the reduction
1099 must be caused by variations in the atmosphere where the SEAP reduces surface solar radiation.
1100 Indeed Figure 7 from the IPCC AR4 shows that, on a globally averaged basis, surface radiative
1101 forcing is controlled by aerosols with the net effect of long-lived greenhouse gases, ozone, aerosols
1102 and land use aligning nearly perfectly with the aerosol direct effect.



1103
 1104 Figure 7: - Source: IPCC AR4 Figure 2.23. Globally and annually averaged temporal
 1105 evolution of the instantaneous all-sky RF (right panel) and surface forcing (left panel) due to various
 1106 agents, as simulated in the MIROC+SPRINTARS model (Nozawa et al., 2005; Takemura et al.,
 1107 2005). This is an illustrative example of the forcings as implemented and computed in one of the
 1108 climate models participating in the AR4. Note that there could be differences in the RFs among
 1109 models. Most models simulate roughly similar evolution of the LLGHGs' RF. [Nozawa et al., 2005]
 1110 and [Takemura et al., 2005].

1111
 1112 Therefore, from the IPCC AR4 and literature it is a plausible hypothesis that the SEAP could
 1113 force the Walker Circulation and trade winds to “relax” by reducing the surface solar radiation
 1114 available to drive convection in the Walker Circulation in the SEAP Area and this paper examines
 1115 the connection between the SEAP, convection in the SEAP Area, the trade winds, the Walker
 1116 Circulation and ENSO events.

1117 However, since the anthropogenic SEAP is a recent event driven by population growth as
 1118 Appendix A and Figure 6 show and ENSO events have been occurring for many centuries to prove
 1119 the hypothesis that the SEAP causes ENSO events it is necessary to show that the natural aerosols
 1120 originating from volcanic eruptions in the SEAP Area can also trigger and sustain ENSO events.

1121 1.7 Volcanic Eruptions and ENSO

1122 The literature includes many attempts to connect volcanic eruptions and ENSO events.
 1123 Neville Nicholls [1988] and N. Nicholls [1990] investigated volcanic eruptions and El Niño events
 1124 and concluded there was no connection. Hirono [1988] investigated the possibility that the 1983
 1125 eruption of El Chichon in Mexico could have triggered the El Niño which followed. Robock et al.
 1126 [1995] investigated the Hirono [1988] hypothesis and found that the eruption did not trigger the El
 1127 Niño event which followed and also noted that “only trade wind collapses in the western equatorial
 1128 Pacific can initiate El Niños”. Handler and Andsager [1990] investigated the volcanic hypothesis
 1129 which states that low-latitude volcanic aerosols are the immediate and only cause of warmer than
 1130 normal SST or El Niño and its inverse using Monte Carlo techniques and found that both aspects of
 1131 the hypothesis were satisfied to “a very high level of statistical significance”. Self et al. [1997]
 1132 investigated volcanic aerosol perturbations and the 16 strongest El Niño events over the last 150

1133 years and found no general correlation. In discussing the evolution of ENSO events *Trenberth et al.*
1134 [2002] suggested that the effects of volcanic eruptions on ENSO events remained unanswered
1135 questions. *Emile-Geay et al.* [2008] focused on very large eruptions which were greater than the
1136 Pinatubo eruption in 1991 and found that small eruptions have no effect. *D Zhang et al.* [2013a]
1137 investigated the effects of large eruptions using AOD in latitudinal bands 0 to 30 and 30 to 90 in both
1138 hemispheres to force the climate model but did not consider the location or the intensity of the
1139 eruption and noted this should be done in the future. *Cane* [2005] reviewed forecasts of ENSO
1140 activity, found that there was no clear picture and suggested solar and volcanic variations in solar
1141 insolation and atmospheric aerosols might have a role. It is also worth noting that *Ammann et al.*
1142 [2003] found that including an improved volcanic eruption dataset in climate model simulations
1143 improved the correlation between the modelled data and observations whilst *Mann et al.* [2005]
1144 stated “Our model experiments reproduce the empirical observations of a short-term ENSO response
1145 to explosive tropical eruptions”

1146 There is therefore obviously great interest in, but no general agreement on, the connection
1147 between volcanic eruptions and ENSO events.

1148 2 METHOD AND DATA

1149 Modelling, satellite and GVP data are used to show that ENSO and the climate variations
1150 commonly linked to ENSO events are accurately explained using mechanisms controlled by the
1151 SEAP.

1152 2.1 Modelling – LME, LE and MERRA-2

1153 The LME [*Otto-Bliesner et al.*, 2016] data from one member of each of the eight forcing
1154 simulations with run number in () (850 (3), All (13), Ozone and Aerosol (Aero) (2), Green House
1155 Gas (GHG) (3), Land use (Land) (3), Orbital (3), Solar (5) and Volcanic (5)) was used to create time
1156 series of 1,156 years and 13,872 months of: aerosol optical depth; air temperature; surface
1157 temperature; omega; wind speed; Oceanic Nino Index; and the global temperature as well as indices
1158 for the Nino 3.4 and 1+2 SST and the SOI (which the IPCC AR5 shows are used to monitor the
1159 status of ENSO). These series were correlated to demonstrate that these indices and parameters are
1160 directly connected to aerosols in the SEAP area.

1161 A similar approach was used for the Large Ensemble (LE) [*Kay et al.*, 2015] using data from
1162 1850 to 2005 with historic forcings and from 2006 to 2100 using RCP 8.5 projections (run 001) and
1163 with the NASA Modern Era Retrospective analysis for Research and Applications release two
1164 (MERRA-2) reanalysis dataset [*Gelaro et al.*, 2017] which includes assimilated aerosols.

1165 LME and LE data is at <https://www.earthsystemgrid.org/> and MERRA-2 data is at
1166 <http://giovanni.gsfc.nasa.gov/giovanni/>

1167 2.2 Satellite Data

1168 The same indices from that IPCC AR5 table were also correlated with four satellite-based
1169 measures of aerosols: The Aerosol Index (AI), obtained from the Total Ozone Mapping Spectrometer
1170 (TOMS) instruments on the N7 and EP satellite platforms; the AOD from the MODIS instrument on
1171 NASA Terra; and the AI from the Ozone Monitoring Instrument (OMI) on NASA Aura.

1172 Note: AI, unlike AOD, is “only sensitive to desert dust and elevated smoke layers. Therefore,
1173 it does not account for aerosols of industrial origin or any kind of aerosol in the lowest 2 km of the
1174 atmosphere” (Personal Communication - NASA). However in the SEAP Area it is useful as we are
1175 investigating biomass burning “smoke” in SON and the CALIPSO data at
1176 https://eosweb.larc.nasa.gov/project/calipso/calipso_table shows smoke at an altitude of 3Km in
1177 October 2015, above the lower limit of AI data.

1178 The following datasets:

- 1179 1. Sea Surface Temperature Niño 3.4 area (5°S-5°N, 170°W-120°W).
1180 <http://www.cpc.ncep.noaa.gov/data/indices/> ;
- 1181 2. Sea Surface Temperature Niño 1 and 2 areas (10°S–0°, 90°W–80°W).
1182 <http://www.cpc.ncep.noaa.gov/data/indices/> ;
- 1183 3. Southern Oscillation Index - Standardized difference of Sea Level Pressure (SLP) - Tahiti
1184 minus Darwin. <http://www.bom.gov.au/climate/current/soihtml1.shtml> ;

1185 and the following:

- 1186 1. Omega (vertical motion in the atmosphere) at 400mb level - CSEAP Area.
1187 <http://www.esrl.noaa.gov/psd/cgi-bin/data/timeseries/timeseries1.pl> (Source 1)
- 1188 2. Rainfall – CSEAP Area. Data NCEP reanalysis (Source 1);
- 1189 3. SST - SEAP Area. Data NCEP reanalysis (Source 1);
- 1190 4. Interpolated OLR – CSEAP Area. Data NOAA NCEP reanalysis (Source 1);
- 1191 5. Trade Wind Index (TWI) (850mb at 5°N-5°S, 175°W-140°W).
1192 <http://www.cpc.ncep.noaa.gov/data/indices/cpac850> (source 2)
- 1193 6. Oceanic Niño Index (ONI). Data NOAA (source 2); and
- 1194 7. Air temperature at 650 hPa. Data MERRA-2 reanalysis.

1195 **2.3 Volcano Data**

1196 Volcanic eruption data from the GVP was processed using the methodology outlined in
1197 Appendix A and analysed against the main ENSO parameters.

1198 **3 RESULTS**

1199 The results in Figures 8, 9, 11 and 15 were calculated using the Excel correlation function
1200 with students two tail t test and colour coded for significance (yellow < 0.01, brown <0.02, green <
1201 0.05 and blue < 0.1).

1202 **3.1 Modelling**

1203 Modelling from the LME and LE was analysed. Due to the significant variation in the mean
1204 and variability in the aerosol and temperature data from both the LME and LE data this data is non-
1205 stationary and must be pre-processed to achieve stationarity before correlating as this paper is
1206 investigating interannual variations. Acceptable stationarity, after testing using a variety of methods
1207 including PAST 3.22 [Hammer *et al.*, 2001], was achieved by the methods shown in Appendix B.

1208 **3.1.1 The Last Millennium Ensemble**

1209 The results of my analysis of the correlation between: the ENSO indices derived from TS
1210 (Skin Temperature) and PSL (Sea Level Pressure); temperature at level 609 and the surface, omega
1211 in the SEAP Area; the global temperature from TS; and the aerosol loading AODVIS (Aerosol
1212 Optical Depth 550 nm) in the SEAP and CSEAP areas averaged from one of each of the eight forcing
1213 regimes are shown in Figure 8. The LME TS from the atmosphere data was used instead of the SST
1214 from the ocean data to avoid having to regrid the ocean data to latitude and longitude (suggested by
1215 the UCAR help desk). The Oceanic Nino Index is a 3 month running average of the Nino 3.4 TS

1216 Note: The volcanic forcing data in the LME cannot of itself demonstrate the connection
1217 between the natural volcanic SEAP and ENSO as it does not have the resolution required to do so. It
1218 is derived from ice cores in the Arctic and Antarctic [*Otto-Bliesner et al.*, 2016] and *Gao et al.*
1219 [2008] who provide the data as only stratospheric sulfate forcing in latitude bands (ten degrees wide),
1220 by altitude and month. For volcanic tephra to travel to the polar regions the tephra must be injected
1221 into the stratosphere requiring a minimum VEI of 3 to 4. Hence all the VEI 0,1,2 and some (50%
1222 assumed) of the VEI 3 eruptions in the SEAP Area must be missing from the dataset. Since this
1223 excludes over 94% of the eruptions in the SEAP Area since 1850 which are used in this paper the
1224 resolution of this LME volcanic forcing dataset is inadequate in itself in terms of eruption size, geo-
1225 space and aerosol type to prove the causation of ENSO by SEAP Area volcanic tephra described in
1226 this paper. Although these LME volcanic forcing runs do provide another independent LME aerosol
1227 forcing dataset which is useful.

1228 **3.1.2 The Large Ensemble**

1229 The LE data used includes historic data from 1850 to 2005 and RCP 8.5 data from 2006 to
1230 2100. The data was analysed in these two parts and the results averaged and shown in the same way
1231 as the LME data in Figure 9.

1232 Note some of the very high correlations from the LME and LE show significance levels much
1233 less than 0.01 due to the correlation magnitude and the length of the time series.

1234

	SEAP T Level 609	SEAP Area TS	SEAP Area Omega	Nino 3.4 U10	Nino 3.4 TS	Nino 1+2 TS	ONI	SOI	Global TS	Nino 3.4 TS & U10 Wind
Monthly Segmented										-0.89
CSEAP	0.94	-0.98	0.95	-0.82	0.96	0.91	0.95	-0.97	0.83	
SEAP	0.99	-0.99	0.76	-0.90	0.93	0.84	0.94	-0.98	0.78	
Interannual Series (September to November Averages - No smoothing)										-0.85
CSEAP	0.38	-0.88	0.82	-0.76	0.79	0.68	0.78	-0.79	0.42	
SEAP	0.50	-0.88	0.87	-0.79	0.77	0.70	0.76	-0.78	0.44	
Interannual Series (April to October Averages - No smoothing)										-0.88
CSEAP	0.58	-0.80	0.80	-0.73	0.85	0.70	0.83	-0.89	0.45	
SEAP	0.76	-0.73	0.81	-0.84	0.83	0.73	0.81	-0.80	.057	
Annual Averages (No smoothing)										-0.92
CSEAP	0.61	-0.77	0.79	-0.82	0.90	0.78	0.87	-0.86	0.58	
SEAP	0.80	-0.64	0.83	-0.87	0.84	0.80	0.81	-0.79	0.66	
Annual Average - Segmented & Averaged (8 segments)										-1.00
CSEAP	0.96	-0.95	0.92	-0.97	1.00	1.00	0.98	-1.00	0.98	
SEAP	0.99	-0.94	0.98	-0.99	0.99	0.98	0.98	-0.97	0.98	

1235
1236
1237
1238

Figure 8: Average correlations of eight runs, one from each of the eight forcings described in the text, from the LME of AODVIS in the CSEAP and SEAP Areas with the ENSO indices, SEAP Area Surface and level 609 Temperature, omega, Nino 3.4 wind speed and the global temperature. Last column correlations of Nino 3.4 TS and U10 wind speed.

1239

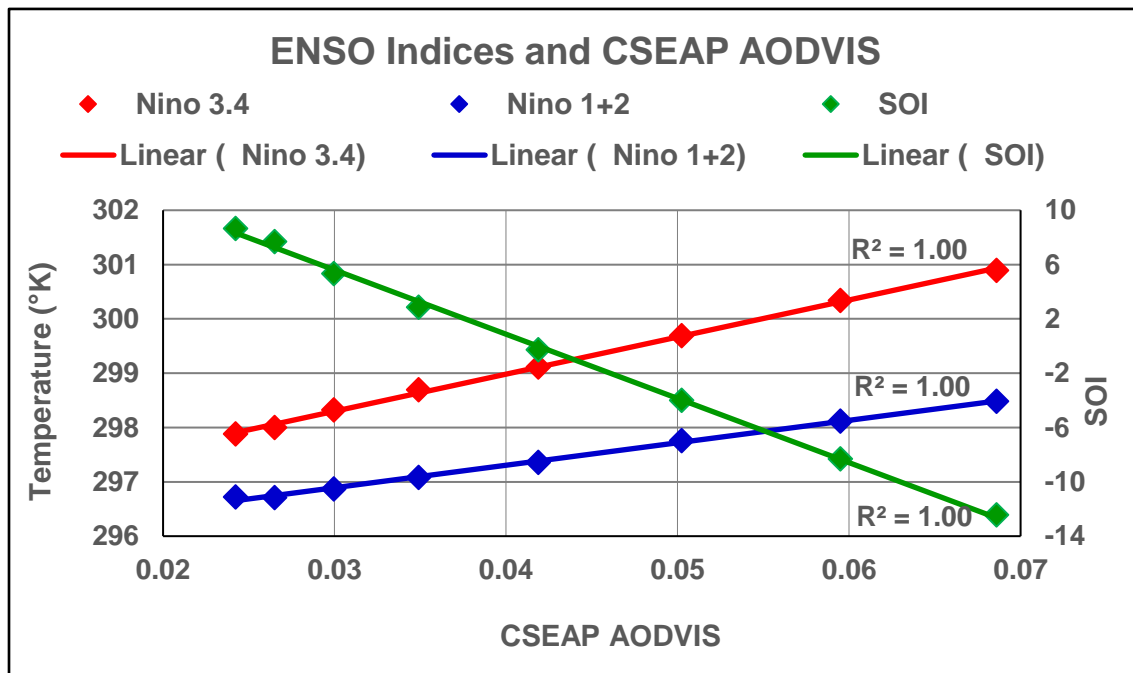
	SEAP T Level 609	SEAP Area TS	SEAP Area Omega	Nino 3.4 U10	Nino 3.4 TS	Nino 1+2 TS	ONI	SOI	Global TS	Nino 3.4 TS & U10 Wind
Monthly Series Segmented										-0.81
CSEAP Area	0.90	-0.93	0.96	-0.94	0.90	0.96	0.86	-0.86	0.90	
SEAP Area	0.88	-0.97	0.83	-0.91	0.93	0.80	0.93	-0.95	0.96	
Interannual Series (September to November Averages - No smoothing)										-0.85
CSEAP Area	0.68	-0.90	0.90	-0.85	0.78	0.75	0.81	-0.73	0.42	
SEAP Area	0.68	-0.85	0.85	-0.82	0.63	0.66	0.76	-0.72	0.44	
Interannual Series (April to October Averages - No smoothing)										-0.94
CSEAP Area	0.68	-0.89	0.91	-0.85	0.88	0.69	0.87	-0.84	0.47	
SEAP Area	0.84	-0.80	0.83	-0.81	0.76	0.57	0.80	-0.76	0.52	
Annual Averages (No smoothing)										-0.96
CSEAP Area	0.64	-0.89	0.92	-0.89	0.92	0.79	0.88	-0.82	0.60	
SEAP Area	0.84	-0.78	0.91	-0.85	0.86	0.73	0.82	-0.77	0.63	
Annual Average - Segmented & Averaged										-0.99
CSEAP Area	0.96	-0.99	0.98	-0.99	0.99	0.97	0.98	-0.97	0.89	
SEAP Area	0.99	-0.99	0.98	-0.99	0.99	0.99	0.99	-0.97	0.94	

1240 Figure 9: Average correlations from the LE (1850 to 2005 and 2006 to 2100) of AODVIS in the CSEAP and SEAP Areas with
 1241 the ENSO indices, SEAP Area Temperature at the surface and level 609, omega and the global surface temperature. Last column
 1242 correlations of Nino 3.4 Area Skin Temp and U10 wind speed. Correlation significance shown is derived from the lowest significance
 1243 of the two correlations. Red indicates one of the two correlations only included two points with the other showing <0.01 significance.

1244 When the LME CSEAP Area AODVIS and Nino Index data from the TS, omega, U10
 1245 wind speed and surface pressure data are segmented and averaged the extraordinary correlations
 1246 in Figure 8 results with graphs of the ENSO data shown in Figure 10 where the segmented and
 1247 averaged data shows the Nino 3.4 TS rising by 3.0°K from 297.9°K to 300.9°K from the segment
 1248 with the lowest AODVIS to the highest. When the same analysis is applied to the LME SOI and
 1249 CSEAP Area AODVIS the SOI falls from +8.7 to -12.4.

1250 It is also worth noting that although the LME AODVIS data from one All Forcing run
 1251 from 1979 to 2005 for the CSEAP Area ranges from 0.025 to 0.063 which is significantly lower
 1252 than the Terra data from April to July from 2000 to 2018 which ranges from 0.18 to 0.35 the data
 1253 still supports the hypothesis that the natural SEAP has always been the cause of ENSO events.
 1254 (Note: April to July is used in this comparison as extreme biomass burning does not occur in
 1255 these months and volcanic forcing is expected to dominate.)

1256 It is therefore obvious with R^2 values of 1.00 in Figure 10 that the LME data proves the
 1257 connection between the aerosol loading in the SEAP/CSEAP Areas and the ENSO indices. The
 1258 causal relationship is discussed later.



1259 Figure 10: Last Millennium Ensemble segmented and averaged annual CSEAP AODVIS,
 1260 Nino 3.4 and 1+2 Skin Temperature (TS) and the LME SOI from 850 to 2005 CE. Data averaged
 1261 from the six of the forcings used – “All” and “Aero” not used as their segments are different.
 1262

1263 It is also worth noting that in two columns of Figures 8 and 9:

- 1264 1. The temperature in the Nino 3.4 area correlates at high levels with the U10 wind
 1265 speed including at -1.00 and -0.99 when the data is segmented and averaged within
 1266 the segments.
- 1267 2. The average global temperature which is known to increase during El Nino events
 1268 [*Foster and Rahmstorf, 2011*] is shown to correlate with the AODVIS in the SEAP
 1269 and CSEAP areas at 0.98, 0.89 and 0.94 when the data is segmented and averaged

1270 with the global average temperature rising by 0.4°C from the segment with the
1271 lowest AOD to the highest.

1272 3.1.3 The NASA MERRA-2 Reanalysis

1273 MERRA-2 which includes assimilated aerosols adds another independent model to the
1274 LME and LE. This dataset is continuous from 1980 to present and at the time of writing included
1275 thirty-nine full years of data.

1276 The MERRA-2 analysis is included in two columns in Figure 11. The column labelled
1277 AOD MERRA-2 correlates the MERRA-2 AOD with the same parameters as the N7, EP, OMI
1278 and Terra AI and AOD. The column labelled AOD MERRA-2 & MERRA-2 was created by
1279 correlating the MERRA-2 AOD with the other parameters which were derived from the
1280 MERRA-2 dataset. Parameters such as the SOI which are not available in MERRA-2 were
1281 calculated using data from the MERRA-2 dataset. The SOI was calculated using the BOM
1282 formula available on their web site at: <http://www.bom.gov.au/climate/current/soi2.shtml> and the
1283 surface pressure near Darwin (130° to 131°E and 12° to 13°S) and Tahiti (149° to 150°W and 17°
1284 to 18°S). The easterly wind component from the same area as the NOAA TWI (140° to 175° W
1285 and 5°S to 5°N) from the MERRA-2 dataset was used as a proxy for the TWI.

1286 For both the MERRA-2 columns in Figure 11 the parameters the IPCC listed as used to
1287 monitor ENSO events correlate at similar levels to the TERRA AOD data and at the same
1288 significance <0.01. The analysis of the SEAP in the column labelled AOD MERRA-2 &
1289 MERRA-2 is effectively a modelling analysis with near random forcings of extreme apparitions
1290 of the SEAP over 39 years which demonstrates exactly the same high correlations as the longer
1291 LME and LE datasets.

1292 3.2 Satellite Data

1293 As shown in Figure 6 the CSEAP AI data contains a significant trend and therefore the
1294 SON AI, AOD and other data was detrended using PAST 3 and then correlated both as a times
1295 series and a detrended time series. The resultant SON and annual correlations are reported in
1296 Figure 11 with the parameters listed in the IPCC AR5 as being used to monitor ENSO events
1297 highlighted in red.

a	Sept Oct Nov – Correlations								
		AOD Terra	AI N7	AI E Probe	AI OMI	AI N7 + EP	AI N7+EP+O	AOD MERRA-	AOD MERRA-2
		2000-18	1979- 1992	1996-2001	2005 - 18	1979...20 01	1979...201 8	1980- 2018	1980-2018
1	Air Temp CSEAP Area MERRA-2 650 hPa	0.67	0.28	0.54	0.69	0.45	0.55	.019	0.12
2	CSEAP Area NCEP Omega	0.91	0.57	0.96	0.62	0.56	0.31	0.80	0.79
3	NOAA TWI	-0.72	-0.69	-0.97	-0.73	-0.76	-0.34	-0.86	0.87
4	SST Niño 3.4	0.77	0.56	0.91	0.65	0.61	0.34	0.74	0.73
5	SST Niño 1 and 2	0.78	0.48	0.96	0.77	0.76	0.34	0.79	0.77
6	SOI	-0.75	-0.64	-0.85	-0.69	-0.45	-0.13	-0.76	-0.73
7	ONI	0.77	0.51	0.92	0.65	0.57	0.26	0.74	0.77
8	SST SEAP Area	-0.66	-0.68	-0.85	-0.20	-0.41	0.11	-0.67	-0.54
9	Rainfall CSEAP Area	-0.58	-0.40	-0.88	-0.35	-0.38	0.18	-0.63	-0.68
10	NOAA Interpl'd OLR	0.85	0.64	0.99	0.50	0.60	0.21	0.82	0.73

1298
1299

1300

b	Sept Oct Nov Detrended using PAST 3 – Correlations								
		AOD Terra	AI N7	AI E Probe	AI OMI	AI N7 + EP	AI N7+EP+O	AOD MERRA-	AOD MERRA- 2
		2000-18	1979- 1992	1996-2001	2005 - 18	1979...20 01	1979...20 18	1980- 2018	1980-2018
1	Air Temp CSEAP Area MERRA-2 650 hPa	0.63	0.08	0.59	0.67	0.25	0.16	0.31	0.37
2	CSEAP Area Omega	0.92	0.79	0.98	0.68	0.74	0.71	0.80	0.78
3	NOAA TWI	-0.71	-0.73	-0.97	-0.63	-0.80	-0.62	-0.87	0.88
4	SST Niño 3.4	0.77	0.67	0.92	0.61	0.73	0.63	0.75	0.75
5	SST Niño 1 and 2	0.77	0.67	0.98	0.71	0.88	0.73	0.79	0.78
6	SOI	-0.74	-0.76	-0.87	-0.65	-0.65	-0.60	-0.75	-0.73
7	ONI	0.76	0.65	0.93	0.61	0.73	0.63	0.74	0.77
8	SST SEAP Area	-0.67	-0.83	-0.83	-0.33	-0.75	-0.65	-0.70	-0.58
9	Rainfall CSEAP Area	-0.68	-0.79	-0.84	-0.58	-0.57	-0.55	-0.65	-0.68
10	NOAA Interpl'd OLR	0.87	0.83	0.97	0.62	0.75	0.69	0.82	0.74

1301

1302

c	Annual – Correlations								
		AOD Terra	AI N7	AI E Probe	AI OMI	AI N7 + EP	AI N7+EP+O	AOD MERRA-	AOD MERRA-2
		2000-18	1979- 1992	1996-2001	2004 - 18	1979...20 01	1979...201 8	1980- 2018	1980-2018
1	CSEAP Area Omega	0.81	0.25	0.99	0.50	0.35	-0.13	0.75	0.71
2	NOAA TWI	-0.62	-0.54	-0.95	-0.85	-0.50	0.09	-0.79	0.74
3	SST Niño 3.4	0.67	0.47	0.95	0.82	0.38	0.11	0.73	0.70
4	SST Niño 1 and 2	0.58	0.36	0.85	0.63	0.55	0.06	0.61	0.59
5	SOI	-0.60	-0.45	-0.93	-0.66	-0.30	0.16	-0.73	-0.76
6	ONI	0.53	0.38	0.88	0.76	0.26	0.00	0.72	0.59
7	SST SEAP Area	-0.41	-0.07	-0.64	0.20	0.19	0.59	-0.47	-0.40
8	Rainfall CSEAP Area	-0.31	0.06	-0.64	0.06	-0.15	0.67	-0.42	-0.47
9	NOAA Interpl'd OLR	0.60	0.48	0.94	0.21	0.49	-0.35	0.70	0.60

1303
1304

1305
1306

d									
Annual Detrended using PAST 3 – Correlations									
		AOD Terra	AI N7	AI E Probe	AI OMI	AI N7 + EP	AI N7+EP+O	AOD MERRA-	AOD MERRA- 2
		2000-18	1979- 1992	1996-2001	2004 - 18	1979...20 01	1979...20 18	1980- 2018	1980-2018
1	CSEAP Area Omega	0.81	0.80	0.99	0.71	0.77	0.37	0.74	0.70
2	NOAA TWI	-0.62	-0.77	-0.91	-0.68	-0.81	-0.21	-0.79	0.74
3	SST Niño 3.4	0.67	0.67	0.91	0.76	0.76	0.36	0.74	0.74
4	SST Niño 1 and 2	0.60	0.68	0.80	0.53	0.73	0.16	0.62	0.61
5	SOI	-0.60	-0.75	-0.89	-0.66	-0.75	-0.30	-0.72	-0.75
6	ONI	0.53	0.61	0.82	0.69	0.69	0.35	0.65	0.61
7	SST SEAP Area	-0.41	-0.56	-0.69	-0.05	-0.57	-0.37	-0.50	-0.41
8	Rainfall CSEAP Area	-0.31	-0.70	-0.47	-0.45	-0.32	-0.03	-0.40	-0.45
9	NOAA Interpl'd OLR	0.61	0.83	0.92	0.64	0.71	0.25	0.69	0.63

1307 Figure 11: Correlations of (a) and (c) time series and (b) and (d) detrended time series of AOD and AI over the CSEAP Area
 1308 with characteristics of ENSO in SON (a) and (b) and annual (c) and (d). The last column AOD MERRA-2 & MERRA-2 uses only
 1309 aerosol and other data from the MERRA-2 reanalysis data set.

1310 Air temp from MERRA-2 dataset at 650hPa. MERRA-2 MERRA-2 at 900 hPa.

1311 MERRA-2 & MERRA-2 Easterly Wind Component is normally negative and reduces in El Niño periods - a positive increase c.f. the
 1312 NOAA TWI which reduces under the same circumstances.

1313 EP AI data was detrended using PAST 3 by excluding 1997 from the data set and reinserting it after detrending to avoid inserting a
 1314 significant trend in the detrending process due to the extreme values of the EP data in 1997, the short duration and the proximity of
 1315 1997 to the start date.

1316 **3.2.1 Air Temperature CSEAP Area**

1317 Figure 11 (a), (b) (1) shows that when the SEAP exists the air temperature at 650 hPa
1318 rises and this correlation confirms that the SEAP is absorbing solar radiation and heating the
1319 upper atmosphere thereby contributing to the temperature inversion compared with periods when
1320 the SEAP does not exist.

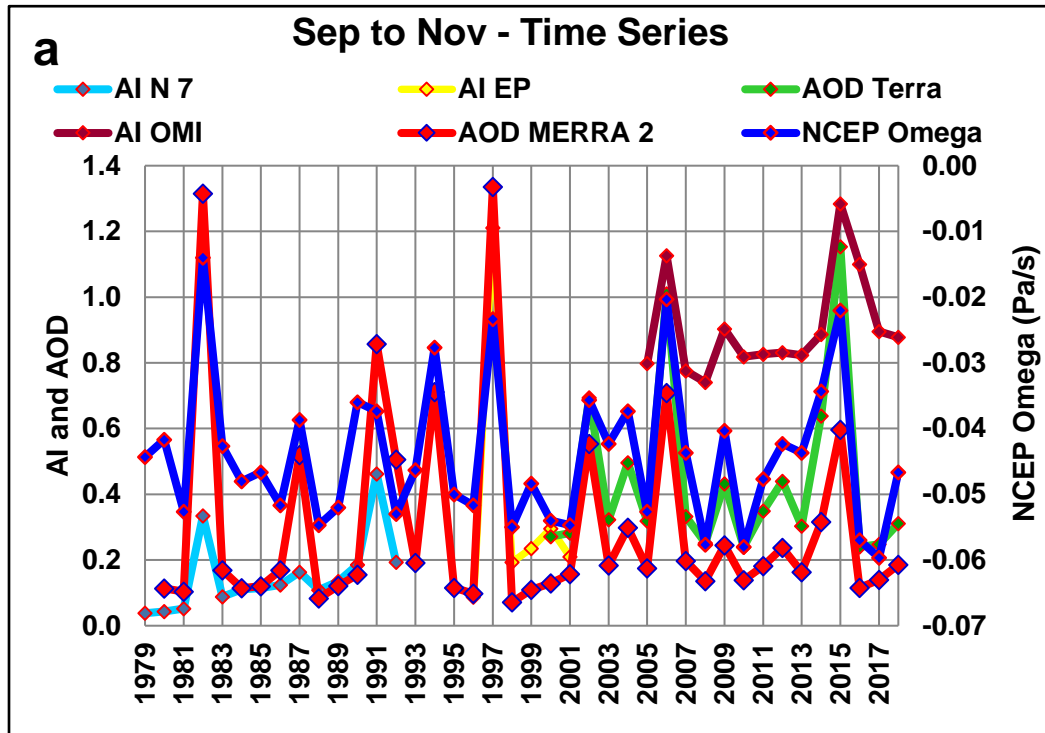
1321 **3.2.2 SEAP Area SST and Rainfall**

1322 During an ENSO event the SEAP Area is prone to reduced rainfall and a cooler SST.
1323 These characteristics are shown to correlate with the AI/AOD of the SEAP in Figure 11.

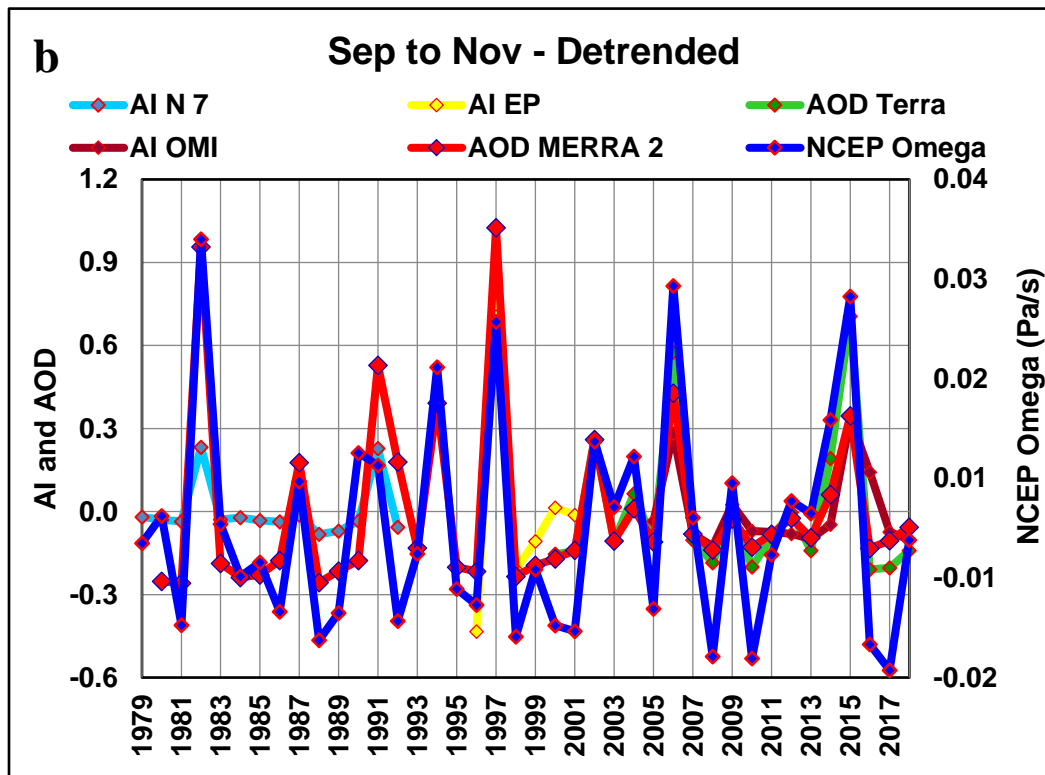
1324 **3.2.3 Convection in the CSEAP Area**

1325 *Tosca et al.* [2015] investigated the effects of anthropogenic aerosols in West Africa and
1326 reported that anthropogenic aerosols in the tropics limit convection, dry the region under the
1327 plume and enable increased fire activity via human ignition due to a positive feedback effect.
1328 This paper also shows a reduction in convection when an aerosol plume exists and the CSEAP
1329 Area AOD and AI is correlated with the NCEP/NCAR reanalysis omega at the 400hPa level in
1330 the same area (Figure 11). Omega is a measure of vertical velocity in the atmosphere positive
1331 values indicate falling motion and negative values rising. A reduction in convection produces an
1332 increase in omega and if an increase in aerosols results in a decrease in convection the
1333 correlations will be positive. The Terra AOD correlates at 0.86 average magnitude and <0.01
1334 significance. The N7, EP and OMI AI data show similar results. The N7 data correlates at lower
1335 magnitudes due to the lower levels of AI in the early part of the N7 data when the effects of the
1336 SEAP would have been greatly reduced. Figure 12 shows graphs of the data.

1337



1338



1339

1340

1341

Figure 12: Average SON CSEAP Area AOD and AI and NCEP Omega (a) time series and (b) detrended using PAST 3.

1342 3.2.4 Trade Wind Speed

1343 The NOAA TWI in Figure 11 (2, 3) shows a significant negative correlation with the AI
1344 and AOD data implying that the Trade Winds and therefore the Walker circulation relax when
1345 the SEAP exists, a primary requirement for the onset of an ENSO event.

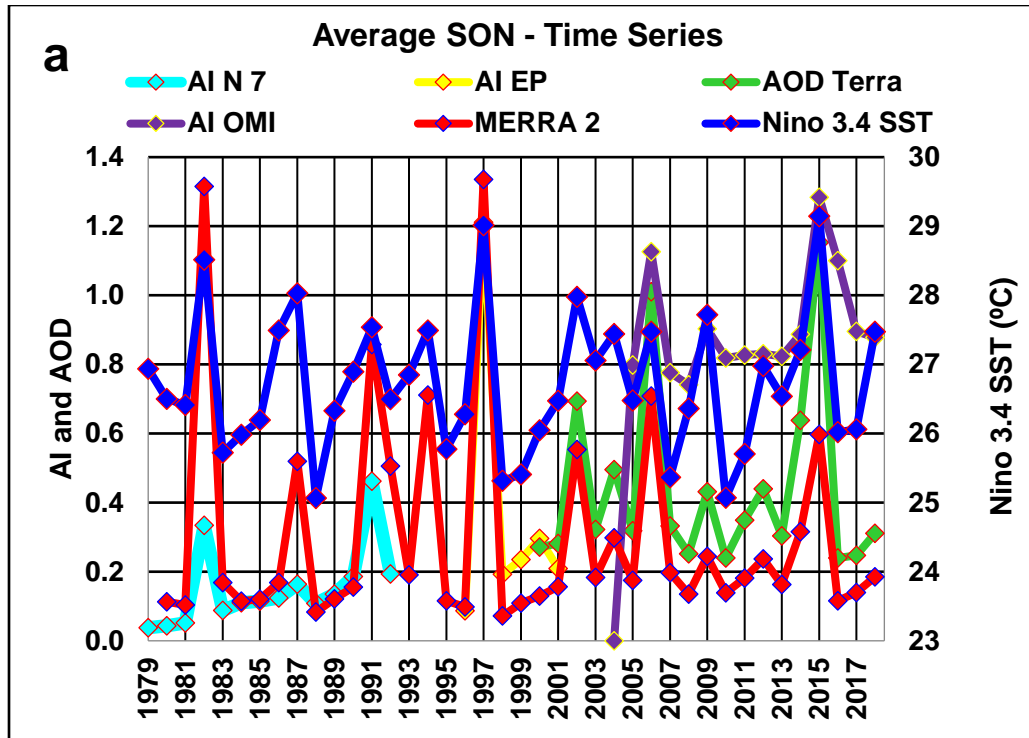
1346 3.2.5 Niño Areas SST and the SOI

1347 The prime indices used to monitor the onset and progress of an ENSO event are the SST
1348 in the Niño 1+2 and 3.4 areas and the SOI. Figure 11 shows that all these indices correlate with
1349 the AI and AOD of the SEAP and when the SEAP exists the Niño 1+2 and 3.4 area SST rises
1350 and the SOI declines – both of which indicate an ENSO event exists. Figure 13 shows AI, AOD
1351 and Niño 3.4 SST. Figure 14 shows the SOI data.

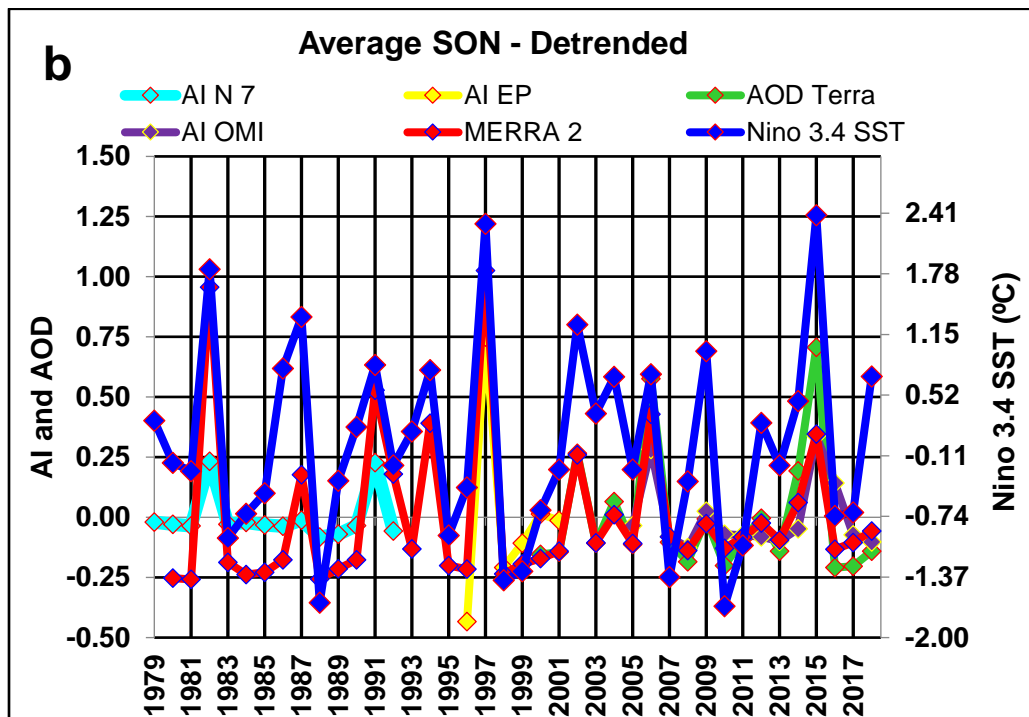
1352 The ONI also shows the same characteristics.

1353

1354



1355



1356

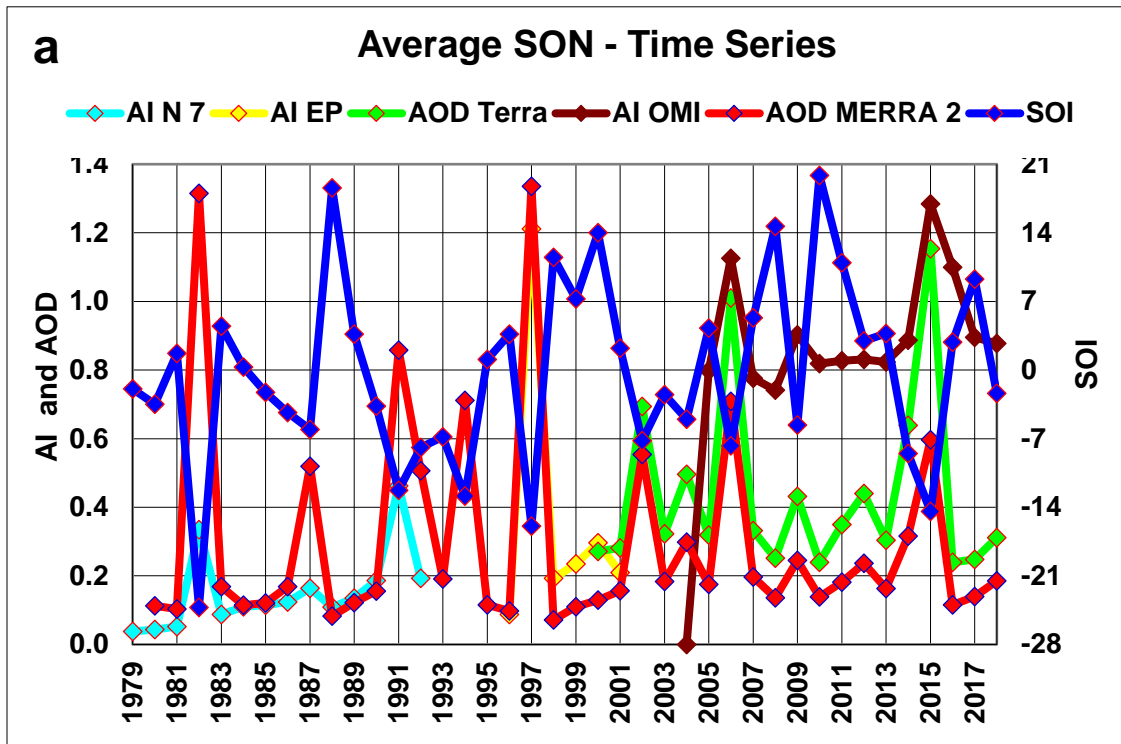
Figure 13: Average SON AOD and AI CSEAP Area and Niño 3.4 SST. (a) time series (b) detrended using PAST 3.

1357

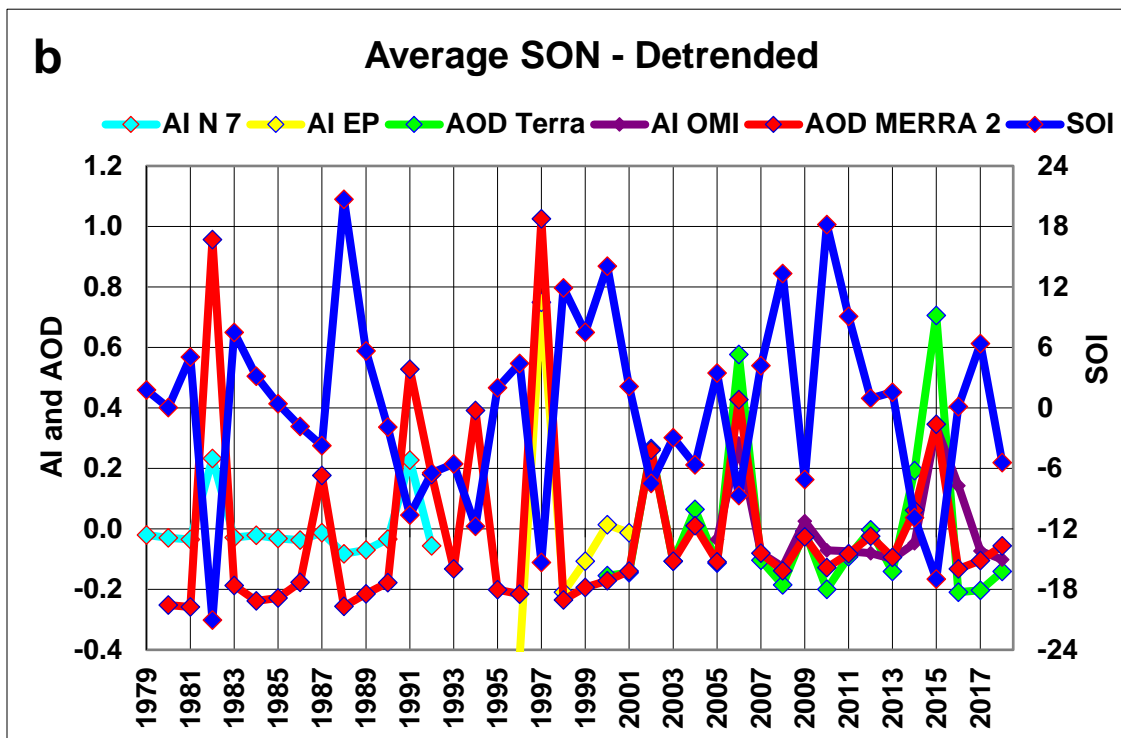
1358

1359

1360



1361



1362

1363 Figure 14: Average SON AOD and AI CSEAP Area and BOM SOI. (a) time series (b)
 1364 detrended using PAST 3.

1365 **3.2.6 Outgoing Longwave Radiation**

1366 The CSEAP Area OLR correlates positively with the AI and AOD of the SEAP implying
1367 that the level of radiation at the surface of the SEAP Area reduces. In October 2015 the level of
1368 OLR was 244 W/m² compared with 209 W/m² in October 2016, a low month of CSEAP Area
1369 AOD.

1370 **3.3 Volcano Data**

1371 The level of VEI Tephra (VEIT) was calculated as shown in Appendix A.

1372 **3.3.1 Tephra, ENSO and CSEAP Area Convection**

1373 The anthropogenic SEAP has only existed in its current form since about 1980 (Figure 6,
1374 Appendix A) and as ENSO events have occurred for centuries the driver of historic ENSO events
1375 must be the natural SEAP which is created by volcanic eruptions (Appendix A).

1376 Previous reported research failed to find a generally accepted link between volcanic
1377 eruptions and ENSO for two reasons:

- 1378 1. In general, only large eruptions were considered and smaller eruptions which only eject
1379 tephra into the troposphere were ignored; and
- 1380 2. A global analysis was undertaken rather than a specific geographic focus on the SEAP
1381 Area which is the only area which can create and sustain an ENSO event because of its
1382 location in the region which drives convection and therefore the entire non-ENSO Walker
1383 Circulation.

1384 In this paper I report the correlation of the volcanic ash plumes emanating from within
1385 the SEAP Area, on a monthly segmented basis with two of the ENSO indices described in the
1386 IPCC AR5:

- 1387 1. The Niño 3.4 SST; and
- 1388 2. The SOI; and with
- 1389 3. SEAP Area omega, vertical velocity in the atmosphere from the NCEP reanalysis;
- 1390 4. The HADCRUT4 global temperature [*Morice et al.*, 2012]; and
- 1391 5. Four monsoon indices

1392 The correlations together with the relevant time periods are shown in Figure 15. The VEIT
1393 correlations show the same effects as the satellite and modelling data when the level of tephra
1394 ejected by the volcanoes in the SEAP area increases: the Niño 3.4 SST rises and the SOI
1395 decreases – both of which being indicative of an ENSO event; CSEAP Area omega and the
1396 global temperature increases and the monsoon indices fall. Figures 16, 17 and 18 show graphs of
1397 the data.

1398

1399

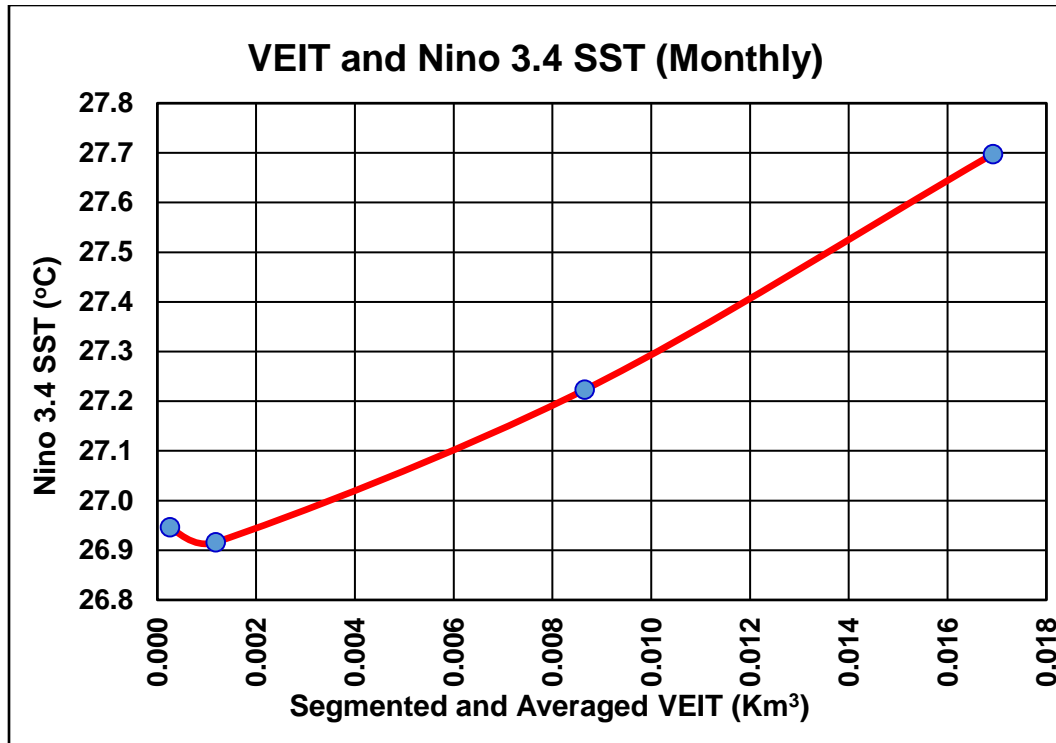
Correlations of VEIT (Monthly Segmented)		
Index	Correlation	Period
Niño 3.4 SST	0.99	1870 – 2018
SOI	-0.99	1876 – 2018
HADCRUT4 Global Temp Anomaly	1.00	1870 - 2018
Omega (400 hPa) (CSEAP Area)	0.98	1948 – 2018
Pre 1980 (Monthly Segmented)		
Niño 3.4 SST	0.98	1870 – 1979
SOI	-1.00	1876 - 1979
HADCRUT4 Global Temp Anomaly	1.00	1870 - 1979
Omega (400 hPa) (CSEAP Area)	0.94	1948 – 1979
Correlations Monsoon Index (Annual Average VEIT)		
Indian Summer	-0.98	1948 - 2018
Western North Pacific	-0.98	1948 - 2018
Webster and Yang	-0.94	1948 - 2018
Australian	-0.99	1948 - 2018

Figure 15: Correlations of segmented and averaged SEAP Area VEIT with indices shown. IPCC Indices highlighted in red.

1400

1401

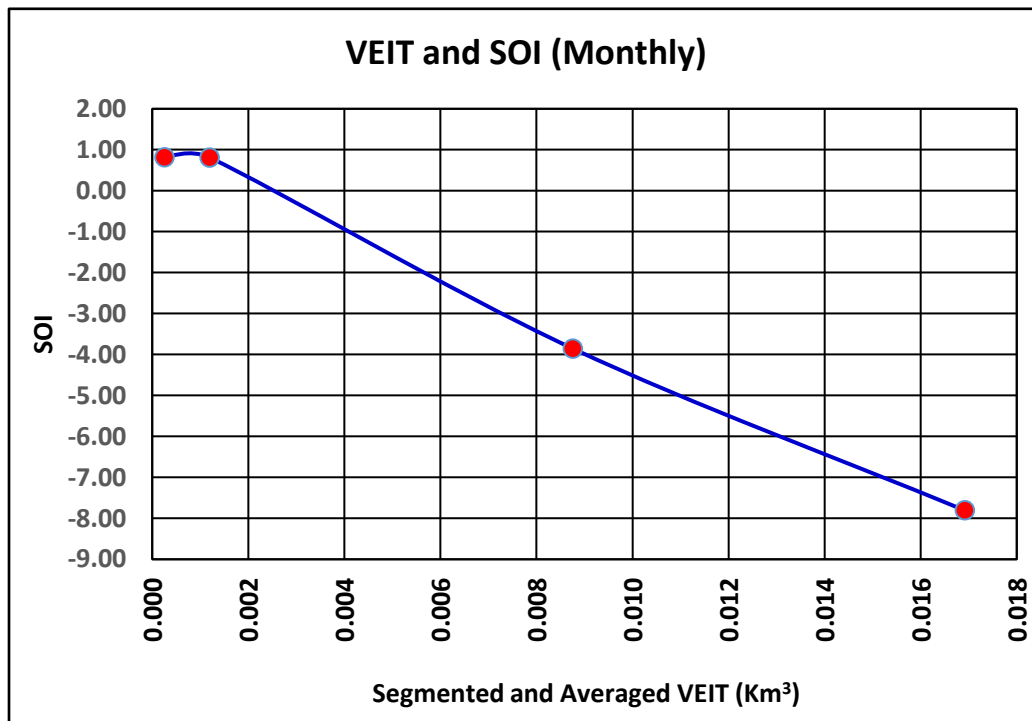
1402



1403

1404 Figure 16: Monthly Segmented and Averaged Niño 3.4 SST and VEIT from Volcanoes in
1405 the SEAP Area. 1870 to 2018

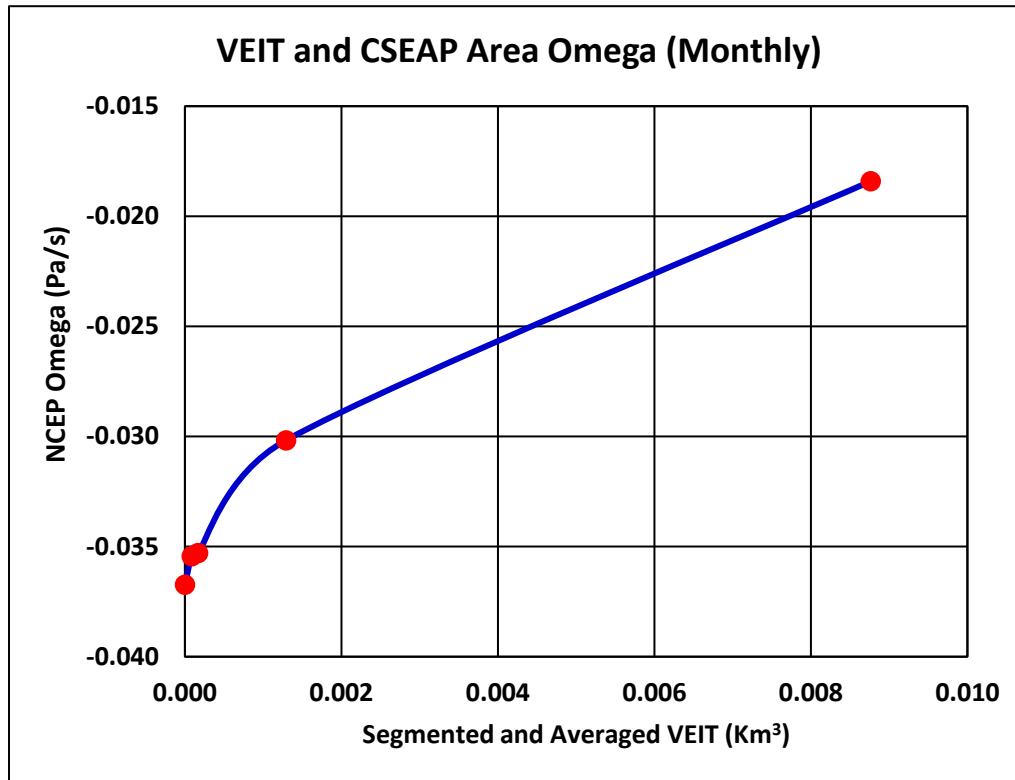
1406



1407

1408 Figure 17: Monthly Segmented and Averaged BOM SOI and VEIT from Volcanoes in
1409 the SEAP area. 1876 to 2018.

1410



1411

1412 Figure 18: NCEP/NCAR Reanalysis CSEAP Area segmented and averaged Monthly
 1413 Omega and VEIT 1948 to 2018.

1414 Figure 15 includes correlations using only data prior to 1980 to demonstrate the volcanic
 1415 connections to ENSO without the contamination of the anthropogenic SEAP in SON which the
 1416 AI/AOD data and Figure 6 shows is much lower in intensity in 1979 and probably did not exist
 1417 in its extreme form prior to this date. Indeed the Representative Concentration Pathways
 1418 inventory version 2.0.5 of Asian black carbon emissions at
 1419 <http://tntcat.iiasa.ac.at/RcpDb/dsd?Action=htmlpage&page=compare> confirms this as from 1850
 1420 to 1950 the emissions from land use change (deforestation), the major source of the SEAP, did
 1421 not change at 0.063 ± 0.02 Tg/year and from 1950 to 1970 increased by 300% [Mieville *et al.*,
 1422 2010].

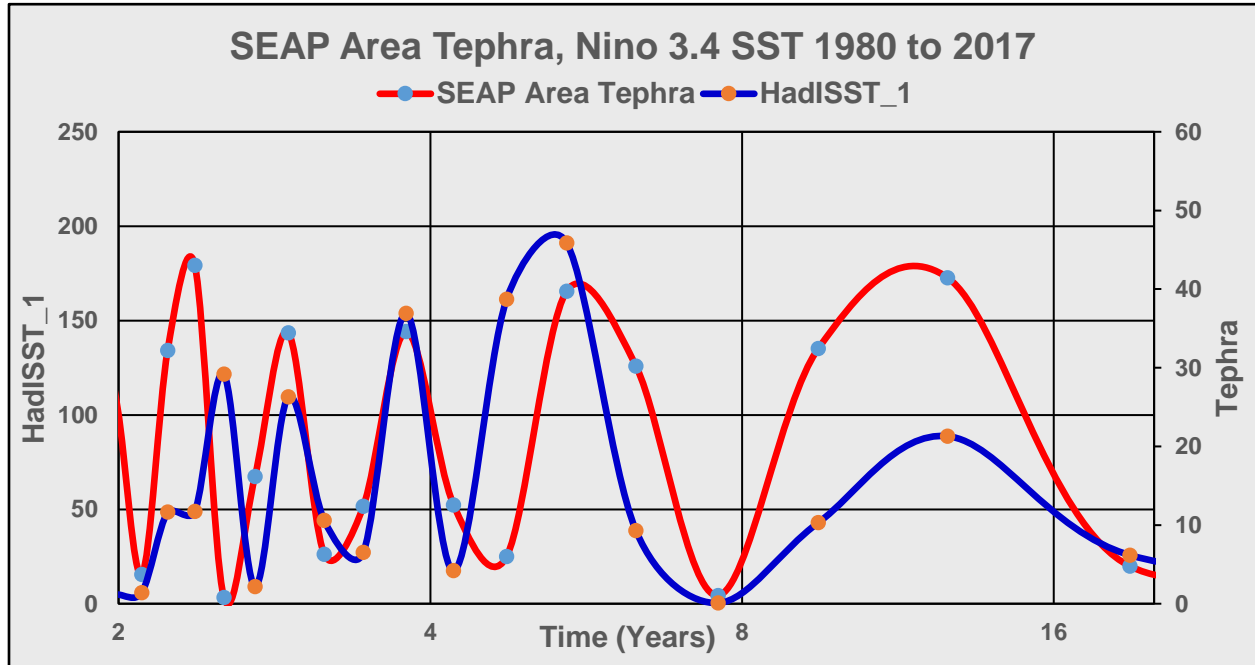
1423 3.3.2 ENSO Return Frequency

1424 In the introduction it was noted in Figure 1 that the ENSO power spectra for the LME
 1425 and HadISST_1 data are very different. The reason is that none of the forcings applied in the
 1426 LME runs included forcing by the natural SEAP at the required resolution.

1427 Figure 19 shows XLSTAT periodograms for the HadISST_1 and SEAP Area tephra data
 1428 from 2 to 19 years with the time axis displayed on a logarithmic scale (base 2) as a linear scale
 1429 compresses the higher frequencies (2 to 5 years) making the comparison difficult. This analysis
 1430 is for the same period as the HadISST_1 in Figure 1, 1980 to 2017, and the spectra are very
 1431 similar with the same number of peaks and troughs which are closely coincident. This similarity

1432 should be compared with the LME data in Figure 1 which shows only one dominant peak at
 1433 about 5 years.

1434 Given the uncertainty in the tephra data which is based on GVP VEI data available as
 1435 integer values on a logarithmic scale the similarity of the spectra in Figure 19 is impressive.



1436
 1437 Figure 19: SEAP Area XLSTAT periodogram for the Nino 3.4 SST and SEAP Area
 1438 Tephra from 1980 to 2017

1439
 1440 **3.3.3 Monsoon Indices**

1441 It was recognized by Sir Gilbert Walker a century ago that there was a connection
 1442 between the Indian monsoon and the SOI and many subsequent papers have explored the
 1443 relationship e.g. [Shukla and Paolino, 1983] , [Maraun and Kurths, 2005] and [Cook et al.,
 1444 2010]. With the high correlations between the volcanic tephra ejected within the SEAP Area and
 1445 ENSO (Nino 3.4 SST and the SOI) four Asian monsoon indices were also correlated with the
 1446 volcanic tephra on an annual basis. The correlations are for the same year for both annual VEIT
 1447 and the monsoon index except for the Australian monsoon index which covers December to
 1448 February where the tephra is the average of the year of the first month of the index. The indices
 1449 used are:

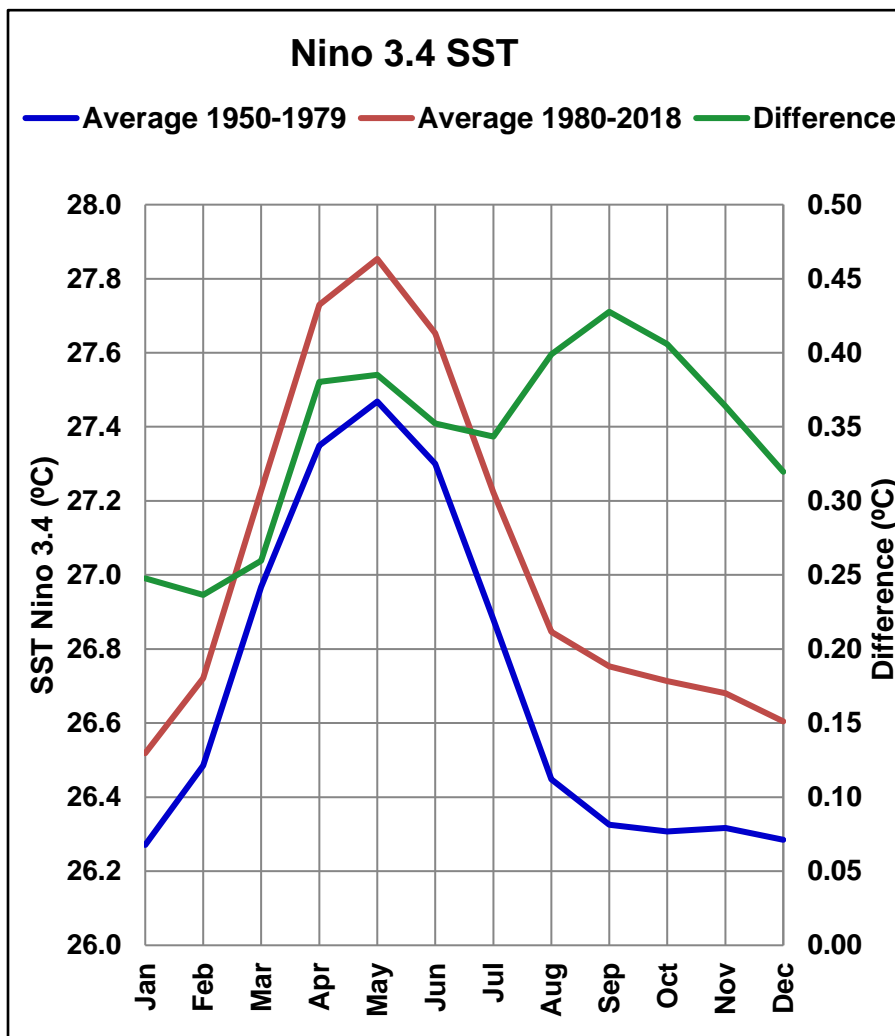
- 1450 1. Indian monsoon index (U850 (5°N -15°N, 40°E-80°E) – U850 (20°N -30°N, 70°E-90°E)
 1451 [Bin Wang and Fan, 1999]
- 1452 2. Webster-Yang monsoon index (U850-U200 averaged over 0-20°N, 40°E-110°E [Webster
 1453 and Yang, 1992]
- 1454 3. East Asia-WNP monsoon index (U850 (5°N -15°N, 100°E-130°E) – U850 (20°N -30°N,
 1455 110°E-140°E) [Bin Wang et al., 2001]

1456 4. Australian monsoon index (U850 averaged over 5°S-15°S, 110°E-130°E [Kajikawa *et al.*,
1457 2010].

1458 The data was calculated using the NCEP reanalysis dataset and the results are in Figure
1459 15.

1460 **3.4 Recent Change in ENSO Character**

1461 ENSO has become more intense in recent decades as Figure 20 demonstrates using the
1462 Nino 3.4 SST which has risen by over 0.3°C in recent decades and especially in Aug-Nov when
1463 the anthropogenic SEAP is at its peak. From the hypothesis: the general rise in all months is due
1464 to the increase in the levels of both the natural and anthropogenic SEAP as Appendix A and
1465 Figure 6 show; and the anomalous rise from Aug to Nov is entirely due to the anthropogenic
1466 SEAP.



1467

1468

1469 Figure 20: NCEP Reanalysis Nino 3.4 SST showing changes in the averages from 1950-
1470 79 and 1980-2018.

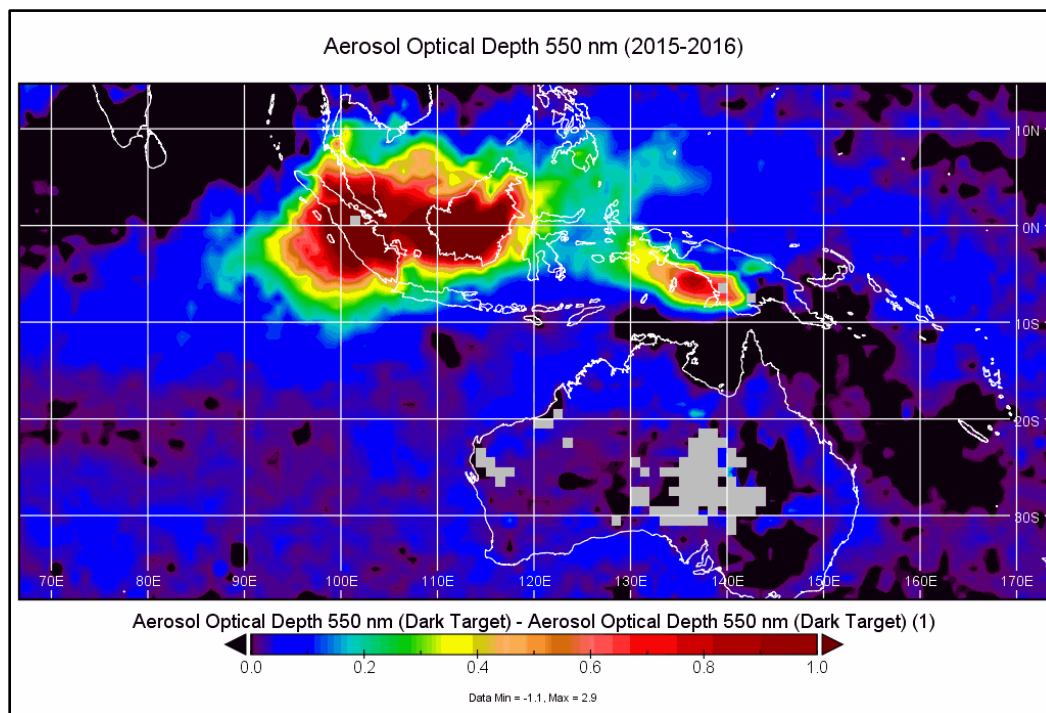
1471

1472 **4 MECHANISMS FOLLOWING THE HYPOTHESIS AND PHYSICAL MODEL**

1473 The changes wrought on climate by extreme events can be shown visually by subtracting
1474 a “normal” year from the “extreme” year in a particular measurement. In this case 2015 was an
1475 extreme year for the AOD of the SEAP Area and 2016 was a “normal” year (Figures 4 and 6)
1476 and this section follows the steps outlined in the hypothesis and physical model using this
1477 technique. It is important to acknowledge that other events in 2015 and 2016 may also have
1478 affected the visualisation results, however as the visualisations show exactly the same effects as
1479 the segmented data and correlations these images are considered to be a reasonable
1480 demonstration of the effects of the SEAP in 2015. The images shown were assembled from the
1481 NCEP/NCAR Reanalysis directly and from the MERRA-2 dataset using NASA Panoply.

1482 **4.1 The SEAP Forms**

1483 The SEAP AOD in SON 2015 was at extreme levels and Figure 21 shows the variation
1484 from the “normal” 2016.



1485

1486 Figure 21: Terra AOD SON 2015-2016

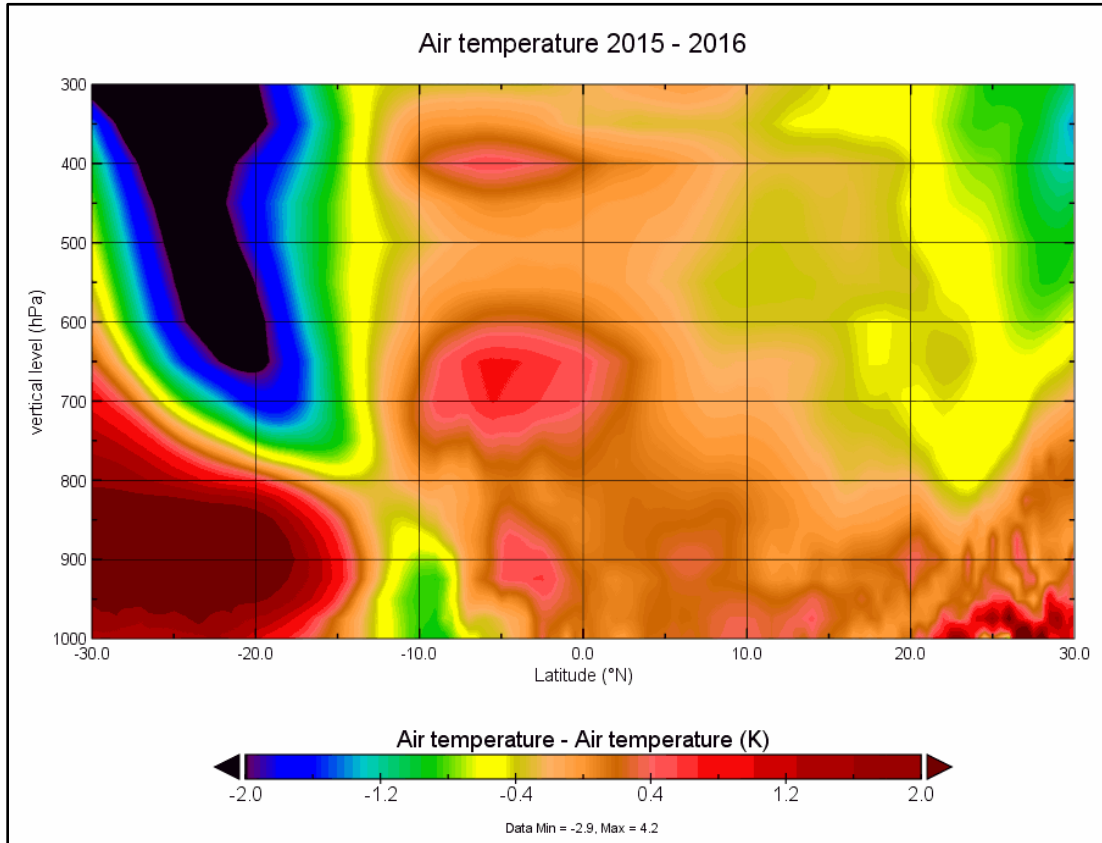
1487

1488

1489

1490 **4.2 Aerosols absorb solar radiation heating the atmosphere**

1491 The SEAP both absorbs and reflects solar radiation which warms the upper atmosphere
1492 as demonstrated in Figure 22 where the atmospheric temperature at 400 and 650 hPa has risen by
1493 about 0.5 and 1.0°K.



1494

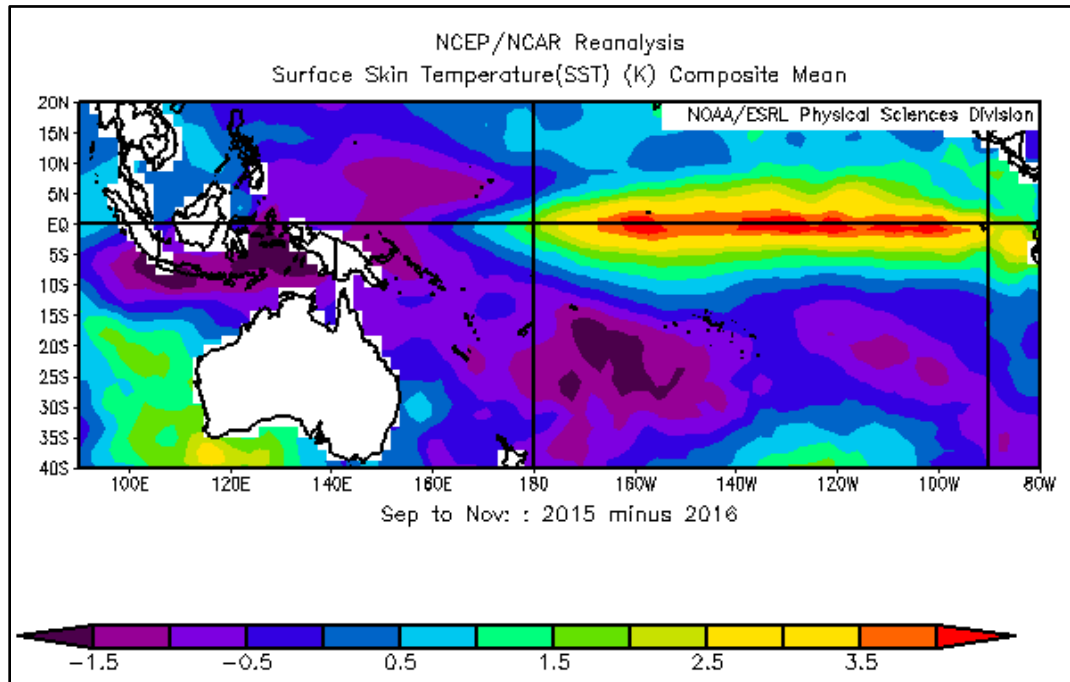
1495 Figure 22: MERRA-2 SON Air Temperature 2015-2016 (Panoply) averaged across the
1496 CSEAP Longitudes

1497

1498

1499 **4.3 Aerosols reduce surface solar radiation cooling the surface**

1500 Figure 23 shows nearly all the SEAP Area sea surface is cooler except the extreme north
1501 and west by over 1°K.

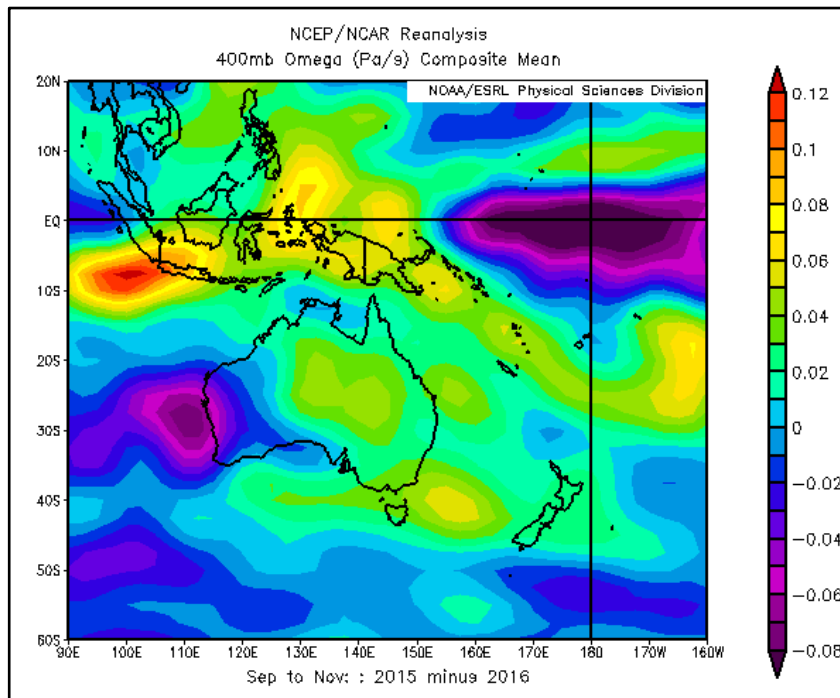


1502

1503 Figure 23: NCEP/NCAR Reanalysis SON SST 2015 - 2016.

1504 **4.4 This creates a temperature inversion which reduces convection**

1505 The effects of aerosols on convection and atmospheric circulation have been extensively
1506 described in the literature as discussed in the introduction. The SEAP absorbs solar radiation
1507 which warms the upper atmosphere and reduces solar radiation at the surface which cools the
1508 lower atmosphere. This alters the vertical temperature profile of the atmosphere with warmer air
1509 above cooler air (relative to the temperatures without the plume) and this stabilises the
1510 atmosphere and reduces convection. This well understood process is confirmed in the SEAP
1511 Area in this paper with the demonstrated correlation of omega with the AOD, AI and ejected
1512 volcanic ash in the area in Figures 8, 9, 11 and 15 and in Figure 24 where nearly all the SEAP
1513 Area is affected except the extreme north and west with omega increasing by up to 0.12.

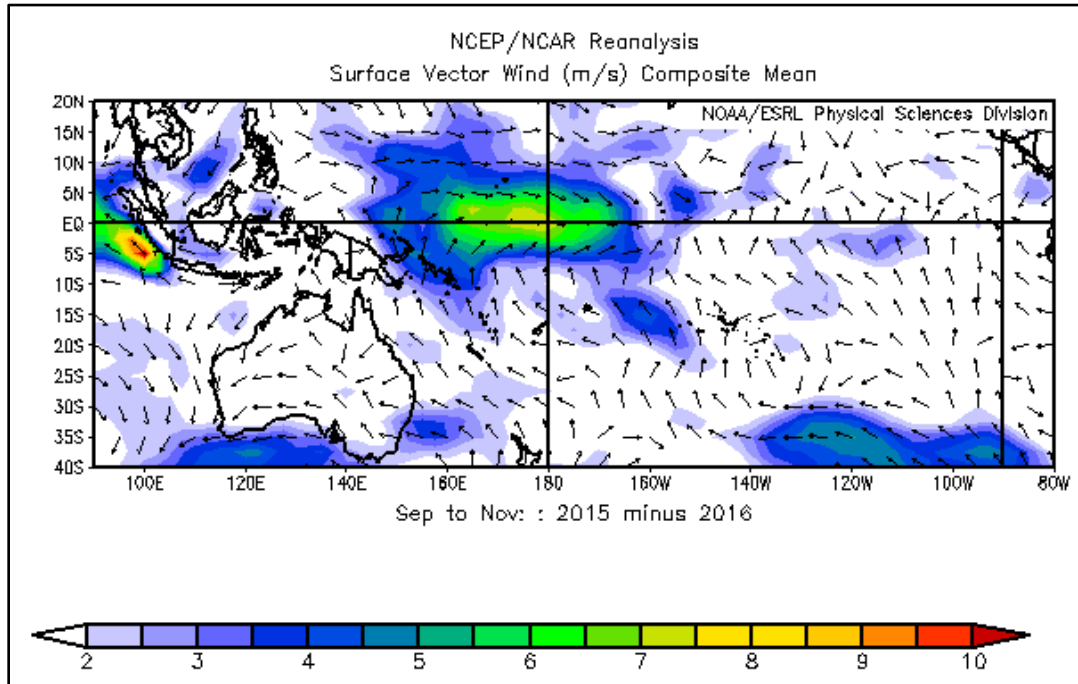


1514

1515 Figure 24: NCEP/NCAR SON omega (400 mb level) 2015-2016

1516 **4.5 Reduced convection in the SEAP Area causes the Trade Winds to relax**

1517 Figure 25 shows the changes in the surface vector winds caused by the SEAP in 2015. It
1518 is clear that the Trade Winds which normally blow east to west across the Pacific Ocean at about
1519 6m/s have effectively stalled near the equator and the dateline in 2015 as an inspection of the
1520 data in the individual years which make up Figure 25 confirms.



1521 Figure 25: NCEP/NCAR Reanalysis SON Surface Vector Wind 2015-2016
1522
1523

1524 **4.6 Reduced Trade Wind speed causes the Nino 3.4 and 1+2 SST to rise**

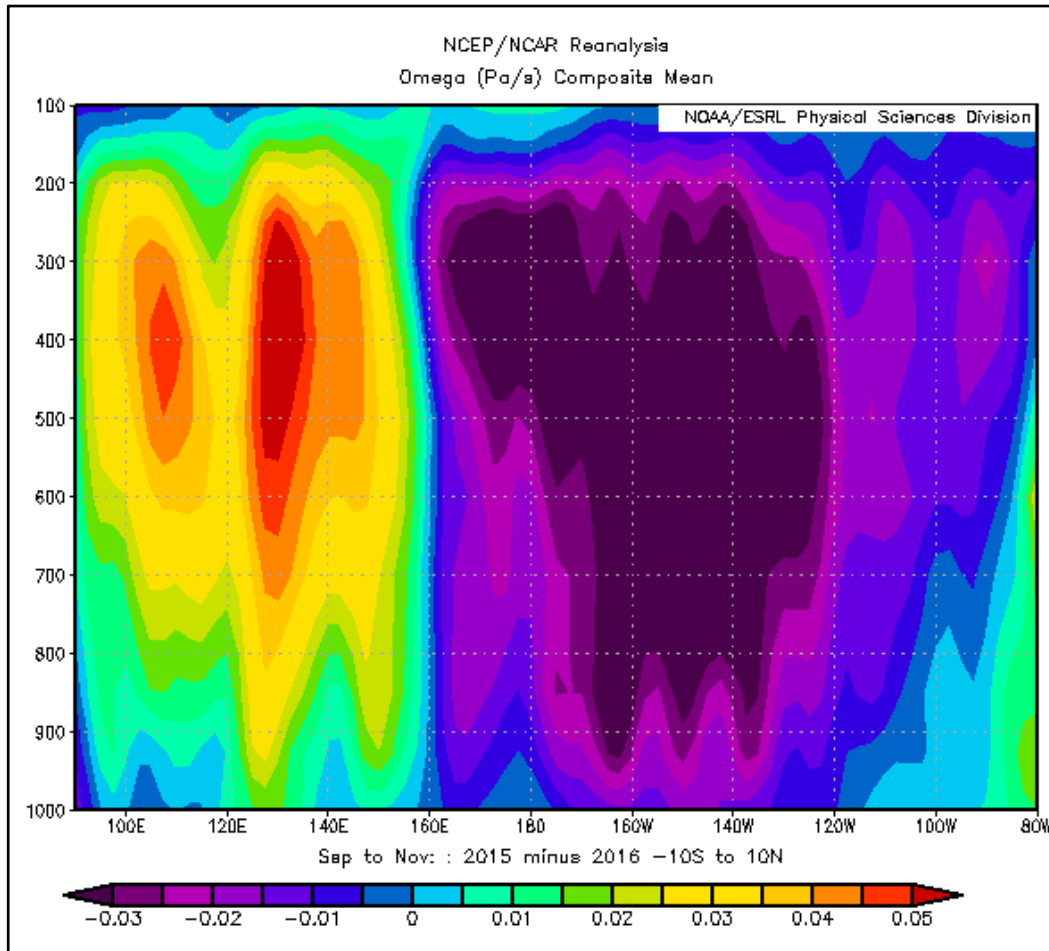
1525 Figure 23 shows a classic warm tongue extending from South America across the Pacific
1526 Ocean with the Nino 3.4 SON SST rising between 2 and 4+°K in 2015 compared to 2016 which
1527 clearly indicates an ENSO event is occurring.

1528 The Nino 1+2 also increases in Figure 23 by 1.5 to 3.5°K, a smaller increase than the
1529 Nino 3.4 Area

1530

1531 **4.7 Higher Nino 3.4 SST causes convection and the Walker circulation relaxes**

1532 Figure 26 shows a vertical cross section of omega from the NCEP/NCAR Reanalysis
1533 from the SEAP Area across the Pacific Ocean averaged across the SEAP Area latitudes. Clearly
1534 Omega has fallen across the Nino 3.4 region indicating increased convection and the opposite
1535 has occurred over the SEAP Area forcing the Walker Circulation to relax/reverse.



1536

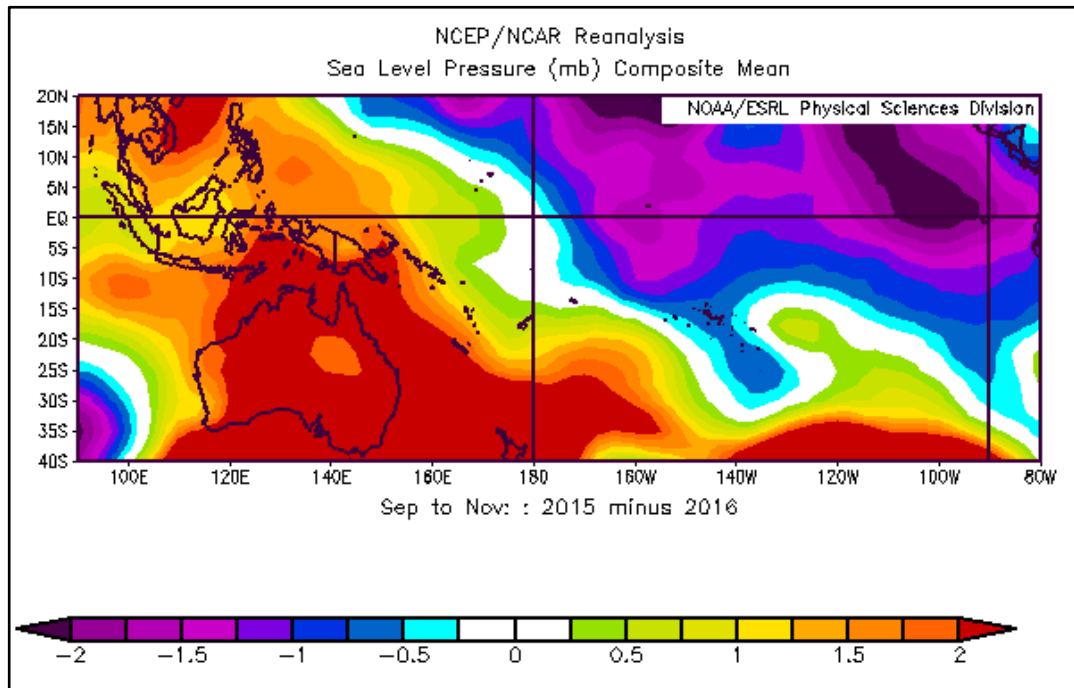
1537 Figure 26: NCEP/NCAR Reanalysis SON Omega averaged across the SEAP Latitudes
1538 2015-2016.

1539

1540

1541 **4.8 The SOI is forced into a negative phase by these changes**

1542 The increased convection in the central Pacific Ocean reduces surface pressure and the
1543 reduced convection in the SEAP Area raises surface pressure. Figure 27 clearly shows the
1544 increase in SLP in Darwin and a reduction in Tahiti which drove the SOI negative in 2015.



1545

1546 Figure 27: NCEP/NCAR Reanalysis SON Sea Level Pressure 2015 -2016

1547

1548 **5 CAUSATION ANALYSIS**

1549 It is clearly understood that correlation between events A and B does not prove causation
1550 from A to B or vice versa. Thus, the causal relationship between the SEAP and the ENSO must
1551 be demonstrated in other ways.

1552 **5.1 Volcanic Eruptions**

1553 The similarity of the power spectra of the Nino 3.4 SST and the SEAP Area tephra and
1554 the clear correlations between volcanic tephra in the SEAP Area and ENSO demonstrated in this
1555 paper show a close relationship exists between the two and since volcanic eruptions are caused
1556 by deep earth tectonic processes and cannot be caused by ENSO events the causal direction must
1557 run from the volcanic eruptions to ENSO.

1558 **5.2 Analysis without Correlation**

1559 Figure 10 shows that the LME Nino 3.4 SST rises by 3.01°C from 297.88°C to 300.89°C
1560 and the SOI falls from +8.65 to -12.4 reflecting accurately the range of these indices from La
1561 Nina to El Nino events without using correlation.

1562 **5.3 Modelling**

1563 **LME:** the LME data used in this paper is forced by the eight agents described above and,
1564 in this modelling, there is no mechanism to create aerosols in south east Asia during an ENSO
1565 event and hence the causal direction must run from the aerosols to the ENSO events.

1566 In addition, the aerosol forcings in all LME runs are fixed at 1850 values except for the
1567 “ozone and aerosol” and “all” runs and there can therefore be no forcing of the aerosols by any
1568 agent within these six runs and the causal direction must flow from the aerosols to the ENSO
1569 events.

1570 **LE:** Aerosols are included as forcing agents in the LE. However, aerosol levels are
1571 specified at decadal intervals in RCP 8.5 and ENSO cannot therefore force the SEAP Area
1572 aerosols on an annual basis and the causal direction must run from the aerosols to the ENSO
1573 events.

1574 **MERRA-2:** The MERRA-2 reanalysis assimilates measured aerosol data and as
1575 Appendix A shows the aerosol sources are volcanoes, gas flares and fires lit by the local
1576 population the causal direction must be from the aerosols to the ENSO events as the aerosols are
1577 assimilated and not generated within the model by ENSO.

1578 **5.4 Satellite Data and Recent Changes in the SEAP**

1579 Figure 20 clearly shown that the character of ENSO as measured by the Nino 3.4 SST has
1580 changed since 1980 when the extreme anthropogenic SEAP started to appear and with the high
1581 correlations of the anthropogenic SEAP in SON with ENSO it is clear that the change is driven

1582 by the SEAP and since Appendix A shows that the anthropogenic SEAP is caused by fires
1583 deliberately lit to clear land the causal direction must run from the SEAP to ENSO.

1584 **5.5 Seasonality of ENSO**

1585 ENSO is highly seasonal and this paper provides an explanation for the seasonality.
1586 Rainfall in the CSEAP area and the Nino 3.4 SST correlate at -0.59 significance <0.05 with the
1587 SST reducing when rainfall in the SEAP Area is high. This clearly supports the hypothesis that
1588 the SEAP is the major cause of ENSO events as the south east Asian monsoon rainfall washes
1589 the aerosols out of the atmosphere enabling convection to be re-established in the region to drive
1590 the Trade Winds and end the ENSO event.

1591 **5.6 Monsoon Indices**

1592 Three of the four monsoon indices in Figure 15 show a statistically significant
1593 relationship to the natural SEAP and since the monsoons cannot cause volcanic eruptions the
1594 causal direction must be from the volcanic tephra to the monsoon.

1595 **5.7 Multiple Independent Datasets**

1596 Seven of eight LME modelling runs (excluding the aerosol forced run as it correlates
1597 with the All forcing run) and the MERRA-2 reanalysis exhibit very low or negative correlations
1598 between the CSEAP AODVIS in the individual runs as shown in the correlation matrix in
1599 Appendix C with an overall average 0.0016. Hence the datasets are independent. The LE is
1600 excluded as the LE aerosols correlate with the LME ALL forcing run.

1601 All these seven LME and MERRA-2 datasets show correlations with the ENSO indices at
1602 significance of <0.01 or less and the chance that all these seven datasets show the same result
1603 and are wrong is the product of the significances i.e. 0.01^{-8} or 10.0^{-16} a vanishingly small
1604 number.

1605 **5.8 Companion Paper**

1606 The companion paper [K A Potts, 2020a] demonstrates that drought in south eastern
1607 Australia (SEAus) which has commonly been attributed the ENSO and/or IOD events is also
1608 caused by the SEAP further confirms the causal relationship flows from the SEAP to all these
1609 events as drought in SEAus cannot create SEAP Area aerosols .

1610 **5.9 Segmented Data**

1611 The climate is a chaotic system and my preferred way to analyse climate data is to
1612 segment, average and compare similar elements as the averaging process will improve the signal
1613 to noise ratio of the analysis. The annual LME AODVIS and ENSO data is segmented on the
1614 basis of the AODVIS data and then averaged and correlated. The three major ENSO indices
1615 when analysed in this way with the CSEAP AODVIS deliver R^2 values of 1.00 (Figure 10)
1616 demonstrating clearly that the SEAP is the major and possibly the only driver of ENSO events.

1617 **5.10 Causal Direction**

1618 Therefore with:

- 1619 7. The volcanic aerosols demonstrating conclusively that SEAP Area aerosols are the cause
1620 of ENSO events;
- 1621 8. The LME data showing a clear connection between the SEAP and ENSO indices without
1622 correlation;
- 1623 9. The LME and MERRA-2 time series analysis showing the same results with a
1624 vanishingly small chance of error;
- 1625 10. The LME data showing, by a preferred analysis method, extremely high correlations
1626 which leave no possibility of other drivers;
- 1627 11. The monsoon indices showing a clear connection to SEAP Area volcanic tephra;
- 1628 12. The support of four satellite datasets showing the same results;

1629 The inevitable conclusion is that the SEAP is the major driver of ENSO events and may
1630 even be the sole driver.

1631 **6 FUTURE RESEARCH**

1632 To finally confirm these conclusions, it is suggested that further LME style analyses are
1633 undertaken in which:

- 1634 1. An aerosol plume is created in the model which ramps up from the naturally low level in
1635 January to reach the same AOD as the extreme SEAP of October 2006 or 2015 in
1636 February, continues at the same level to October and ramps down in November to the
1637 naturally low level in December. This plume to be applied in the model with random
1638 returns from 2 to 10 years to mimic the actual return frequency of ENSO;
- 1639 2. Repeating 1 with reducing levels of AOD from February to October to determine the
1640 minimum AOD level over SE Asia which is required to cause an ENSO event.

1641 These analyses will confirm the conclusions in this paper and conclusively demonstrate
1642 that ENSO events are caused by the SEAP and determine the AOD levels required to do so.

1643 **7 CONCLUSIONS**

1644 The LME with 1.156 annual and 13,872 monthly time series data points, LE with 251
1645 years of data including 75 years of RCP 8.5 data, MERRA-2, measured aerosol datasets from
1646 four satellites and the GVP volcanic eruption data all confirm the direct connection between the
1647 SEAP and ENSO in multiple independent ways.

1648 Causal analysis showing that the relationship must flow from the SEAP to ENSO.

1649 Power spectra showing a clear, close relationship between the natural SEAP and the Nino
1650 3.4 area SST derived from the HadISST-1 datasets which is lacking in the LME data.

1651 Correlations of the LME and LE CSEAP Area AOD with Nino 3.4 TS and the SOI show
1652 average R^2 values for these two major ENSO indicators at 0.79 and 0.72 (time series) and 1.00
1653 (segmented) respectively.

1654 I therefore conclude that the SEAP is unique and based on these values is the major and
1655 possibly the sole trigger and sustaining agent for ENSO events and that the hypothesis is proved.

1656 This conclusion brings six important elements into climate change analysis:

1657 **First:** Aerosol Regional Dimming, the Surface Radiative Forcing caused by the annual
1658 apparitions of continental scale aerosol plumes, the anthropogenic elements of which did not
1659 occur before the middle of the 20th century, is an important, recent element driving climate
1660 change. The eight plumes noted in this paper both reflect and absorb/reradiate solar radiation at
1661 levels depending on their aerosol chemistry and affect the local hydrologic cycle and large scale
1662 atmospheric circulation systems such as the Hadley and Walker Cells as this paper and its
1663 companion [*K A Potts, 2020a*] demonstrate. These plumes mainly exist in the tropics and the
1664 effects only occur in the season in which the plume exist as the residence time of aerosols in the
1665 troposphere is short – the IPCC AR5 [*Stocker et al., 2013*] states “1 to 3 weeks” for volcanic
1666 aerosols.

1667 **Second:** The natural volcanic tephra plumes from all volcanic eruptions and not just large
1668 eruptions must be included in climate modelling as they are the prime cause of ENSO events and
1669 are therefore the primary climate forcing agent on an interannual basis;

1670 **Third:** All eight major continental scale, aerosol plumes shown in Figure 3 must be
1671 included in climate models as their effects are significant;

1672 **Fourth:** Climate models must incorporate these plumes at temporal and geographic
1673 resolutions which will adequately model their effects. Global and seasonal or annual averages are
1674 not sufficient as the climate forcing effects of the plumes only exist when the plume exists and
1675 the averaging process reduces the intensity of the plumes and destroys their seasonal effects.

1676 **Fifth:** Since the SEAP causes ENSO events it follows that this aerosol plume causes an
1677 increase in the global temperature, most likely through the modification of the large-scale
1678 atmospheric circulation systems (especially convection in SE Asia) instead of just cooling the
1679 region under the plume through direct surface forcing as is commonly assumed. It is also likely
1680 that the increases in the AI and AOD of the SEAP since 1980 in non-extreme years such as 1999
1681 and 2001 will also have affected the global temperature. This requires further investigation.

1682 **Sixth:** The effects of combinations of the eight anthropogenic, continental scale aerosol
1683 plumes require investigation as the combined effects of such plumes may be radically different to
1684 the effects of individual plumes.

1685 Finally I concur with *Booth et al. [2012]* that emissions of carbonaceous aerosols are
1686 directly addressable by government policy actions and suggest that this is an urgent necessity to
1687 mitigate future anthropogenic ENSO events in the Austral spring which *Timbal and Drosdowsky*
1688 [*2013*] link to drought in Australia.

1689 **8 APPENDIX A - SOURCES OF THE SOUTH EAST ASIAN AEROSOL PLUME**1690 **8.1 Biomass burning**

1691 Biomass burning in the tropics is part of the annual agricultural cycle and usually occurs
 1692 at the end of the dry season before the start of the local monsoon. In the SEAP Area the monsoon
 1693 commences in November and the biomass burning aerosol plume is at its most intense in SON.
 1694 The increase in biomass burning in the SEAP Area in recent decades has been driven by the
 1695 increasing population of the SEAP Area. The population of Indonesia, Malaysia and Papua New
 1696 Guinea has increased from 77 to 277 million between 1950 and 2010 (United Nations
 1697 <https://www.un.org/en/development/desa/population/publications/database/index.asp>). This
 1698 increasing population has forced: an increase in food production from tropical agriculture with
 1699 its attendant smoke/aerosols; and increased rainforest clearing to provide living space and
 1700 agricultural land. There has also been increasing levels of commercial activity including
 1701 rainforest logging. In SON in 1982, 1991, 1997, 2002, 2004, 2006, 2009, 2014 and 2015 the
 1702 AOD or AI increased significantly compared to the intervening years (Figure 6) due to the
 1703 clearing of the rainforest for palm oil plantations.

1704 *Applegate et al.* [2001] found that there were a number of direct causes of fire in the
 1705 1997-98 fires in Indonesia:

- 1706 • Fire being used to assist with land clearing;
- 1707 • Fire used as a weapon in land tenure or land use disputes;
- 1708 • Accidental or escaped fires;
- 1709 • Fire connected with resource extraction.

1710 Neither climate change nor ENSO events are identified as a primary cause of fire in
 1711 1997-98 and the other major fire events in 1982/1983, 1987, 1991 and 1994 although this is
 1712 commonly stated to be the case in the literature relating to ENSO events. ENSO is only noted as
 1713 a reason for the spread of fire started by the causes noted above in certain years.

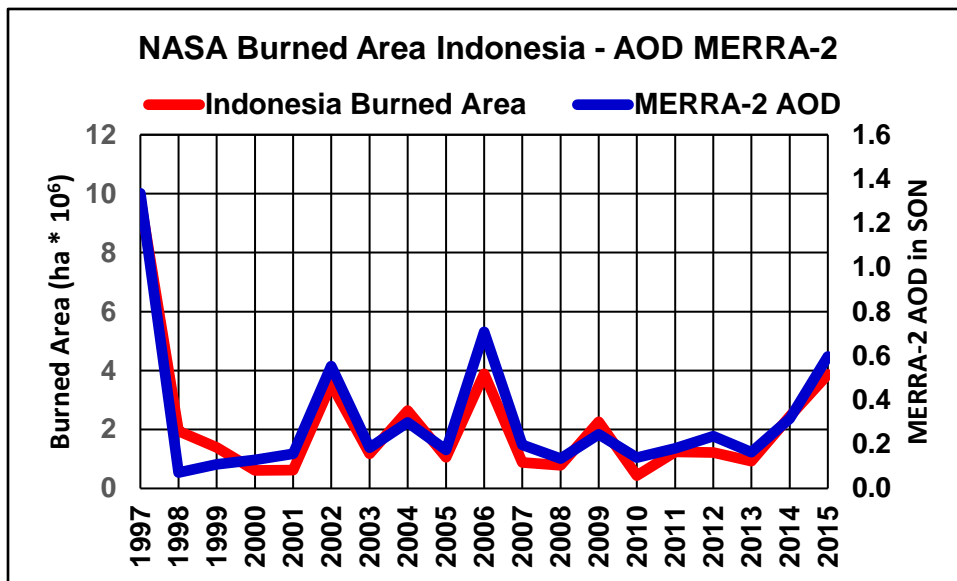
1714 The 6th International Wildland Fire Conference held by the United Nations International
 1715 Strategy for Disaster Reduction and their Food and Agriculture Organization in Korea, in 2015
 1716 released the Pyeongchang Declaration “Fire Management and Sustainable Development”
 1717 (<https://gfmc.online/allgemein/korea-2015.html>) which stated in the Regional Statement for
 1718 southeast Asia that “Most vegetation fires occurring in the member countries of the
 1719 Association of Southeast Asian Nations are due to human interventions, notably by local
 1720 communities and industrial corporations.”

1721 Reports in the popular press as well as governments in the region attribute the cause of
 1722 such fires to land clearing in Indonesia and on Nov 9 2006 Reuters reported “Environment
 1723 ministers from five Southeast Asian countries endorsed a plan of action on Thursday to fight
 1724 forest fires in Indonesia that have spread choking smoke across the region.” and “Indonesia's
 1725 neighbours have grown increasingly frustrated by the fires, most of which are deliberately lit by
 1726 farmers or by timber and palm oil plantation companies to clear land for cultivation.” In
 1727 September 2015 the Times in London reported that “Singapore has taken legal measures against
 1728 Indonesian businesses for the vast forest fires that are choking millions of people across
 1729 southeast Asia.” See CIFOR at

1730 [http://blog.cifor.org/37016/clearing-the-smoke-the-causes-and-consequences-of-](http://blog.cifor.org/37016/clearing-the-smoke-the-causes-and-consequences-of-indonesias-fires?fnl=en)
 1731 [indonesias-fires?fnl=en](http://blog.cifor.org/37016/clearing-the-smoke-the-causes-and-consequences-of-indonesias-fires?fnl=en) which suggests that 115,000 were burning in Indonesia in October 2015.

1732 The connection between AOD in the CSEAP Area and fire is demonstrated in three ways:

1733 **One:** The burned areas in Indonesia from NASA at
 1734 [https://search.earthdata.nasa.gov/projects?p=C1457414586-SEDAC!C1457414586-](https://search.earthdata.nasa.gov/projects?p=C1457414586-SEDAC!C1457414586-SEDAC&q=burned%20area%20indonesia&tl=1563231391!4!!)
 1735 [SEDAC&q=burned%20area%20indonesia&tl=1563231391!4!!](https://search.earthdata.nasa.gov/projects?p=C1457414586-SEDAC!C1457414586-SEDAC&q=burned%20area%20indonesia&tl=1563231391!4!!) [Center for International Earth
 1736 Science Information Network - CIESIN - Columbia University, 2018] from 1997 to 2015 was
 1737 extracted. Correlating the MERRA-2 AOD in SON, the burning season, with the areas burned in
 1738 Indonesia gives 0.96. The data is shown in Figure 28
 1739



1740

1741

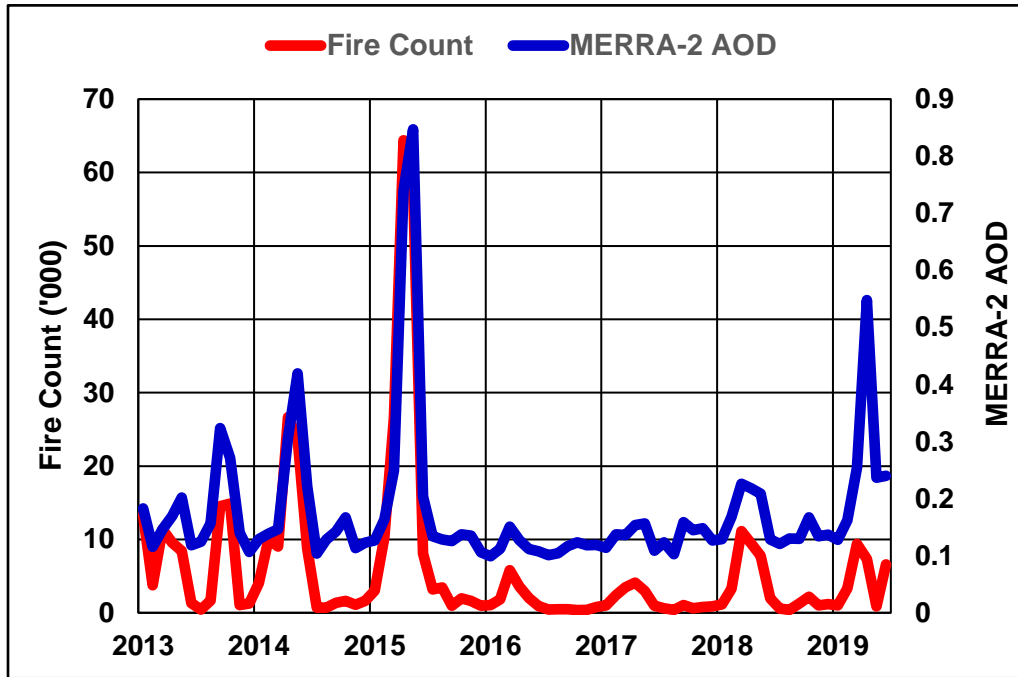
1742

1743

Figure 28: NASA MERRA-2 AOD in SON and Area Burned.

1744 **Two:** The Indonesian archived active fires (NASA) from August 2013 to 2019 from the
1745 Global Forest Watch at
1746 https://data.globalforestwatch.org/datasets/de1fe5832831464cbd64aaa8f2d54781_0/data

1747 was downloaded and the average number of fires locations each month were extracted
1748 which correlate with the MERRA-2 AOD at 0.95 (significance < 0.01) (Figure 29).
1749
1750
1751

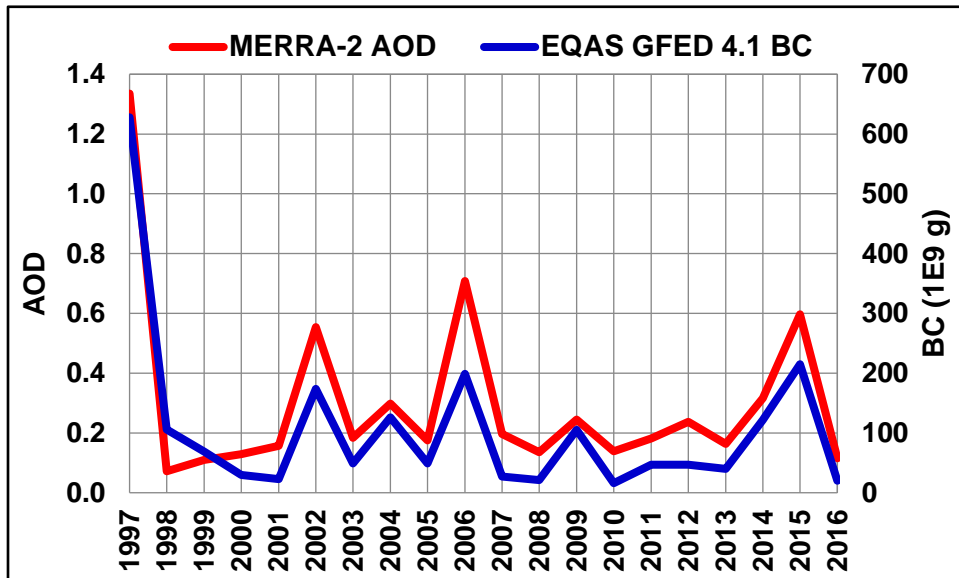


1752
1753 Figure 29: Indonesian Global Fire Watch Archived Fires (NASA) and NASA MERRA-2
1754 AOD

1755
1756

1757 **Three:** Correlating the Black Carbon (BC) Emissions from the Global Fire Emissions
 1758 Database (GFED4.1) [Randerson *et al.*, 2017] for the Equatorial Asian (EQAS) Region and of
 1759 similar extent to the SEAP Area) from fires at [https://daac.ornl.gov/cgi-](https://daac.ornl.gov/cgi-bin/dsviewer.pl?ds_id=1293)
 1760 [bin/dsviewer.pl?ds_id=1293](https://daac.ornl.gov/cgi-bin/dsviewer.pl?ds_id=1293) for the period 1997 to 2016 with the SON AOD of the CSEAP Area
 1761 gives 0.96. The data is shown in Figure 30.

1762



1763

1764 Figure 30: Equatorial Asian Region black carbon emissions from the GFED database 4.1
 1765 and the CSEAP Area SON MERRA-2 AOD.

1766 Together the burned area, fire and BC data show that the extreme AOD in SON in some
 1767 years was created by fire in south east Asia, mainly Indonesia.

1768

1769 **8.2 Gas Flares**

1770 Gas Flares in the oil production industry increased in number over recent decades as oil
1771 production in south east Asia (Indonesia, Malaysia, Thailand and Brunei) increased from
1772 567,000 to 2,087,000 barrels of oil per day between 1965 and 2018 (BP Statistical Review of
1773 World Energy 2019).

1774 The World Bank has established the GGFRP which estimates SE Asia flares 4.03 billion
1775 m³ of natural gas each year and the gas flare locations are shown in Figure 2. NOAA identifies
1776 about 387 flare locations in the SEAP Area. Images of such flares producing aerosols are easily
1777 found in Google Earth (Figure 31) or at the GGFRP web site.

1778

1779



1780

1781 Figure 31: LNG Badak. Credits: Left Ridho Akbari, Right Fauzi (from Google Earth)

1782

1783

1784 **8.3 Volcanoes**

1785 Figure 2 shows the GVP overlay of volcano locations, each red triangle is either one or a
1786 cluster of volcanoes.

1787 The level of tectonic activity, shown by earthquakes, in the SEAP Area increased from
1788 the early 1980's to 2005, declined to 2009 and has since increased again. The USGS provides
1789 earthquake data from 1973 and Figure 32 and shows that the average number of
1790 earthquakes/month in the SEAP Area was 71 between 1973 and 1982. The red line marks this
1791 average plus 3 standard deviations calculated from the same period and shows that from 1995 to
1792 2009 there was a significant (> 3 std deviations) increase in the number of earthquakes which
1793 peaked at 1,303 in January 2005 after the Boxing Day earthquake and Tsunami. In May 2009 the
1794 number of earthquakes fell below the red line for the first time since January 1995 but in 2013
1795 started increasing again.

1796 The GVP database of volcanic eruptions [Venzke, 2013] shows that the SEAP Area
1797 hosted over 18% of all the global volcanic eruptions from 1500 to 2018 whilst covering only 3%
1798 of the Earth's surface. *Simkin and Siebert* [2000] reported that 16 volcanoes have been erupting
1799 nearly continuously for 30 years and that 5 of these volcanoes are in the SEAP Area. Hence the
1800 SEAP Area hosts an unusually high percentage of the global volcanic activity and within it
1801 Indonesia is "the most volcanically active nation on Earth" (USGS)
1802 <https://www.usgs.gov/center-news/revolutionizing-volcano-monitoring-indonesia>).

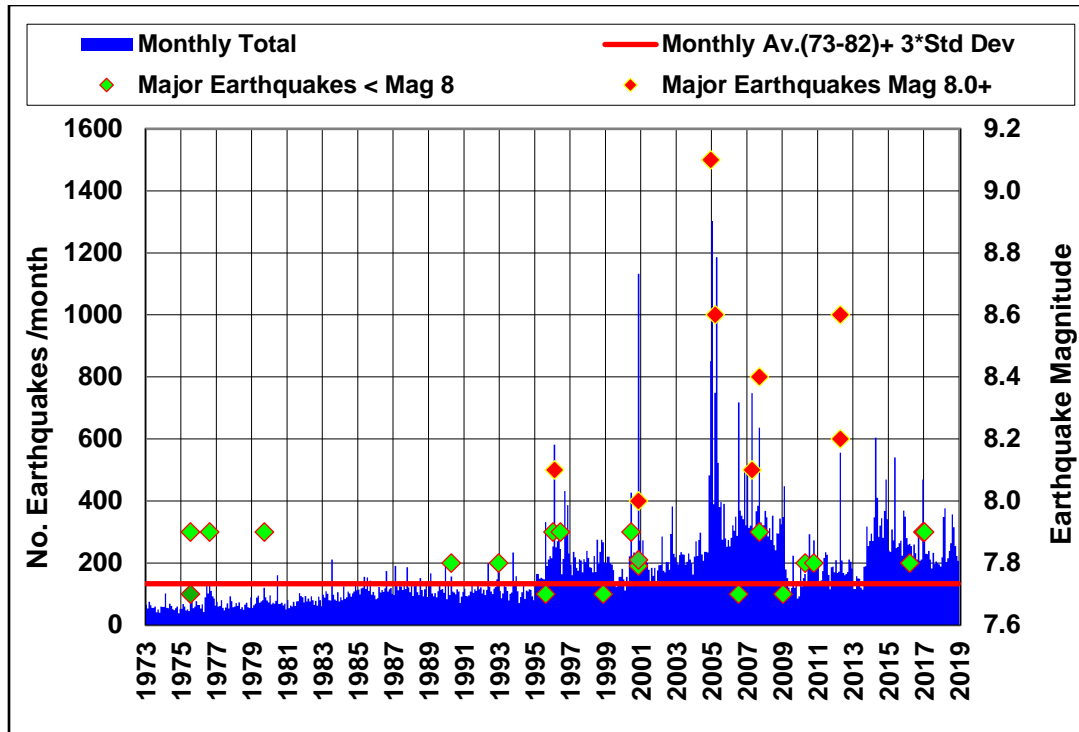
1803 It is also worth noting that the median duration of a volcanic eruption is 7 weeks [*Simkin*
1804 *and Siebert*, 2000]. The IPCC AR5 in Figure 1 of section FAQ 11.2 notes that the effect of
1805 volcanic eruptions on the lower atmosphere (and therefore the surface) is "cooling because the
1806 reduction of sunlight overwhelms any increased downward energy emitted by the volcanic
1807 cloud" and also states the residence time in the troposphere of "1 to 3 weeks" for volcanic ash.
1808 Hence a volcanic ash plume will have a median residence time of 8 to 10 weeks in the
1809 atmosphere – 7 weeks of eruption followed by 1 to 3 weeks of residence.

1810 The volume of Tephra ejected by volcanoes in the SEAP Area was calculated as shown
1811 below. The VEIT data was summed for each decade from 1890 to the present and when
1812 restricted to the April to October Figure 33 shows the 2000 to 2009 VEIT level was 2.89 times
1813 the 20th century average.

1814 **AOD and Volcanic Tephra:** The MERRA-2 AOD of the CSEAP Area averaged over
1815 the months January to August, which avoids the extreme plumes in SON, correlates with the
1816 tephra ejected by volcanoes in the same months at 0.73 from 1980 to 2014 (significance <0.1).
1817 For the full year from 1980 to 2014 the correlation is 0.83 (significance <0.05) and excluding the
1818 years of extreme SON aerosols (October AOD > 0.7) to avoid contaminating the analysis with
1819 the extreme plumes caused by biomass burning the correlation is the same, 0.83 (significance
1820 <0.05)

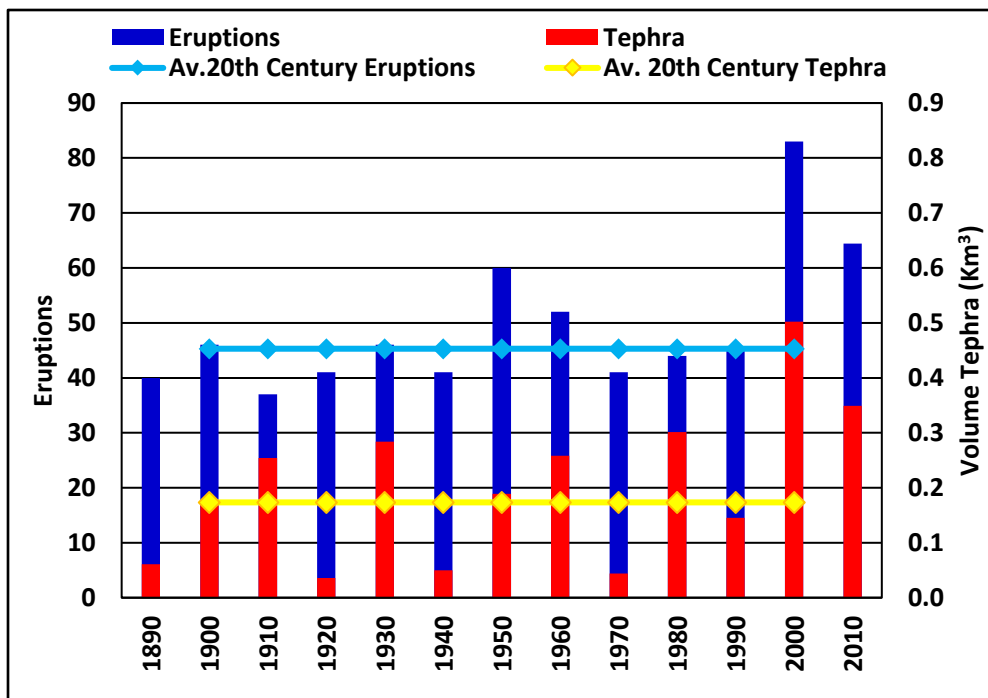
1821 **Spread of tropospheric Volcanic Tephra:** Figure 34 shows an image of the eruption of
1822 the Sangeang Volcano in Indonesia which continued for 1.5 years from May 2014 to November
1823 2015 (GVP database) at an estimated VEI of 3 (GVP) suggesting the majority of the tephra
1824 remained in the troposphere. This image demonstrates how quickly the aerosol plume spreads
1825 from a point source to about 250 km width in the lower right of the image after travelling about
1826 400 Km. Noting that Indonesia, which covers a significant part of the SEAP Area, is "the most

1827 volcanically active nation on Earth” (USGS) it is easy to see how volcanic tephra from multiple
1828 simultaneous eruptions can significantly affect the AOD of the SEAP Area.



1829

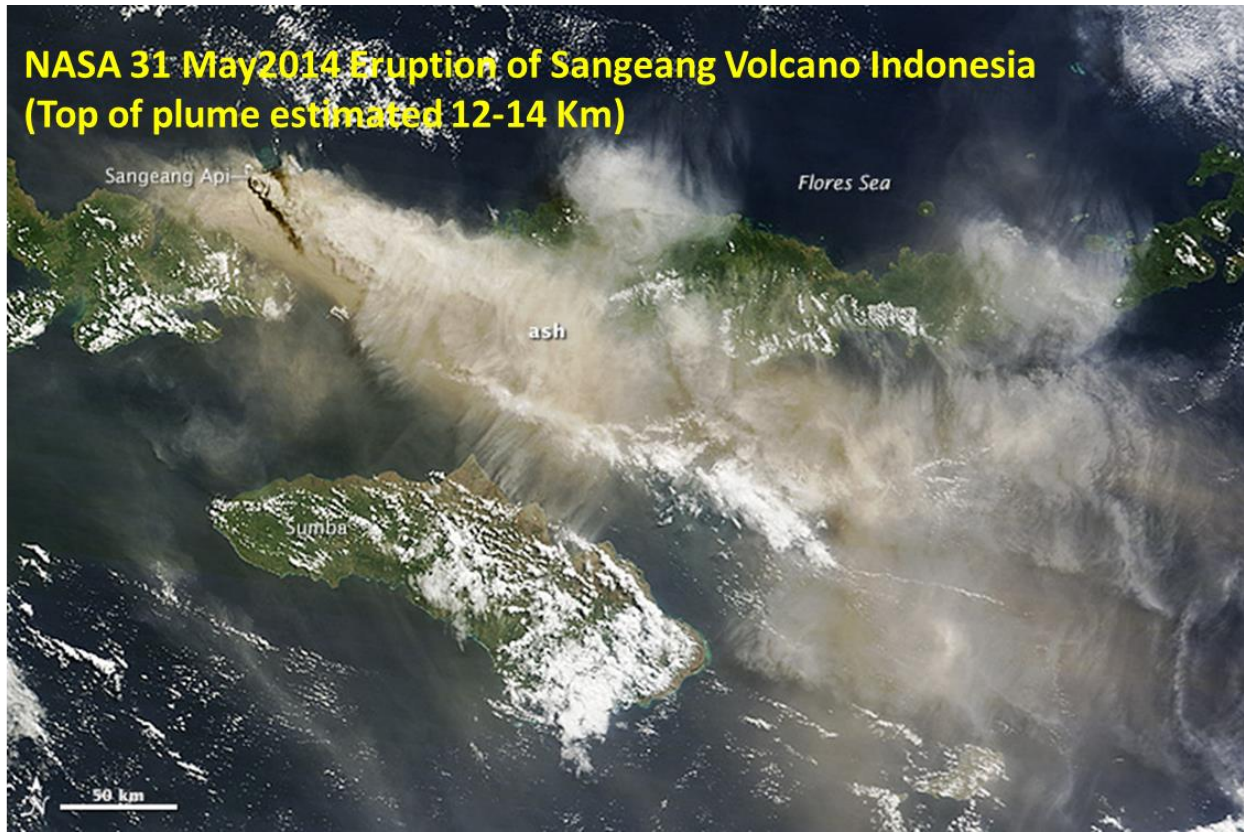
1830 Figure 32: Total Monthly Earthquakes 1973 – 2018 SEAP Area with major events
1831 Magnitude 7.7+ shown. Source: USGS Earthquake database.



1832

1833 Figure 33: Decadal total and average volcanic eruptions and tephra volume in the SEAP
1834 Area from April to October. Averages from 1900 to 1999. Source GVP Database. (Note the 2010
1835 column is for 2010 to 2018, 9 years, and has been increased pro rata to be comparable to the
1836 other decades).

1837



1838
1839

1840

Figure 34: Aerosol plume emanating from Sangeang Volcano May 2014. Source NASA.

1841

1842

1843

1844

1845

1846 **8.4 Volcano Data Processing**

1847 The volcanic eruption data was downloaded from the Global Volcanism Program
1848 database at http://volcano.si.edu/list_volcano_holocene.cfm [Venzke, 2013]. Then:

- 1849 • Eruptions from 1870 were extracted from the dataset;
- 1850 • The VEI was extracted. Any eruptions with no VEI listed were allocated a VEI of 0;
- 1851 • The VEIT in Km³ was calculated using the table in *Newhall and Self* [1982];
- 1852 • The eruption start year was extracted;
- 1853 • The eruption start month was extracted and eruptions with no start month were
1854 allocated sequentially to January then February and so on;
- 1855 • The end year and month was extracted. For eruptions with no end date the end date
1856 was calculated using the start date and the median eruption length in [Simkin and
1857 Siebert, 2000] of 7 weeks;
- 1858 • The length of each eruption in months was calculated and the total VEIT for the
1859 eruption was allocated equally to each month of the eruption starting with the start
1860 month and ending with the end month.
- 1861 • The VEIT for each month from 1870 to 2018 was summed;
- 1862 • The summed monthly VEIT was then smoothed with a 12 month running average
1863 and carried forward to the various analyses;
- 1864 • In the analyses of the Nino 3.4, 1+2 SST and the SOI (Nino Parameters) the VEIT
1865 data was allocated to segments 0 to 0.001, >0.001 to 0.004, >0.004 to 0.01 and >0.01
1866 and averaged and the corresponding monthly Nino Parameter allocated to the same
1867 segment and averaged;
- 1868 • The VEIT and Nino Parameters were then correlated and displayed on scatter plots.

1869 **Note:**

- 1870 • The BOM SOI data runs from 1876 to 2019
- 1871 • The NOAA ESRL Nino 3.4 and 1+2 SST run from 1870 to 2018
- 1872 • The NCEP Omega data runs from 1948 to 2018
- 1873 • Due to the significantly different time periods of the Nino Parameter data and the
1874 omega data the segment boundaries for the omega data were: 0.00005, 0.0001,
1875 0.0002, 0.00855 and >0.00855

1876 **9 APPENDIX B – PROCESSING SEQUENCE FOR LME AND LE DATA**

1877 The LME and LE data was processed through the following routes as required:

- 1878 1. No Processing;
- 1879 2. Deseasonalised;
- 1880 3. Normalised: Some of the data exhibits a non-linear trend which was removed by dividing the data at time t by the running
- 1881 average from time t-3 to t+3 and then multiplying the result by the average of the whole data set;
- 1882 4. Smoothed with a running 12 point average centered on time t (t-5 to t+6);
- 1883 5. Note: the ONI, IOD and SOI include both negative and positive values and the normalising was carried out using the
- 1884 absolute values of these indices to avoid anomalies which occur when true averages resulted in values close to zero.

1885 The processing route for each analysis is shown in Figure 35 and the key in Figure 36.

Last Millennium Ensemble													
Forcing	Run	SEAP Area			El Niño					IOD	Australia		Global
		T Level 609	TS	Omega	3.4 TS	1+2 TS	ONI	SOI	U 10	IOD	MSLP	Rain	TS
850	03												
All	13												
Aerosol	02												
Greenhouse	03												
Land	03												
Orbital	03												
Solar	05												
Volcanic	05												
Large Ensemble													
1850 to 2005													
2006 to 2100													

1886

1887

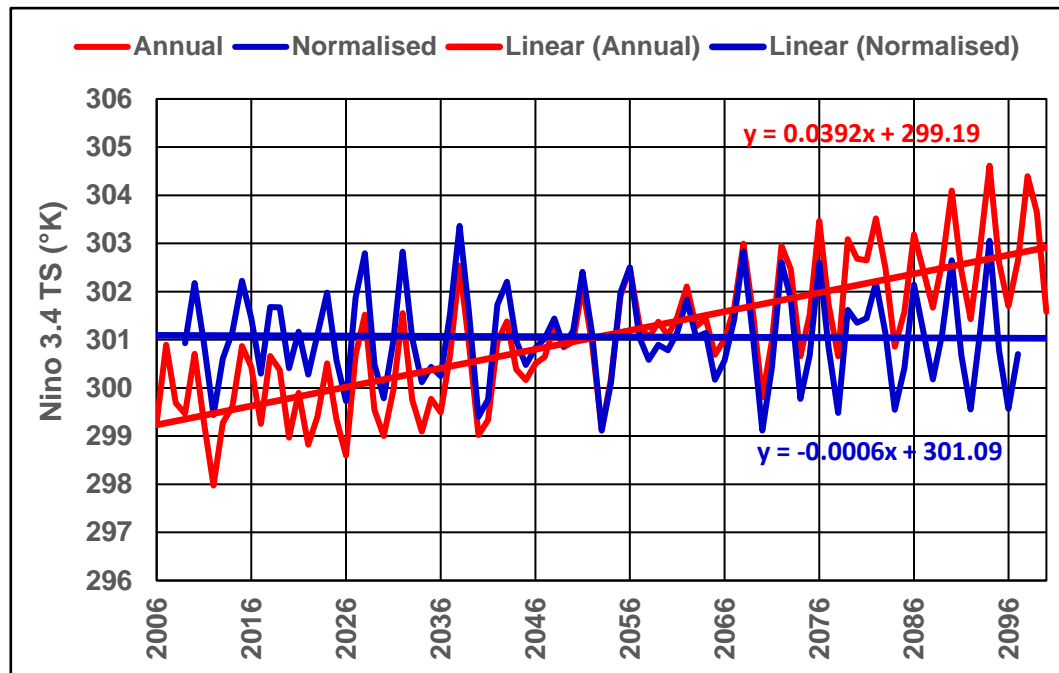
Figure 35: Processing route for each parameter including time series and segmented data.

	Time Series			Segmented	
	Annual	Apr-Oct	SON	Annual	monthly
	None			None	None
	Normalised			None	None
	Normalised			Normalised	None
	Normalised			Normalised	Normalised
	Normalised			Normalised	Normalised & Smoothed 12 Av.
	Normalised			Normalised	Deseasonalised & normalised
	Normalised			Normalised	Averaged 12 points

1888

1889

Figure 36: Key for processing routes



1890

1891

Figure 37: Effect of normalising Nino 3.4 TS data from the LE RCP 8.5 data.

1892 The effect of the normalization process is described in [Dettling, 2014] p34 and is shown in Figure 37 where the trend in TS
1893 under RCP 8.5 has been reduced from 3.72°K to -0.057°K across the data set and the interannual variation is virtually unchanged.

1894 **10 APPENDIX C – CORRELATION MATRIX FOR LME, LE AND MERRA-2**

1895

	850	All	GHG	Land Use R3	Orbital R3	Ozone Aerosol R2	Solar	Volcanic R5	MERRA 2
850	1.00	0.02	0.03	-0.04	0.08	-0.08	0.07	-0.02	-0.37
All	0.02	1.00	0.02	0.00	-0.02	0.54	-0.04	-0.02	0.12
GHG	0.03	0.02	1.00	0.00	0.09	-0.06	0.04	0.01	-0.05
Land Use R3	-0.04	0.00	0.00	1.00	0.00	0.02	0.00	0.02	-0.03
Orbital R3	0.08	-0.02	0.09	0.00	1.00	0.12	-0.01	0.03	-0.09
Ozone Aerosol R2	-0.08	0.54	-0.06	0.02	0.12	1.00	-0.15	0.12	-0.09
Solar	0.07	-0.04	0.04	0.00	-0.01	-0.15	1.00	-0.07	0.25
Volcanic R5	-0.02	-0.02	0.01	0.02	0.03	0.12	-0.07	1.00	-0.39
MERRA 2	-0.37	0.12	-0.05	-0.03	-0.09	-0.09	0.25	-0.39	1.00
Average	-0.04	0.08	0.01	0.00	0.03	0.05	0.01	-0.04	-0.08

1896

1897 Figure 38: Correlation matrix for LME and MERRA-2 CSEAP AOD/AODVIS. The average
 1898 excludes the self-correlations which return 1.00.

1899 There is only one significant positive correlation between the All and Ozone Aerosol data in
 1900 Figure 38 hence 8 of the 9 data sets are independent.

3. Acknowledgments and Data

1901 I acknowledge:

1902 NASA: Analyses and visualizations used in this paper were produced with the Giovanni
1903 online data system, developed and maintained by the NASA GES DISC; the mission scientists and
1904 Principal Investigators who provided the data used in this paper including the CALIPSO data; and Dr
1905 Robert Schmunk for the Panoply data viewer;

1906 The Hadley Centre for the HadISST_1 dataset;

1907 Google EarthTM and the copyright holders noted on the images for the images of the Earth
1908 and gas flares;

1909 The Global Forest Watch at
1910 https://data.globalforestwatch.org/datasets/defaultfe5832831464cbd64aaa8f2d54781_0/data for the fire
1911 data;

1912 Oak Ridge National Laboratory and NASA for the Global Fire Emissions Database
1913 (GFED4.1s) for the BC Emissions for the Equatorial Asian Region at [https://daac.ornl.gov/cgi-](https://daac.ornl.gov/cgi-bin/dsvviewer.pl?ds_id=1293)
1914 [bin/dsvviewer.pl?ds_id=1293](https://daac.ornl.gov/cgi-bin/dsvviewer.pl?ds_id=1293)

1915 The Climate and Global Dynamics Division of ESSL at NCAR for the SEAP SST, Omega
1916 and Niño 1+2 and 3.4 SST data;

1917 The Indonesian burned areas data from NASA at
1918 [https://search.earthdata.nasa.gov/projects?p=C1457414586-SEDAC!C1457414586-](https://search.earthdata.nasa.gov/projects?p=C1457414586-SEDAC!C1457414586-SEDAC&q=burned%20area%20indonesia&tl=1563231391!4!!)
1919 [SEDAC&q=burned%20area%20indonesia&tl=1563231391!4!!](https://search.earthdata.nasa.gov/projects?p=C1457414586-SEDAC!C1457414586-SEDAC&q=burned%20area%20indonesia&tl=1563231391!4!!)

1920 NOAA: Data and images provided by the NOAA/OAR/ESRL PSD, Boulder, Colorado, USA,
1921 from their Web site at <http://www.esrl.noaa.gov/psd/> ; the Trade Wind data by the Climate Prediction
1922 Centre;

1923 The CESM1(CAM5) Last Millennium Ensemble Community Project and supercomputing
1924 resources provided by NSF/CISL/Yellowstone;

1925 The CESM Large Ensemble Community Project and supercomputing resources provided by
1926 NSF/CISL/Yellowstone;

1927 The United Nations Department of Economic and Social Affairs Population Division for the
1928 world population statistics;

1929 The United Nations Forest Resources Assessment reports for the burned area data

1930 The Australian Bureau of Meteorology for the Walker Circulation images, SOI data and SOI
1931 formula at <http://www.bom.gov.au>;

1932 The U.S. Geological Survey for the earthquake information at: [https://www.usgs.gov/natural-](https://www.usgs.gov/natural-hazards/earthquake-hazards/science/20-largest-earthquakes-world?qt-science_center_objects=0#qt-science_center_objects)
1933 [hazards/earthquake-hazards/science/20-largest-earthquakes-world?qt-science_center_objects=0#qt-](https://www.usgs.gov/natural-hazards/earthquake-hazards/science/20-largest-earthquakes-world?qt-science_center_objects=0#qt-science_center_objects)
1934 [science_center_objects](https://www.usgs.gov/natural-hazards/earthquake-hazards/science/20-largest-earthquakes-world?qt-science_center_objects=0#qt-science_center_objects) ;

1935 BP for the oil production statistics at [http://www.bp.com/en/global/corporate/energy-](http://www.bp.com/en/global/corporate/energy-economics/statistical-review-of-world-energy.html)
1936 [economics/statistical-review-of-world-energy.html](http://www.bp.com/en/global/corporate/energy-economics/statistical-review-of-world-energy.html);

1937 The Global Volcanism Program at the Smithsonian Institution for the volcano eruption data at
1938 <http://volcano.si.edu/> ;

- 1939 Warwick Goldsworthy and Andrew Metcalfe for discussion and comments;
- 1940 The anonymous reviewers whose comments greatly improved the paper.
- 1941 All data supporting the conclusions is available from the sources shown in the text.
- 1942 This research project was funded personally by the author and his wife Julie.

4. References

- 1943 Allen, R. J., S. C. Sherwood, J. R. Norris, and C. S. Zender (2012), Recent Northern Hemisphere tropical expansion
 1944 primarily driven by black carbon and tropospheric ozone, *Nature*, *485*(7398), 350-354, doi:10.1038/nature11097.
 1945 Ammann, C. M., G. A. Meehl, W. M. Washington, and C. S. Zender (2003), A monthly and latitudinally varying
 1946 volcanic forcing dataset in simulations of 20th century climate, *Geophysical Research Letters*, *30*(12), n/a-n/a,
 1947 doi:10.1029/2003GL016875.
 1948 Applegate, G., U. Chokkalingam, and Suyanto (2001), The Underlying Causes and Impacts of Fires in South-east Asia,
 1949 *Center for International Forestry Research and International Centre for Research in Agroforestry*.
 1950 Barry, R. G., and R. J. Chorley (2010), *Atmosphere Weather and Climate* Routledge, Abingdon UK.
 1951 Blake, S. A. P., S. C. Lewis, A. N. LeGrande, and R. L. Miller (2018), Assessing the impact of large volcanic eruptions
 1952 of the last millennium (850–1850 CE) on Australian rainfall regimes, *Clim. Past*, *14*(6), 811-824, doi:10.5194/cp-14-811-
 1953 2018.
 1954 Booth, B. B., N. J. Dunstone, P. R. Halloran, T. Andrews, and N. Bellouin (2012), Aerosols implicated as a prime driver
 1955 of twentieth-century North Atlantic climate variability, *Nature*, *484*(7393), 228-232, doi:10.1038/nature10946.
 1956 Brown, J. N., and A. V. Fedorov (2010), How Much Energy Is Transferred from the Winds to the Thermocline on ENSO
 1957 Time Scales?, *Journal of Climate*, *23*(6), 1563-1580, doi:10.1175/2009JCLI2914.1.
 1958 Cane, M. A. (2005), The evolution of El Niño, past and future, *Earth and Planetary Science Letters*, *230*(3–4), 227-240,
 1959 doi:<http://dx.doi.org/10.1016/j.epsl.2004.12.003>.
 1960 Center for International Earth Science Information Network - CIESIN - Columbia University (2018), Global Fire
 1961 Emissions Indicators, Country-Level Tabular Data: 1997-2015, edited, NASA Socioeconomic Data and Applications
 1962 Center (SEDAC), Palisades, NY.
 1963 Cook, E. R., K. J. Anchukaitis, B. M. Buckley, R. D. D'Arrigo, G. C. Jacoby, and W. E. Wright (2010), Asian Monsoon
 1964 Failure and Megadrought During the Last Millennium, *Science*, *328*(5977), 486-489, doi:10.1126/science.1185188.
 1965 Dettling, D. M. (2014), Applied Time Series Analysis, *Zurich University of Applied Sciences*,
 1966 https://stat.ethz.ch/education/semesters/ss2014/atsa/Scriptum_v140523.pdf.
 1967 Duncan, B. N., I. Bey, M. Chin, L. J. Mickley, T. D. Fairlie, R. V. Martin, and H. Matsueda (2003), Indonesian wildfires
 1968 of 1997: Impact on tropospheric chemistry, *Journal of Geophysical Research: Atmospheres*, *108*(D15), 4458,
 1969 doi:10.1029/2002JD003195.
 1970 Emile-Geay, J., R. Seager, M. A. Cane, E. R. Cook, and G. H. Haug (2008), Volcanoes and ENSO over the Past
 1971 Millennium, *Journal of Climate*, *21*(13), 3134-3148.
 1972 Enfield, D. B. (1989), El Niño, past and present, *Reviews of Geophysics*, *27*(1), 159-187, doi:10.1029/RG027i001p00159.
 1973 Forster, P., et al. (2007), Changes in Atmospheric Constituents and in Radiative Forcing. In: *Climate Change 2007: The*
 1974 *Physical Science Basis. Contribution of Working Group I to the Fourth Assessment Report of the Intergovernmental*
 1975 *Panel on Climate Change* [Solomon, S., D. Qin, M. Manning, Z. Chen, M. Marquis, K.B. Averyt, M. Tignor and H.L.
 1976 Miller (eds.)] Cambridge University Press, Cambridge, United Kingdom and New York, NY, USA.
 1977 Foster, G., and S. Rahmstorf (2011), Global temperature evolution 1979–2010, *Environ. Res. Lett.*, *6*,
 1978 doi:10.1088/1748-9326/6/4/044022.
 1979 Gao, C., A. Robock, and C. Ammann (2008), Volcanic forcing of climate over the past 1500 years: An improved ice
 1980 core-based index for climate models, *Journal of Geophysical Research: Atmospheres*, *113*(D23),
 1981 doi:10.1029/2008jd010239.
 1982 Gelaro, R., et al. (2017), The Modern-Era Retrospective Analysis for Research and Applications, Version 2 (MERRA-2),
 1983 *Journal of Climate*, *30*(14), 5419-5454, doi:10.1175/jcli-d-16-0758.1.
 1984 Hammer, Ø., D. A. T. Harper, and P. D. Ryan (2001), PAST: Paleontological statistics software package for education
 1985 and data analysis. , *Palaeontologia Electronica* *4*(1): 9pp, 9pp.
 1986 Handler, P., and K. Andsager (1990), Volcanic aerosols, El Niño and the Southern Oscillation, *International Journal of*
 1987 *Climatology*, *10*(4), 413-424, doi:10.1002/joc.3370100409.
 1988 Hansell, R. A., S. C. Tsay, Q. Ji, K. N. Liou, and S. C. Ou (2003), Surface aerosol radiative forcing derived from
 1989 collocated ground-based radiometric observations during PRIDE, SAFARI, and ACE-Asia, *Appl Opt*, *42*(27), 5533-5544.
 1990 Hegerl, G. C., F. W. Zwiers, P. Braconnot, N. P. Gillett, Y. Luo, J. A. Marengo Orsini, N. Nicholls, J. E. Penner, and P.
 1991 A. Stott (2007), Understanding and Attributing Climate Change. In: *Climate Change 2007: The Physical Science Basis.*
 1992 *Contribution of Working Group I to the Fourth Assessment Report of the Intergovernmental Panel on Climate Change*
 1993 *[Solomon, S., D. Qin, M. Manning, Z. Chen, M. Marquis, K.B. Averyt, M. Tignor and H.L. Miller (eds.)]*. Cambridge
 1994 University Press, Cambridge, United Kingdom and New York, NY, USA.
 1995 Hirono, M. (1988), On the trigger of El Niño Southern Oscillation by the forcing of early El Chichón volcanic aerosols,
 1996 *Journal of Geophysical Research: Atmospheres*, *93*(D5), 5365-5384, doi:10.1029/JD093iD05p05365.

- 1997 Huang, B., P. W. Thorne, V. F. Banzon, T. Boyer, G. Chepurin, J. H. Lawrimore, M. J. Menne, T. M. Smith, R. S. Vose,
 1998 and H.-M. Zhang (2017), Extended Reconstructed Sea Surface Temperature, Version 5 (ERSSTv5): Upgrades,
 1999 Validations, and Intercomparisons, *Journal of Climate*, 30(20), 8179-8205, doi:10.1175/jcli-d-16-0836.1.
- 2000 IPCC (2007), IPCC Assessment Report 4 Glossary.
- 2001 Kajikawa, Y., B. Wang, and J. Yang (2010), A multi-time scale Australian monsoon index, *International Journal of*
 2002 *Climatology*, 30(8), 1114-1120, doi:10.1002/joc.1955.
- 2003 Kalnay, E., et al. (1996), The NCEP/NCAR 40-Year Reanalysis Project, *Bulletin of the American Meteorological*
 2004 *Society*, 77(3), 437-471, doi:10.1175/1520-0477(1996)077<0437:TNYRP>2.0.CO;2.
- 2005 Kaufman, Y. J., B. N. Holben, D. Tanré, I. Slutsker, A. Smirnov, and T. F. Eck (2000), Will aerosol measurements from
 2006 Terra and Aqua Polar Orbiting satellites represent the daily aerosol abundance and properties?, *Geophysical Research*
 2007 *Letters*, 27(23), 3861-3864, doi:10.1029/2000GL011968.
- 2008 Kay, J. E., et al. (2015), The Community Earth System Model (CESM) Large Ensemble Project: A Community Resource
 2009 for Studying Climate Change in the Presence of Internal Climate Variability, *Bulletin of the American Meteorological*
 2010 *Society*, 96(8), 1333-1349, doi:10.1175/bams-d-13-00255.1.
- 2011 Kirchstetter, T. W. (2004), Evidence that the spectral dependence of light absorption by aerosols is affected by organic
 2012 carbon, *Journal of Geophysical Research*, 109(D21), doi:10.1029/2004jd004999.
- 2013 Kirtman, B., et al. (2013), Near-term Climate Change: Projections and Predictability. In: Climate Change 2013: The
 2014 Physical Science Basis. Contribution of Working Group I to the Fifth Assessment Report of the Intergovernmental Panel
 2015 on Climate Change Stocker, T.F., D. Qin, G.-K. Plattner, M. Tignor, S.K. Allen, J. Boschung, A. Nauels, Y. Xia, V. Bex
 2016 and P.M. Midgley (eds.]. *Rep.*, IPCC, Cambridge, United Kingdom and New York, NY, USA.
- 2017 Lamarque, J. F., et al. (2010), Historical (1850–2000) gridded anthropogenic and biomass burning emissions of reactive
 2018 gases and aerosols: methodology and application, *Atmospheric Chemistry and Physics*, 10(15), 7017-7039,
 2019 doi:10.5194/acp-10-7017-2010.
- 2020 Levy II, H., D. T. Shindell, A. Gilliland, M. D. Schwarzkopf, and L. W. Horowitz (2008), Executive Summary in
 2021 Climate Projections Based on Emissions Scenarios for Long-Lived and Short-Lived Radiatively Active Gases and
 2022 Aerosols. H. Levy II, D.T. Shindell, A. Gilliland, M.D. Schwarzkopf, L.W. Horowitz, (eds.). A Report by the U.S.
 2023 Climate Change Science Program and the Subcommittee on Global Change Research, Washington, D.C.
- 2024 Maher, N., S. McGregor, M. H. England, and A. S. Gupta (2015), Effects of volcanism on tropical variability,
 2025 *Geophysical Research Letters*, 42(14), 6024-6033, doi:10.1002/2015GL064751.
- 2026 Mann, M. E., M. A. Cane, S. E. Zebiak, and A. Clement (2005), Volcanic and Solar Forcing of the Tropical Pacific over
 2027 the Past 1000 Years, *Journal of Climate*, 18(3), 447-456, doi:10.1175/JCLI-3276.1.
- 2028 Maraun, D., and J. Kurths (2005), Epochs of phase coherence between El Niño/Southern Oscillation and Indian
 2029 monsoon, *Geophysical Research Letters*, 32(15), n/a-n/a, doi:10.1029/2005GL023225.
- 2030 McGregor, G. R., and S. Nieuwof (1977), *Tropical Climatology*, 207 pp., John Wiley and Sons.
- 2031 McGregor, S., A. Timmermann, M. F. Stuecker, M. H. England, M. Merrifield, F.-F. Jin, and Y. Chikamoto (2014),
 2032 Recent Walker circulation strengthening and Pacific cooling amplified by Atlantic warming, *Nature Clim. Change*, 4(10),
 2033 888-892, doi:10.1038/nclimate2330
 2034 <http://www.nature.com/nclimate/journal/v4/n10/abs/nclimate2330.html#supplementary-information>.
- 2035 McPhaden, M. J., et al. (1998), The Tropical Ocean-Global Atmosphere observing system: A decade of progress, *Journal*
 2036 *of Geophysical Research: Oceans*, 103(C7), 14169-14240, doi:10.1029/97JC02906.
- 2037 McPhaden, M. J., S. E. Zebiak, and M. H. Glantz (2006), ENSO as an Integrating Concept in Earth Science, *Science*,
 2038 314(5806), 1740-1745, doi:10.1126/science.1132588.
- 2039 Menon, S., J. Hansen, L. Nazarenko, and Y. Luo (2002), Climate Effects of Black Carbon Aerosols in China and India,
 2040 *Science*, 297(5590), 2250-2253, doi:10.1126/science.1075159.
- 2041 Meyers, G., P. McIntosh, L. Pigot, and M. Pook (2007), The Years of El Niño, La Niña, and Interactions with the
 2042 Tropical Indian Ocean, *Journal of Climate*, 20(13), 2872-2880, doi:10.1175/jcli4152.1.
- 2043 Mieville, A., C. Granier, C. Lioussé, B. Guillaume, F. Mouillot, J. F. Lamarque, J. M. Grégoire, and G. Pétron (2010),
 2044 Emissions of gases and particles from biomass burning during the 20th century using satellite data and an historical
 2045 reconstruction, *Atmospheric Environment*, 44(11), 1469-1477, doi:<http://dx.doi.org/10.1016/j.atmosenv.2010.01.011>.
- 2046 Morice, C. P., J. J. Kennedy, N. A. Rayner, and P. D. Jones (2012), Quantifying uncertainties in global and regional
 2047 temperature change using an ensemble of observational estimates: The HadCRUT4 data set, *Journal of Geophysical*
 2048 *Research: Atmospheres*, 117(D8), n/a-n/a, doi:10.1029/2011JD017187.
- 2049 Murray Darling Basin Authority (2011), Annual Report 2010-11 *Rep.*
- 2050 Newhall, C. G., and S. Self (1982), The volcanic explosivity index (VEI) an estimate of explosive magnitude for
 2051 historical volcanism, *Journal of Geophysical Research: Oceans*, 87(C2), 1231-1238, doi:10.1029/JC087iC02p01231.

- 2052 Nicholls, N. (1988), Low latitude volcanic eruptions and the El Niño-Southern Oscillation, *Journal of Climatology*, 8(1),
2053 91-95, doi:10.1002/joc.3370080109.
- 2054 Nicholls, N. (1990), Low-latitude volcanic eruptions and the El Niño/Southern Oscillation: A reply, *International*
2055 *Journal of Climatology*, 10(4), 425-429, doi:10.1002/joc.3370100410.
- 2056 Nicholls, N., B. Lavery, C. Frederiksen, W. Drosowsky, and S. Torok (1996), Recent apparent changes in relationships
2057 between the El Niño-Southern Oscillation and Australian rainfall and temperature, *Geophysical Research Letters*, 23(23),
2058 3357-3360, doi:10.1029/96GL03166.
- 2059 Novakov, T., V. Ramanathan, J. E. Hansen, T. W. Kirchstetter, M. Sato, J. E. Sinton, and J. A. Sathaye (2003), Large
2060 historical changes of fossil-fuel black carbon aerosols, *Geophysical Research Letters*, 30(6), 1324,
2061 doi:10.1029/2002GL016345.
- 2062 Nozawa, T., T. Nagashima, H. Shiogama, and S. A. Crooks (2005), Detecting natural influence on surface air
2063 temperature change in the early twentieth century, *Geophysical Research Letters*, 32(20), n/a-n/a,
2064 doi:10.1029/2005GL023540.
- 2065 Ott, L., B. Duncan, S. Pawson, P. Colarco, M. Chin, C. Randles, T. Diehl, and E. Nielsen (2010), Influence of the 2006
2066 Indonesian biomass burning aerosols on tropical dynamics studied with the GEOS-5 AGCM, *Journal of Geophysical*
2067 *Research: Atmospheres*, 115(D14), D14121, doi:10.1029/2009JD013181.
- 2068 Otto-Bliesner, B. L., E. C. Brady, J. Fasullo, A. Jahn, L. Landrum, S. Stevenson, N. Rosenbloom, A. Mai, and G. Strand
2069 (2016), Climate Variability and Change since 850 CE: An Ensemble Approach with the Community Earth System
2070 Model, *Bulletin of the American Meteorological Society*, 97(5), 735-754, doi:10.1175/bams-d-14-00233.1.
- 2071 Potts, K. A. (2017), Poster: The South East Asian Aerosol Plume: The Cause of All El Niño Events, in *AGU 2017 Fall*
2072 *Meeting*, edited, Earth and Space Science Open Archive (ESSOAr, New Orleans, USA,
2073 doi:<https://doi.org/10.1002/essoar.10500075.1>.
- 2074 Potts, K. A. (2018), Poster: How the Natural & Anthropogenic Aerosol Plume over S. E. Asia caused the Millennium
2075 Drought, in *AMOS-ICSHMO 2018*, edited, Sydney, Australia, doi:<https://doi.org/10.1002/essoar.10500083.1>.
- 2076 Potts, K. A. (2020a), How Extreme Apparitions of the Volcanic and Anthropogenic South East Asian Aerosol Plume
2077 caused the Millennium Drought in South Eastern Australian. First Attribution and Mechanism using data from the Last
2078 Millennium Ensemble, Large Ensemble, MERRA-2 Reanalysis, four Satellites and the Global Volcanism Program.
- 2079 Potts, K. A. (2020b), How Extreme Apparitions of the Volcanic and Anthropogenic South East Asian Aerosol Plume
2080 Trigger and Sustain El Niño Events. First Attribution and Mechanism using data from the Last Millennium Ensemble,
2081 Large Ensemble, MERRA-2 Reanalysis, four Satellites and the Global Volcanism Program.
- 2082 Power, S., F. Tseitkin, S. Torok, B. Lavery, R. Dahni, and B. McAvaney (1998), Australian temperature, Australian
2083 rainfall and the Southern Oscillation, 1910-1992: coherent variability and recent changes, *Aust. Met. Mag.*, 47.
- 2084 Predybaylo, E., G. L. Stenchikov, A. T. Wittenberg, and F. Zeng (2017), Impacts of a Pinatubo-size volcanic eruption on
2085 ENSO, *Journal of Geophysical Research: Atmospheres*, 122(2), 925-947, doi:doi:10.1002/2016JD025796.
- 2086 Ramanathan, V. (2006), ATMOSPHERIC BROWN CLOUDS: HEALTH, CLIMATE AND AGRICULTURE
2087 IMPACTS, *Scripta Varia* 106.
- 2088 Randerson, J. T., G. R. Van Der Werf, L. Giglio, G. J. Collatz, and P. S. Kasibhatla (2017), Global Fire Emissions
2089 Database, Version 4.1 (GFEDv4), edited, ORNL Distributed Active Archive Center, doi:10.3334/ORNLDAAAC/1293.
- 2090 Rayner, N. A., D. E. Parker, E. B. Horton, C. K. Folland, L. V. Alexander, D. P. Rowell, E. C. Kent, and A. Kaplan
2091 (2003), Global analyses of sea surface temperature, sea ice, and night marine air temperature since the late nineteenth
2092 century, *Journal of Geophysical Research: Atmospheres*, 108(D14), doi:doi:10.1029/2002JD002670.
- 2093 Remer, L. A., et al. (2009), Executive Summary, in *Atmospheric Aerosol Properties and Climate Impacts*, A Report by
2094 the U.S. Climate Change Science Program and the Subcommittee on Global Change Research [Mian Chin, Ralph A.
2095 Kahn, and Stephen E. Schwartz (eds.)]. National Aeronautics and Space Administration, Washington, D.C., USA.
- 2096 Remer, L. A., et al. (2005), The MODIS Aerosol Algorithm, Products, and Validation, *Journal of the Atmospheric*
2097 *Sciences*, 62(4), 947-973, doi:10.1175/JAS3385.1.
- 2098 Robock, A., K. E. Taylor, G. L. Stenchikov, and Y. Liu (1995), GCM evaluation of a mechanism for El Niño triggering
2099 by the El Chichón ash cloud, *Geophysical Research Letters*, 22(17), 2369-2372, doi:10.1029/95GL02065.
- 2100 Rotstain, L. D., et al. (2007), Have Australian rainfall and cloudiness increased due to the remote effects of Asian
2101 anthropogenic aerosols?, *Journal of Geophysical Research: Atmospheres*, 112(D9), D09202,
2102 doi:10.1029/2006JD007712.
- 2103 Rotstain, L. D., M. A. Collier, M. R. Dix, Y. Feng, H. B. Gordon, S. P. O'Farrell, I. N. Smith, and J. Syktus (2009a),
2104 Improved simulation of Australian climate and ENSO-related rainfall variability in a global climate model with an
2105 interactive aerosol treatment, *International Journal of Climatology*, n/a-n/a, doi:10.1002/joc.1952.

- 2106 Rotstayn, L. D., M. D. Keywood, B. W. Forgan, A. J. Gabric, I. E. Galbally, J. L. Gras, A. K. Luhar, G. H. McTainsh, R.
 2107 M. Mitchell, and S. A. Young (2009b), Possible impacts of anthropogenic and natural aerosols on Australian climate: a
 2108 review, *International Journal of Climatology*, 29(4), 461-479, doi:10.1002/joc.1729.
 2109 Self, S., M. R. Rampino, J. Zhao, and M. G. Katz (1997), Volcanic aerosol perturbations and strong El Niño events: No
 2110 general correlation, *Geophysical Research Letters*, 24(10), 1247-1250, doi:10.1029/97GL01127.
 2111 Shukla, J., and D. A. Paolino (1983), The Southern Oscillation and Long-Range Forecasting of the Summer Monsoon
 2112 Rainfall over India, *Monthly Weather Review*, 111(9), 1830-1837, doi:doi:10.1175/1520-
 2113 0493(1983)111<1830:TSOALR>2.0.CO;2.
 2114 Simkin, T., and L. Siebert (2000), Earth's volcanoes and eruptions: an overview p. 249-261. , in *Encyclopedia of*
 2115 *Volcanoes*, , edited by S. H. Academic Press, San Diego.
 2116 Solomon, S., et al. (2007), Technical Summary. In: Climate Change 2007: The Physical Science Basis. Contribution of
 2117 Working Group I to the Fourth Assessment Report of the Intergovernmental Panel on Climate Change [Solomon, S., D.
 2118 Qin, M. Manning, Z. Chen, M. Marquis, K.B. Averyt, M. Tignor and H.L. Miller (eds.)]. Cambridge University Press,
 2119 Cambridge, United Kingdom and New York, NY, USA.
 2120 Stocker, T. F., et al. (2013), Technical Summary. In: Climate Change 2013: The Physical Science Basis. Contribution of
 2121 Working Group I to the Fifth Assessment Report of the Intergovernmental Panel on Climate Change *Rep.*,
 2122 Intergovernmental Panel on Climate Change, Cambridge, United Kingdom and New York, NY, USA.
 2123 Sturman, A. P., and N. J. Tapper (1996), The Weather and Climate of Australia and New Zealand. Oxford University
 2124 Press Australia 476.
 2125 Takemura, T., T. Nozawa, S. Emori, T. Y. Nakajima, and T. Nakajima (2005), Simulation of climate response to aerosol
 2126 direct and indirect effects with aerosol transport-radiation model, *Journal of Geophysical Research: Atmospheres*,
 2127 110(D2), n/a-n/a, doi:10.1029/2004JD005029.
 2128 Timbal, B., et al. (2010), Understanding the anthropogenic nature of the observed rainfall decline across south-eastern
 2129 Australia, *Centre for Australian Weather and Climate Research, Technical Report 026*.
 2130 Timbal, B., and W. Drosowsky (2013), The relationship between the decline of Southeastern Australian rainfall and the
 2131 strengthening of the subtropical ridge, *International Journal of Climatology*, 33(4), 1021-1034, doi:10.1002/joc.3492.
 2132 Timmreck, C. (2012), Modeling the climatic effects of large explosive volcanic eruptions, *Wiley Interdisciplinary*
 2133 *Reviews: Climate Change*, 3(6), 545-564, doi:doi:10.1002/wcc.192.
 2134 Tosca, M. G., D. J. Diner, M. J. Garay, and O. V. Kalashnikova (2015), Human-caused fires limit convection in tropical
 2135 Africa: First temporal observations and attribution, *Geophysical Research Letters*, 42(15), 2015GL065063,
 2136 doi:10.1002/2015GL065063.
 2137 Trenberth, K. E., J. M. Caron, D. P. Stepaniak, and S. Worley (2002), Evolution of El Niño–Southern Oscillation and
 2138 global atmospheric surface temperatures, *Journal of Geophysical Research: Atmospheres*, 107(D8), AAC 5-1-AAC 5-17,
 2139 doi:10.1029/2000JD000298.
 2140 Trenberth, K. E., D. P. Stepaniak, and J. M. Caron (2000), The Global Monsoon as Seen through the Divergent
 2141 Atmospheric Circulation, *Journal of Climate*, 13(22), 3969-3993, doi:doi:10.1175/1520-
 2142 0442(2000)013<3969:TGMAS>2.0.CO;2.
 2143 Ummerhofer, C. C., M. H. England, P. C. McIntosh, G. A. Meyers, M. J. Pook, J. S. Risbey, A. S. Gupta, and A. S.
 2144 Taschetto (2009), What causes southeast Australia's worst droughts?, *Geophysical Research Letters*, 36(4),
 2145 doi:10.1029/2008gl036801.
 2146 Venzke, E. (2013), Volcanoes of the World v. 4.4.3, edited by S. I. G. V. Program, doi:
 2147 <http://dx.doi.org/10.5479/si.GVP.VOTW4-2013>.
 2148 Wang, B., and S. An (2002), A mechanism for decadal changes of ENSO behavior: roles of background wind changes,
 2149 *Climate Dynamics*, 18(6), 475-486, doi:10.1007/s00382-001-0189-5.
 2150 Wang, B., and Z. Fan (1999), Choice of South Asian Summer Monsoon Indices, *Bulletin of the American Meteorological*
 2151 *Society*, 80(4), 629-638, doi:doi:10.1175/1520-0477(1999)080<0629:COSASM>2.0.CO;2.
 2152 Wang, B., R. Wu, and K.-M. Lau (2001), Interannual Variability of the Asian Summer Monsoon: Contrasts between the
 2153 Indian and the Western North Pacific–East Asian Monsoons, *Journal of Climate*, 14(20), 4073-4090,
 2154 doi:doi:10.1175/1520-0442(2001)014<4073:IVOTAS>2.0.CO;2.
 2155 Wang, C. (2002), Atmospheric Circulation Cells Associated with the El Niño–Southern Oscillation, *Journal of Climate*.
 2156 Wang, C. (2004), A modeling study on the climate impacts of black carbon aerosols, *Journal of Geophysical Research:*
 2157 *Atmospheres*, 109(D3), D03106, doi:10.1029/2003JD004084.
 2158 Wang, G., and H. H. Hendon (2007), Sensitivity of Australian Rainfall to Inter–El Niño Variations, *Journal of Climate*,
 2159 20(16), 4211-4226, doi:10.1175/jcli4228.1.
 2160 Webster, P. J., and S. Yang (1992), Monsoon and Enso: Selectively Interactive Systems, *Quarterly Journal of the Royal*
 2161 *Meteorological Society*, 118(507), 877-926, doi:10.1002/qj.49711850705.

2162 Winker, D. M., M. A. Vaughan, A. Omar, Y. Hu, K. A. Powell, Z. Liu, W. H. Hunt, and S. A. Young (2009), Overview
2163 of the CALIPSO Mission and CALIOP Data Processing Algorithms, *Journal of Atmospheric and Oceanic Technology*,
2164 26(11), 2310-2323, doi:10.1175/2009jtecha1281.1.
2165 Zebiak, S. E., and M. A. Cane (1987), A Model El Niño–Southern Oscillation, *Monthly Weather Review*, 115(10),
2166 2262-2278, doi:10.1175/1520-0493(1987)115<2262:AMENO>2.0.CO;2.
2167 Zhang, D., R. Blender, and K. Fraedrich (2013a), Volcanoes and ENSO in millennium simulations: global impacts and
2168 regional reconstructions in East Asia, *Theoretical & Applied Climatology*, 111(3/4), 437-454, doi:10.1007/s00704-012-
2169 0670-6.
2170 Zhang, R., et al. (2013b), Have Aerosols Caused the Observed Atlantic Multidecadal Variability?, *Journal of the*
2171 *Atmospheric Sciences*, 70(4), 1135-1144, doi:10.1175/JAS-D-12-0331.1.

2172

2173

2174

2175